



TAMPEREEN TEKNILLINEN YLIOPISTO
TAMPERE UNIVERSITY OF TECHNOLOGY

Heino Kuuluvainen
On the Surface Interaction of Aerosol Particles



Julkaisu 1461 • Publication 1461

Tampereen teknillinen yliopisto. Julkaisu 1461
Tampere University of Technology. Publication 1461

Heino Kuuluvainen

On the Surface Interaction of Aerosol Particles

Thesis for the degree of Doctor of Science in Technology to be presented with due permission for public examination and criticism in Tietotalo Building, Auditorium TB109, at Tampere University of Technology, on the 10th of March 2017, at 12 noon.

Tampereen teknillinen yliopisto - Tampere University of Technology
Tampere 2017

Doctoral candidate: Heino Kuuluvainen, M.Sc.
Aerosol Physics Laboratory
Faculty of Natural Sciences
Tampere University of Technology
Tampere, Finland

Supervisor: Jorma Keskinen, Prof.
Aerosol Physics Laboratory
Faculty of Natural Sciences
Tampere University of Technology
Tampere, Finland

Pre-examiners: Sergey A. Grinshpun, Prof.
Department of Environmental Health
University of Cincinnati
Cincinnati, USA

Gerhard Kasper, Prof.
Institut für Mechanische Verfahrenstechnik
Karlsruhe Institute of Technology
Karlsruhe, Germany

Opponent: Alfred P. Weber, Prof.
Institute of Particle Technology
Clausthal University of Technology
Clausthal-Zellerfeld, Germany

Painopaikka:
Juvenes Print
Suomen Yliopistopaino Oy
Tampere 2017

ISBN 978-952-15-3913-8 (printed)
ISBN 978-952-15-3921-3 (PDF)
ISSN 1459-2045

Abstract

Aerosol particles interact with surfaces in different environments and applications. The knowledge of fundamental surface interaction phenomena can be used to investigate the structural properties of particles, describe the performance of different instruments, and develop new applications. In this thesis, particle rebound from a surface as well as the transfer of the electric charge during rebound and resuspension were studied. The research was based on the experimental and numerical characterization of these surface interaction phenomena. Along with the fundamental understanding obtained for the interaction between aerosol particles and surfaces, new methods were developed and applied for specific aerosols, such as fungal spores.

The critical velocity of rebound, which is the smallest incident velocity for a particle to rebound, was determined in a wide particle size range combining the separate groups of previous results. The main instrument developed during the research of this thesis, a variable nozzle area impactor (VNAI), was used throughout the wide size range for different particle and surface materials. The particle material was found to have a significant effect on the critical velocity of rebound. On the contrary, the effect of the surface material was observed to be much smaller, at least for the hard surface materials studied in the experiments. Also the critical velocity for oblique impacts in the impactor was characterized. It was found that the critical velocity of rebound significantly decreased with the increasing obliquity of the impact. Based on the results of this thesis, the effect of materials and obliquity on the critical velocity can be estimated quantitatively and exploited in the development of new applications, such as impactors and collectors.

The triboelectric charge transfer during rebound was characterized for nanoparticles with a new simplified method developed for an electrical low pressure impactor (ELPI). In addition, the charge transfer was measured for fungal spores and standard test dusts during rebound and resuspension. The results of this thesis showed that the triboelectric charging of particles during resuspension correlated with the triboelectric charging during rebound. Spores of different fungal species were found to obtain both positive and negative charges from substrates of different materials. The information on the triboelectric charging and rebound behavior can be used for predicting the particle dynamics in different environments and designing new applications, for instance, in ventilation and filtration systems.

Preface

The thesis work has been conducted in the Aerosol Physics Laboratory at Tampere University of Technology (TUT) during the years 2012–2017. I am grateful for the facilities and infrastructure provided by the laboratory. The financial support from the TUT’s Graduate School is greatly acknowledged. The research conducted in this thesis was also funded by Tekes and Nessling Foundation. In addition, I thank for the personal grants given by the Emil Aaltonen Foundation.

I express my greatest gratitude to my supervisor and the head of the Aerosol Physics Laboratory, Prof. Jorma Keskinen, for providing me the opportunity to work in the research group and guiding me through the years of research. Prof. Sergey A. Grinshpun and Prof. Gerhard Kasper are acknowledged for the pre-examination of the thesis and valuable feedback. The publications included in this thesis would not have been finished without the contribution of all the co-authors. I would like to thank especially Dr. Anssi Arffman for the inventions and computational work that enabled the successful research. I am also grateful to Dr. Juha Harra for being a forerunner of my scientific career and peer-reviewing almost every word I have written. I thank my colleague Dr. Sampo Saari, Dr. Jacob Mensah-Attipoe and Dr. Pertti Pasanen from University of Eastern Finland, and Prof. Tiina Reponen from University of Cincinnati for introducing me to the research of bioaerosols. The personnel from the Department of Materials Science at TUT and from the workshop of the Department of Physics at TUT are acknowledged for their efforts to the experimental research.

The former members of the research group, Prof. Annele Virtanen, Dr. Jonna Kannosto, and Dr. Erkkka Saukko are especially acknowledged for their guidance at the early stage of my career. Along with the thesis work, I have had the privilege to explore many different fields of aerosol science. I want to thank Dr. Topi Rönkkö, Prof. Jyrki M. Mäkelä, and Prof. Miikka Dal Maso for that. All the current and former co-workers at the Aerosol Physics Laboratory deserve my special thanks for creating a great atmosphere to work.

I am grateful to my parents, siblings, and grandparents for supporting me during my studies and life in general. I also wish to thank all my fellow students and other friends. Finally, I want to thank my beloved wife Kaisa-Tuulia. Because of her, I have taken giant steps also as a person during the last years.

Tampere, February 2017



Heino Kuuluvainen

Contents

Abstract	iii
Preface	v
Symbols and abbreviations	ix
List of publications	xi
Author's contribution	xiii
1 Introduction	1
1.1 Aim and scope	2
2 Surface interaction phenomena	5
2.1 Adhesion	6
2.2 Rebound	7
2.3 Resuspension	10
2.4 Charge transfer	11
3 Methods	15
3.1 Aerosol instruments	15
3.2 Numerical simulation and analysis	20
3.3 Generation of particles	24
4 Results and discussion	29
4.1 Critical velocity of rebound	29
4.2 Triboelectric charging	33
5 Conclusions	37
Bibliography	39
Publications	45

Symbols and abbreviations

α	material coefficient of rebound
β	precharge sensitivity of charge transfer
η_{cr}	critical collection efficiency
ρ_{eff}	effective density
A	Hamaker constant
AF	ammonium fluorescein ($C_{20}H_{16}NO_5$)
Ag	silver
Al	aluminum
<i>A.v.</i>	<i>Aspergillus versicolor</i>
C_C	slip correction factor
C_R	coefficient of restitution
<i>C.c.</i>	<i>Cladosporium cladosporioides</i>
CFD	computational fluid dynamics
CPC	condensation particle counter
Cu	copper
d_a	aerodynamic diameter
d_p	particle diameter (mobility diameter)
DENSMO	real-time effective density monitor
DMA	differential mobility analyzer
E_{adh}	adhesion energy
ELPI	electrical low pressure impactor
F_{adh}	adhesion force
FCE	Faraday cup electrometer
FSSST	fungal spore source strength tester

HR-LPI	high-resolution low-pressure impactor
I	electric current
KHP	potassium biphthalate
L_{cr}	critical slit length
LAS-X	laser aerosol spectrometer
LDV	laser Doppler velocimetry
n	average number of elementary charges
NaCl	sodium chloride
Mo	molybdenum
OPS	optical particle sizer
P	penetration
<i>P.b.</i>	<i>Penicillium brevicompactum</i>
PTFE	polytetrafluoroethylene
q	electric charge
q_c	contact charge
R^2	coefficient of determination
SEM	scanning electron microscope
SiC	silicon carbide
SMPS	scanning mobility particle sizer
SOA	secondary organic aerosol
TEM	transmission electron microscope
UV-APS	ultra-violet aerodynamic particle sizer
v	velocity
v_{cr}	critical velocity of rebound
VNAI	variable nozzle area impactor
VOAG	vibrating orifice aerosol generator
z_0	separation distance

List of publications

- Paper I** Heino Kuuluvainen, Anssi Arffman, Erkka Saukko, Annele Virtanen, and Jorma Keskinen, “A new method for characterizing the bounce and charge transfer properties of nanoparticles,” *Journal of Aerosol Science*, vol. 55, pp. 104–115, 2013. doi: 10.1016/j.jaerosci.2012.08.007
- Paper II** Anssi Arffman, Heino Kuuluvainen, Juha Harra, Ossi Vuorinen, Paxton Juuti, Jaakko Yli-Ojanperä, Jyrki M. Mäkelä, and Jorma Keskinen, “The critical velocity of rebound determined for sub-micron silver particles with a variable nozzle area impactor,” *Journal of Aerosol Science*, vol. 86, no. 9, pp. 32–43, 2015. doi: 10.1016/j.jaerosci.2015.04.003
- Paper III** Heino Kuuluvainen, Anssi Arffman, Anssi Järvinen, Juha Harra, and Jorma Keskinen, “The effect of materials and obliquity of the impact on the critical velocity of rebound,” *Aerosol Science and Technology*, Published online 14 Nov 2016. doi: 10.1080/02786826.2016.1260088
- Paper IV** Heino Kuuluvainen, Sampo Saari, Jacob Mensah-Attipoe, Anssi Arffman, Pertti Pasanen, Tiina Reponen, and Jorma Keskinen, “Triboelectric charging of fungal spores during resuspension and rebound,” *Aerosol Science and Technology*, vol. 50, no. 2, p. 187–197, 2016. doi: 10.1080/02786826.2016.1141164

Author's contribution

- Paper I** A new method for characterizing the bounce and charge transfer properties of nanoparticles was designed and evaluated. The method consisted of experiments and a numerical analysis. The author designed and performed the experiments, was responsible for the numerical analysis except the computational fluid dynamics, and wrote most of the paper.
- Paper II** The critical velocity of rebound was determined for spherical silver aerosol particles in a wide size range using a new impactor design, experimental methods, and a numerical analysis. The first authorship was shared between the author and Anssi Arffman, who was responsible for the impactor design and the numerical simulations. The author had the main responsibility of the experiments, data analysis, preparation of the figures, and writing the paper.
- Paper III** Experiments for spherical ammonium fluorescein particles were conducted in order to investigate the effect of different materials and obliquity of the impact on the critical velocity of rebound. The author was responsible of the experiments and data analysis, except the numerical simulation. The author also prepared the figures and wrote most of the paper.
- Paper IV** The triboelectric charging of fungal spores during rebound and resuspension was studied with different experimental setups. The author had the main responsibility of designing and performing the experiments, except the fungal spore sample preparation. Furthermore, the author carried out the data analysis and wrote most of the paper.

1 Introduction

The idea of an elastic ball traveling around a room and rebounding from the walls is often associated with molecules to describe the kinetic theory of gases. Even if the world of molecules is far beyond the world of macroscopic objects, the principles of the interaction with a surface are basically the same. The simple interaction between a spherical object and a surface is one of the most fascinating problems in physics. Even if the problem is easy to understand, it may not be easy to characterize by means of theoretical and experimental physics. Between the macroscopic and molecular worlds, there is the area of aerosol particles with four magnitudes of particle sizes. Aerosol particles are known to adhere easily on surfaces but they may also rebound. In the wide size range of aerosol particles, the challenges are many, but we are on the way to combine the world of molecules to the world of macroscopic objects.

In aerosol physics, particle rebound from a surface has often been considered as an unwanted phenomenon causing artifacts in inertial impactors (Chang et al., 1999; Dzubay et al., 1976), reduction of the collection efficiency in filtration (Heim et al., 2005; Hubbard et al., 2014), and triboelectric charging of particles in medical inhalators (Matsusaka et al., 2010). Recently, particle rebound has also been recognized as a significant source of uncertainty in aerosol mass spectrometers (Kang et al., 2015). In order to prevent the unwanted rebound in different applications, practical innovations and improvements have been introduced, such as porous and greased substrates in impactors, as well as different materials and geometries in filters and medical inhalators. Some of these innovations and improvements would not have been realized without a strong know-how and characterization of the particle rebound phenomenon. The development in instrumentation may also in future lead to various applications where particle rebound can be a problem. In order to solve the problems, profound knowledge of the phenomenon is required.

Particle rebound has also been utilized in different applications. Virtanen et al. (2010) found an amorphous solid state of secondary organic aerosol (SOA) particles by investigating the bounce behavior of the particles in a cascade impactor. The discovery has led to the development of more sophisticated methods to study the phase state of SOA particles as a function of the relative humidity (Bateman et al., 2014; Saukko et al., 2012). The phase state and viscosity of amorphous particles are important properties for atmospheric aerosols because of their ability to act as cloud condensation nuclei. Recently, the research has been turned into the chase of viscosity, where the measurement of particle rebound has a significant role (Pajunoja et al., 2015). Another field of aerosol physics in which the particle–surface interaction has been utilized to investigate particle properties is the field of engineered nanoparticles. Froeschke et al. (2003) observed the fragmentation of agglomerates and estimated the binding energies between primary particles in an agglomerate. Similar studies were conducted more recently by Seipenbusch et al. (2007)

and Ihalainen et al. (2014). A quantitative analysis of the phase state and agglomerate binding energy practically requires reliable determination of the particle impact velocity.

One of the typical pathways for an aerosol particle close to a surface is that the particle first deposits and is later resuspended. Resuspension may occur as a result of mechanical, aerodynamic, or electrostatic disturbance. Especially in indoor environments, resuspension caused by everyday activities, such as walking or cleaning, is a significant process affecting the concentration and dynamics of the particles. Experimental and theoretical characterization of resuspension is not straightforward, and it has usually been studied in specific conditions. For instance, the experimental setups for resuspension studies have been designed to mimic human walking (Gomes et al., 2007) and natural wind (Nicholson, 1993). The similarities of the resuspension and rebound phenomena from the point of view of triboelectric charge transfer have not been studied before.

The theoretical framework of this thesis is mainly formed by three previous studies. Dahneke (1971) introduced the basic theory for the critical velocity of rebound that is the smallest incident velocity with which a particle rebounds from a surface. John et al. (1980) formulated the theory for the triboelectric charge transfer during rebound and Wall et al. (1990) specified the theory of the critical velocity. Despite of the theoretical knowledge, the rebound and charge transfer phenomena are very difficult to predict in any case without experiments. The critical velocity of rebound has previously been determined experimentally or using a combination of experimental and numerical methods for micron-sized particles (Wall et al., 1990) and nanoparticles (Rennecke and Weber, 2013a). There is a substantial gap between these two sets of results with respect to the particle size range and with respect to the order of magnitude of the critical velocity if the values would be extrapolated to the same size range. Lack of knowledge also exists in the experimental characterization of the charge transfer phenomenon. John et al. (1980) investigated the phenomenon thoroughly for micron-sized particles but no data exists for nanoparticles or bioaerosols.

Chapter 2 of the thesis presents the fundamental surface interaction phenomena for aerosol particles including adhesion, rebound, resuspension, and charge transfer. The phenomena are described from the theoretical point of view, as well as from an aspect of the previous experimental knowledge. Both experimental and numerical methods were exploited in the research of this thesis. These methods, including the test particle generation, are described in Chapter 3. The results of this work are reviewed in Chapter 4 and concluded with the final remarks in Chapter 5.

1.1 Aim and scope

The aim of this thesis is to provide new information on the fundamental aerosol physics related to the surface interaction of particles. The research is mainly focused on the phenomena of particle rebound and triboelectric charge transfer, the latter of which is also connected to the resuspension of particles. Despite of its fundamental nature, the thesis also includes characterization of specific indoor aerosols. The main objectives of this thesis are listed below.

- To determine the critical velocity of rebound in a wide particle size range and identify its dependency on the particle and surface materials.
- To analyze the triboelectric charging of fungal spores and nanoparticles during resuspension and rebound from substrates of different materials.

- To estimate the relevance of the critical velocity and triboelectric charging for instrumentation and indoor environments.

The first objective was partly realized in all publications of this thesis. **Paper I** introduced a method with which the critical velocity of rebound could be estimated for polydisperse aerosols in the nanoparticle size range. In **Paper II**, the critical velocity was more accurately determined for silver particles in a wide sub-micron size range. **Paper III** revealed the effect of different surface materials and **Paper IV** presented the critical velocity for fungal spores.

The second objective regarding the triboelectric charging was realized in **Paper I** and **IV**. The charge transfer of sodium chloride and levoglucosan nanoparticles during rebound in an impactor was characterized in **Paper I**. More profound study on the triboelectric charging of particles was carried out in **Paper IV** for micron-sized particles, such as fungal spores, and different surface materials.

The last objective of this thesis was directly connected to **Paper I** and **IV** that brought out the aspect of instrumentation and indoor environments, respectively. Furthermore, the last objective was partly realized also in **Paper II** and **III**, as well as in the introduction part of the thesis.

2 Surface interaction phenomena

In this chapter, the surface interaction of aerosol particles is reviewed. The interaction can be understood through four basic phenomenon which are adhesion, rebound, resuspension, and charge transfer (see Figure 2.1). Adhesion is the basis of the particle–surface interaction and it is also involved in rebound and resuspension. An adhesion force F_{adh} , arising from the molecular interaction of a particle and a surface, affects the particle in the adhesion force field within a distance h from the surface. In order to rebound or be resuspended, the particle has to escape from the adhesion force field. Triboelectric charge transfer between the particle and the surface may occur during rebound or resuspension.

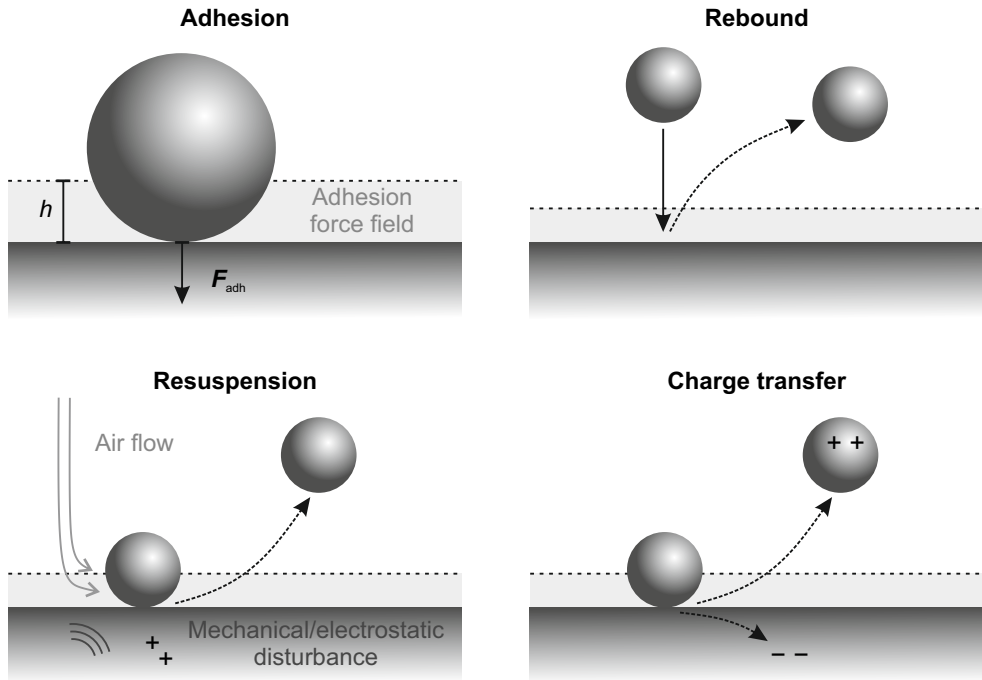


Figure 2.1: A schematic of the surface interaction phenomena introduced in this chapter. The light-gray area represents an adhesion force field within a height h from the surface, where an adhesion force F_{adh} affects the particle.

2.1 Adhesion

The definition of adhesion may vary between different applications and different fields of physics. According to Mittal (1975), adhesion is the sticking together of two similar or dissimilar materials. Other definitions restrict it to the case of two dissimilar materials. Many applications, such as adhesive tapes and glues, aim at maximizing the effect of adhesion. If there is strong adhesion between two materials or objects, the adhesion force F_{adh} is significant and the objects are firmly stuck together. The adhesion force can be measured by searching the minimum force required to separate the objects. Another quantitative approach to adhesion arise from the work done by the adhesion force and the adhesion energy. The work for an object on a surface can be written as (Mittal, 1975)

$$W = \int_0^h F_{\text{adh}}(z) dz \quad (2.1)$$

where z is the distance from the surface and h is the height of the adhesion force field. The work defined through this equation equals the adhesion energy E_{adh} . The height of the adhesion force field may depend on the materials and objects involved but, for aerosol particles, it is in the order of a few atomic layers (Hinds, 1999). Even if the adhesion force and energy are conceptually effortless to understand, there are numerous different theories trying to explain the interaction. The theories can be based on the analysis of macroscopic, microscopic, or molecular phenomena, and applications may require the use of several levels of theories (Ebnesajjad, 2006).

Aerosol particles adhere easily on different surfaces. This is a feature that distinguishes aerosol particles from molecules and macroscopic objects (Hinds, 1999). Gas molecules are known to rebound from surfaces, whereas the forces affecting macroscopic objects, such as the gravitational force, are often stronger than the adhesion force. In aerosol physics, adhesion is important for many applications. Many types of filters and collectors have been based on the tendency of aerosol particles to adhere on surfaces (Dzubay and Barbour, 1983; Miaskiewicz-Peska and Lebkowska, 2012). Recently, the role of adhesion has become more important in the field of engineered nanoparticles, where the properties of surfaces can be changed with various nanoparticle coatings. The functional coatings may be, for example, hydrophobic or hydrophilic (Stepien et al., 2011).

The most important adhesion forces affecting aerosol particles are the London–van der Waals forces. They are electrostatic intermolecular forces arising from the movement of electrons that may result in positively or negatively charged regions or poles in molecules. Due to the work of R. S. Bradley and H. C. Hamaker in the 1930s, an expression for attractive force and energy between two spheres was integrated and formed (Hamaker, 1937). Adapting the notation of Dahneke (1971), the depth of the potential well corresponding to the adhesion energy for two spheres with diameters d_1 and d_2 adhering to each other is given by

$$E_{\text{adh}} = \frac{Ad}{12z_0} \quad (2.2)$$

where A is the Hamaker constant and z_0 is the equilibrium separation distance of the spheres. The dimension d is the ratio $d_1 d_2 / (d_1 + d_2)$ and it represents directly the diameter of a sphere on a flat surface for which $d_2 \rightarrow \infty$. The separation distance arising from the surface roughness of the spheres or surface may change during the adhesion process but it is usually assumed to be 0.4 nm (Hinds, 1999). According to Kleman and Lavrentovich

(2003), typical values for the Hamaker constant are in the range of $0.4-4 \times 10^{-19}$ J. The Hamaker constant values for different material pairs can be calculated using the Lifshitz theory and experimentally determined dielectric properties of materials (Bergström, 1997). However, only a limited amount of data exists for different material pairs and the values have not been proven to be applicable to the interaction of aerosol particles and surfaces. In addition to the London–van der Waals forces, two other mechanisms may have an effect on the adhesion of aerosol particles. The first mechanism is based on the attractive electrostatic force between a charged particle and the image charge generated to a surface. The other one arises from the surface tension of the water remained between a particle and a surface. However, these mechanisms are significant compared to the London–van der Waals forces only for highly charged particles and ambient conditions above 90 % relative humidity, respectively (Hinds, 1999).

2.2 Rebound

Even though aerosol particles are inclined to adhere, they may also rebound from surfaces. A theory for particle rebound was introduced by Dahneke (1971). The basic idea in the theory is that the sum of the initial kinetic energy and the potential energy of the adhesion force field, reduced by the energy losses during the impact, has to be larger than the adhesion energy for a particle to rebound. Generally, the potential energy seen by the incoming particle may differ from the potential energy seen by the rebounding particle. The energy balance equation on the capture limit can be written as

$$(E_{k,i} + E_{p,i}) C_R^2 = E_{p,r} \quad (2.3)$$

where $E_{k,i}$ is the kinetic energy of the incoming particle, $E_{p,i}$ is the potential energy seen by the incoming particle, $E_{p,r}$ is the potential energy seen by the rebounding particle and C_R is the coefficient of restitution. In this notation, the coefficient of restitution can be considered as a ratio of the normal rebound velocity and the normal impact velocity relatively close to the surface compared to the height of the adhesion force field.

Dahneke (1971) assumed that the potential energy seen by the incoming particle is the same for the rebounding particle. By setting this potential energy equal to the adhesion energy and using the definition of the kinetic energy, we can derive from Equation (2.3) the capture limit velocity, i.e. the critical velocity of rebound

$$v_{cr} = \left(\frac{2E_{adh}}{m} \frac{1 - C_R^2}{C_R^2} \right)^{1/2} \quad (2.4)$$

where m is the particle mass. The particle mass can also be expressed as $m = \frac{\pi}{6} \rho d_p^3$, where d_p is the particle diameter and ρ is the density. By using Equation (2.2) for the adhesion energy with the particle diameter d_p , the critical velocity becomes

$$v_{cr} = \alpha d_p^{-1} \quad (2.5)$$

where

$$\alpha = \left(\frac{A(1 - C_R^2)}{\pi z_0 \rho C_R^2} \right)^{1/2} \quad (2.6)$$

is the material coefficient of rebound. In this expression, also used by Dahneke (1971), the critical velocity of rebound is inversely proportional to the particle diameter and

the material coefficient includes the effects of adhesion as well as the energy losses. The effects of adhesion are included in the Hamaker constant and all the energy losses are implemented in the coefficient of restitution. By contrast, Wall et al. (1990) took into account a fraction of the energy losses in the difference of the potential energies seen by the incoming and rebounding particles.

The energy losses have an important role in the collision of a particle and a surface. Through some mechanisms, such as acoustic waves and flexural work, the energy losses may occur in the surface (Dahneke, 1971), but these can usually be ignored in the case of aerosol particles and rigid surfaces. The most important energy loss mechanism is the plastic deformation of the particle. Rogers and Reed (1984) developed a model based on the elastic and plastic deformation and applied it for impacts and adhesion of large copper microspheres. More recently, different approaches to calculate the effect of material properties, corresponding to the material coefficient of rebound in Equation (2.5), have been introduced. In spite of the different approaches based on an elastic (Wang and Kasper, 1991) or plastic (Weir and McGavin, 2008) behavior of particles, the inverse proportionality to the particle size has remained.

A schematic in Figure 2.2 shows the ratio of the rebound velocity v_r and the impact velocity v_i as a function of the impact velocity for a particle interacting with a surface. The observation is reduced to the normal velocity components perpendicular to the surface. Conceptually, the velocity ratio v_r/v_i may also be called as the coefficient of restitution, even if the velocities would be defined outside the adhesion force field. Consequently, the coefficient of restitution is equal to zero with low impact velocities until it rapidly increases at the critical velocity and reaches the constant value defined as C_R . The theory of Dahneke (1971) leads to a simple step function, but, in the theory of Wall et al. (1990), the difference in the potential energies seen by the incoming and rebounding particles dominate the energy losses close to the onset of rebound, and the value of C_R is not reached until at higher velocities. Wall et al. (1990) measured directly the velocity ratio for micron-sized particles and the results agreed with the theoretical dependency. If the impact velocity is further increased, the coefficient of restitution may begin to decrease again at some point because of the onset of plastic deformation. The impact velocity corresponding to this transition from elastic to plastic deformation can be used to calculate the energy required for the transition and the yield limit of the particle material. For micron-sized particles, the onset of plastic deformation has been experimentally determined to be at impact velocities above 20 m/s (Dahneke, 1975; Wall et al., 1990) and investigated from a theoretical point of view (Tsai et al., 1990). Schöner et al. (2014) were able to determine the coefficient of restitution for nanoparticles with impact velocities above 20 m/s. They found both elastic and plastic regions, depending on the particle size, and an agreement with molecular dynamics simulations.

In the case of oblique impacts, the normal components of the velocities are usually observed instead of the total velocities in order to study the critical velocity and the coefficient of restitution. It has been found that the capture limit for the normal velocity component may be lower in oblique impacts than in normal impacts. The experimental results with large microspheres, reviewed by Brach et al. (2000), showed that the coefficient of restitution may increase with a decreasing contact angle on rough surfaces, even up to unrealistically high values above unity with contact angles smaller than 10° . This is also illustrated in the schematic in Figure 2.2. With rough surfaces, a part of the energy related to the tangential velocity component may contribute to the normal rebound velocity during the collision and cause values above unity for the coefficient of restitution. Wang and

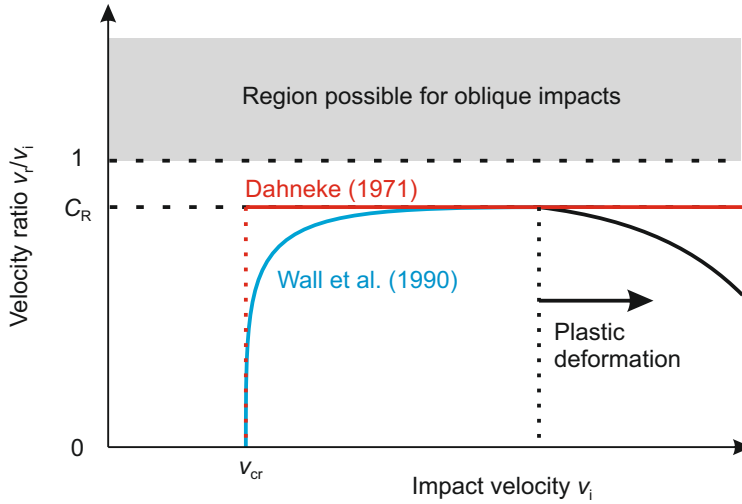


Figure 2.2: A schematic presentation for the ratio of the particle rebound velocity and the impact velocity as a function of the incoming velocity. The velocity ratio can also be called as the coefficient of restitution. The theoretical functions used by Dahneke (1971) and Wall et al. (1990) are shown.

John (1988) concluded that the critical velocity of micron-sized particles determined with an impactor was lower than the critical velocity based on a direct velocity measurement (Wall et al., 1990), because of the tangential velocity in the impactor. However, no quantitative analysis was presented on the effect of the obliquity on the critical velocity. Recently, also the model of Chen et al. (2015) predicted a rapidly decreasing critical velocity with an increasing contact angle.

Different methods have been used in the experimental research of the critical velocity of rebound. The direct measurement of the particle impact and rebound velocities, based on optical methods, is practically limited to the size range above one micron. Rogers and Reed (1984) used a high speed camera for large copper and glass spheres above $10\ \mu\text{m}$ in size, and Wall et al. (1990) measured the velocities of spherical ammonium fluorescein (AF) particles of $2\text{--}7\ \mu\text{m}$ using laser Doppler velocimetry (LDV). Another approach to determine the critical velocity of rebound has been to combine the measurement of the collection efficiency in impactors or granular beds and the theoretical characterization of the flow field. This method is applicable also for smaller particles but the theoretical characterization of the flow field includes uncertainties. In the size range above one micron or slightly below, impactors have been used in the experiments to determine the critical velocity for different particle materials, such as ammonium fluorescein (Wang and John, 1988), latex (Cheng and Yeh, 1979), and uranine (Esmen et al., 1978). D’Ottavio and Goren (1982) determined the critical velocity similarly by using a granular bed instead of an impactor for potassium biphthalate (KHP) particles. Recently, the combination of impactor measurements and computational fluid dynamics (CFD) simulations has extended the size range of experimentally determined critical velocities to nanoparticles. Rennecke and Weber (2013a) measured the collection efficiency of a single stage low pressure impactor as a function of the impaction pressure and were able to determine the critical impaction pressure corresponding to the onset of rebound. The critical velocity of rebound was subsequently calculated from the critical impaction pressure. The particle

materials used by Rennecke and Weber (2013a) were silver (Ag) and sodium chloride (NaCl). Methods for determining the critical velocity were also developed in this thesis. A straightforward method to determine the material coefficient of rebound for polydisperse nanoparticles was presented in **Paper I** and a new type of an impactor, introduced in **Paper II**, enabled more accurate determination of the critical velocity for monodisperse particles in controlled impaction conditions. In **Paper III**, the results obtained with the latter method were widely compared to the previous results, and the differences between various methods were discussed.

Figure 2.3 shows the critical velocity of rebound as a function of the particle size from the previous studies introduced above. The data include combinations of different particle and surface materials which are listed in the figure legend. The critical velocity values seem to form two groups: the results for nanoparticles and the results for micron-sized particles. With respect to the particle size, there was a substantial gap between these groups with no existing experimental data. Furthermore, a difference of several orders of magnitude would be seen between these two groups if the critical velocities were extrapolated to the same size range, excluding the data of Esmen et al. (1978). The majority of experimental results predicted a size dependency where the negative exponent of the particle diameter is larger than in the theory. Usually, it has been explained with a transition from elastic to plastic deformation with the decreasing particle size (Rennecke and Weber, 2013a; Wall et al., 1990), corresponding to a size dependency of the Hamaker constant or the coefficient of restitution in Equation (2.6). The results of this thesis fill the gap between the two groups of the previous critical velocity results. In **Paper II**, the critical velocity of rebound was determined in a wide sub-micron size range for spherical silver particles. The results obtained for ammonium fluorescein particles on different surfaces in **Paper III** revealed the effect of materials and obliquity of the impact on the critical velocity. In addition, the critical velocity of fungal spores was determined in **Paper IV**, which can be relevant in ventilation systems and in the filtration of indoor aerosols.

2.3 Resuspension

Resuspension is the detachment of a particle from a surface, including the transport away. It can be considered as an important phenomenon affecting the aerosol concentrations and dynamics both in indoor and outdoor environments. Particles may be resuspended under an air flow, or through a mechanical or electrostatic disturbance (Figure 2.1). Resuspension by a jet of air can be referred as re-entrainment or blow-off. In resuspension, a particle has to overcome the adhesion energy, but the forces required for resuspension can be less than 1% of the static adhesion forces required for the detachment in a centrifuge (Hinds, 1999). Rolling and sliding can be involved and relieve the detachment in re-entrainment and blow-off before the particle becomes airborne. This was supported by Reeks and Hall (2001) who performed experiments in a centrifuge to measure adhesive forces and in a blower to measure the forces required for resuspension. They found a kinetic model taking into account rolling and sliding to have the best agreement with the experiments. Boor et al. (2013) reviewed previous studies on resuspension and found differences between monolayer and multilayer deposits.

In this thesis, resuspension was studied from an aspect of indoor aerosols. Every day activities in indoor environments, such as walking and cleaning, significantly increase the particle concentrations through resuspension (Thatcher and Layton, 1995). It has been shown that also allergen-containing particles, such as fungal spores and bacteria,

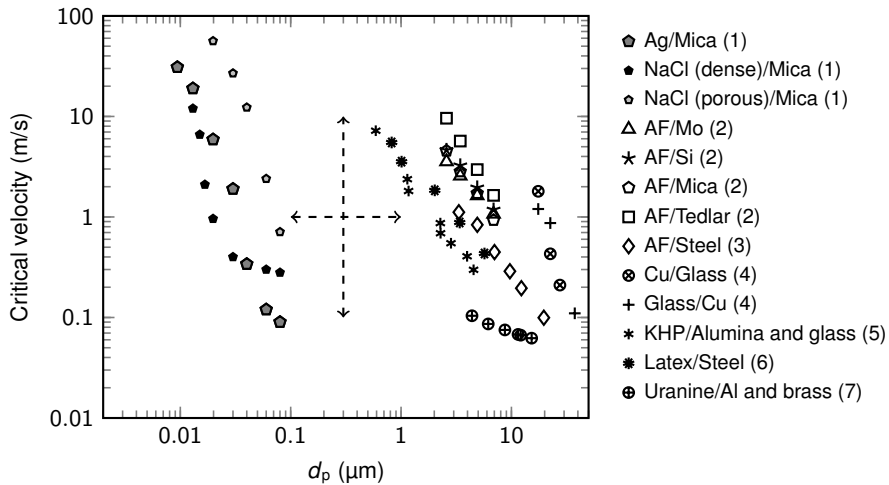


Figure 2.3: The critical velocity of rebound as a function of the particle size from previous studies of (1) Rennecke and Weber (2013a), (2) Wall et al. (1990), (3) Wang and John (1988), (4) Rogers and Reed (1984), (5) D’Ottavio and Goren (1982), (6) Cheng and Yeh (1979) and (7) Esmen et al. (1978). The legend shows the material of the particle/surface. AF refers to ammonium fluorescein and KHP to potassium biphthalate. The dashed arrows illustrate the unexplored size range and the substantial difference between the results for nanoparticles and micron-sized particles. (Adapted from **Paper II**.)

may easily be resuspended under mechanical and aerodynamic disturbances from human walking and other activities (Gomes et al., 2007; Reponen et al., 1992). The inhalation of fungal spores has been found to cause respiratory diseases and allergies (Douwes et al., 2003). According to Mendell et al. (2011), water damages and subsequent mold growth in buildings often lead to the release of fungal spores and degrade the indoor air quality. In indoor air, an important factor, affecting the dynamics of fungal spores, is their charging state. Previously, Lee et al. (2004) found that airborne fungal spores usually carry a net negative charge in most environments. Their charging state also differ significantly from non-biological particles (Mainelis et al., 2001). **Paper IV** presents a new aspect on the origin of the charging state of fungal spores by observing the triboelectric charging during resuspension and rebound. Triboelectric charging is likely to occur for fungal spores after the detachment from different surfaces in indoor environments. Thus, the resuspension of fungal spores from different surface materials relevant for indoor environments was studied in **Paper IV**.

2.4 Charge transfer

Everyday static electricity is mostly triboelectric. Two dissimilar materials, brought into contact and then separated, may gain electric charges of different polarity. The transferred charge depends on the electrochemical potential, the contact area and the relaxation time between the materials. Lowell and Rose-Innes (1980) showed that different combinations of insulating and conductive materials should be treated distinctly from a theoretical point of view. Free electron models can be used for the conductive materials, whereas the insulating materials require the use of Fermi levels in models (Matsusaka et al., 2010). However, the triboelectric effect is still poorly understood in general, and

there are problems in the reproducibility of experiments (Castle, 1997; Ireland, 2009).

A triboelectric series is a list of materials sorted according to their charge affinity with relation to other materials. The materials on the top of the series are most willing to donate electrons and the materials on the bottom of the series most willing to receive electrons. Many of the triboelectric series found in the literature are qualitative and based on a single experiment that may be difficult to reproduce. In some of the series, the data has been gathered from different sources resulting in an extensive list, but there can be a high uncertainty in the relative position of different materials in the list. However, it is also possible to obtain quantitative or semi-qualitative triboelectric series by measuring the charge, charge affinity, or charge density with relation to a reference material (Diaz and Felix-Navarro, 2004; Park et al., 2008). In **Paper IV** of this thesis, a triboelectric series was formed, based on the charge transfer results of micron-sized aerosol particles and different surface materials.

The charge transfer from an aerosol particle to a surface during rebound can in principle be divided into two separate processes. The first one is the transfer of pre-existing charge and the second process is the triboelectric contact charging. John et al. (1980) formulated a theory where both of these factors were derived theoretically for a spherical particle and a smooth surface starting from the mechanical properties of materials and the elasticity theory of Hertz. As a result, the total charge transferred during rebound is given by

$$q_{\text{tot}} = q_c + \beta q_0 \quad (2.7)$$

where q_c is the contact charge, q_0 is the precharge, and β is a constant describing precharge sensitivity of the process. The theory also predicts that the contact charge is dependent on the cube of the particle diameter and proportional to $v_i^{0.6}$ for insulating materials and to $v_i^{0.8}$ for conductive materials, where v_i is the impact velocity. In some studies (Watanabe et al., 2007; Yamamoto and Scarlett, 1986), a concept of an equilibrium charge has been used to describe the transferred charge during rebound instead of the contact charge. The equilibrium charge refers to the value of the pre-existing charge with which the total charge transferred is zero.

The experimental values for q_c and β were also determined by John et al. (1980). The measurements were carried out by using an inertial impactor, equipped with different metal substrates, and particles with a diameter of 3–7 μm . The particle materials were sodium chloride, methylene blue and potassium biphthalate. They found that the contact charge was dependent on the substrate material, but the substrate did not significantly affect the precharge sensitivity of the process and the value of β . For methylene blue particles the average value of β was 0.043 ± 0.009 , for potassium biphthalate 0.036 ± 0.016 and for sodium chloride 0.42 ± 0.05 . As an example of the size dependency of the contact charge, John et al. (1980) obtained for sodium chloride particles on a steel substrate $q_c = 124 \cdot d_p^{2.45}$, where d_p is the particle diameter in micrometers and the unit of the result is in elementary charges. In addition, the contact charge was found to be directly proportional to the impact velocity in the experiments. Wang and John (1988) were able to explain theoretically the direct proportionality and the inconsistency with the theory of John et al. (1980) by taking into account the plastic deformation of particles.

The increased use of powders in industrial processes has motivated researchers to study the triboelectric charging in many applications (Matsusaka et al., 2010). Especially pharmaceutical powders are prone to electrostatic charging causing many problems during manufacturing processes and aerosolization in medical inhalators (Watanabe et al., 2007).

However, because of a lack of interest towards sub-micron particles in this respect, only a few studies of the charge transfer behavior of nanoparticles have been published. Weber and Wu (2009) measured the charge transfer of metal nanoparticles as a function of the impact velocity and found a transition from elastic to plastic behavior by comparing the experimental results to the theory of Wang and John (1988). More recently, Rennecke and Weber (2014) carried out similar experiments with a higher resolution and were also able to distinguish an elastoplastic transition regime. In **Paper I** of this thesis, the charge transfer of nanoparticles was characterized for polydisperse aerosols. The new method developed for a cascade impactor provided a simple manner to measure the contact charge but also evaluated the performance of the instrument. The triboelectric charging has not been studied previously for biological aerosols, such as fungal spores or bacteria. **Paper IV** presented the values of q_c and β for fungal spores and different surface materials measured during rebound. In addition, the charging during resuspension was connected to the corresponding contact charge values measured during rebound.

3 Methods

Both experimental and computational methods were used during the research of this thesis. This chapter presents an overview of the applied methods. The work was mainly conducted in the Aerosol Physics Laboratory of the Department of Physics at Tampere University of Technology (TUT), except the electron microscopy analysis performed in the Department of Materials Science at TUT and the fungal spore sample preparation performed in the Department of Environmental Science at University of Eastern Finland. Some of the applied methods were established in the research of aerosol physics, but others were introduced for the first time during the research of this thesis.

3.1 Aerosol instruments

Detection of particle–surface interaction

The interaction of an aerosol particle and a surface can be studied in an inertial impactor. It is an instrument that classifies aerosol particles in an air flow according to their aerodynamic size and consists of an air flow nozzle above a collection substrate. The collection efficiency for an impactor as a function of the particle size is a sigmoid function where larger particles are collected and smaller particles continue in the flow through the impactor. In this thesis, two different impactors were used to study the particle–surface interaction. An electrical low pressure impactor (ELPI) was used in **Paper I** and a variable nozzle area impactor (VNAI) was used in **Paper II, III, and IV**. In addition, resuspension and rebound were studied with a single impactor stage of an ELPI in **Paper IV**. These instruments are introduced in detail later in this chapter.

Figure 3.1 illustrates the possible pathways for an aerosol particle in the particle–surface interaction with respect to the detection of particle rebound, resuspension, and charge transfer. Particles can be detected at three different stages of the process, either at the impaction substrate, upstream of the impactor, or downstream of the impactor. In addition, it is possible to measure the transferred charge at the impaction substrate. The detection methods can be divided into electrical and optical methods. The optical detection methods are applicable for relatively large particles in an air flow close to ambient pressure, upstream and downstream of an impactor. On the contrary, electrical detection methods can be used to measure smaller particles in an air flow even in low-pressure conditions. Furthermore, the particles collected on the impaction substrate and the transferred charge can be detected using electrical methods. It should be noted that optical methods connected to the condensation growth of particles are also applicable for very small particles down a few nanometers but they cannot be used in low-pressure conditions downstream of an impactor.

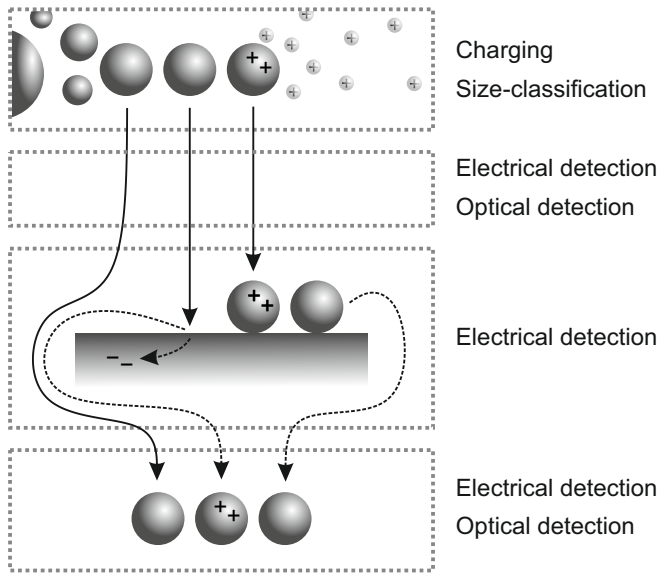


Figure 3.1: Possible pathways for an aerosol particle in the particle–surface interaction. Different detection methods can be used at different stages of the process to characterize particle rebound, resuspension, and charge transfer. In some cases, the particles may require charging or size-classification before the detection.

Aerosol particles can be detected electrically from an air flow by using a Faraday cup electrometer (FCE). It consists of a filter inside a Faraday cage which is connected to an electrometer. When charged particles are collected by the filter inside the Faraday cage, an electric current is measured by the electrometer. Similarly, an impactor can be placed inside a Faraday cage connected to an electrometer, which enables the measurement of the collected particles and transferred charge. In this thesis, the electrical detection was used in **Paper I, II, and IV** for impactors and filters. The electrical detection of particles may require charging. That can be carried out by using a unipolar diffusion charger or a bipolar radioactive neutralizer. In the latter, the particles have to be classified further, for example, with a differential mobility analyzer (DMA). The main purpose of the DMA is to classify particles according to their mobility size, but, in the output of the instrument, the particles are also positively or negatively charged and can be measured using electrical detection. This was exploited in **Paper II**. In addition, a DMA was used for the size-classification of particles in **Paper III**.

Optical methods can be used to detect particles upstream and downstream of the impactor. Devices based on the optical detection consist of a laser focused on the aerosol beam and a detector measuring the light scattered from the particles. In this thesis, an optical particle sizer (OPS) was used in **Paper II and IV**, a laser aerosol spectrometer (LAS-X) in **Paper IV**, and an ultra-violet aerodynamic particle sizer (UV-APS) was used in **Paper III**. The main purpose of these instruments was to measure the particle concentration and the collection efficiency of the impactor. However, the instruments are also capable of measuring the size distribution of particles. The UV-APS measures the aerodynamic size distribution and the OPS measures a size distribution as a function of the instrument specific optical diameter. In **Paper I**, a scanning mobility particle sizer (SMPS) was used to measure the mobility size distribution of particles. The SMPS consists of a DMA

and a condensation particle counter (CPC), the latter of which is an instrument based on the condensation growth and optical detection of particles.

Electrical low pressure impactor

An electrical low pressure impactor (ELPI) is a cascade impactor consisting of impactors with different collection efficiency curves placed on top of each other. In addition, there is a unipolar corona charger and twelve electrometers connected to the impactor stages for the electrical detection of particles. The ELPI was introduced by Keskinen et al. (1992) and it was developed to a commercial product during the 1990s. A thorough performance evaluation of the instrument was carried out by Marjamäki et al. (2000) including the measurement of the impactor collection efficiency curves and the efficiency of the corona charger. More recently, a filter stage (Marjamäki et al., 2002) and an additional impactor stage (Yli-Ojanperä et al., 2010) were introduced to improve the nanoparticle resolution of the ELPI. With these modifications the size range of the instrument is from 7 nm to 10 μm . The volumetric flow of the instrument is 10 lpm.

In a normal operation of the ELPI, the impactor substrates are usually coated with vacuum grease (e.g. Apiezon-L) in order to prevent particle rebound. Some solid particles with a high tendency to rebound may even require the use of porous substrates. The effect of substrate porosity on the collection efficiency curves of an ELPI was characterized by Marjamäki and Keskinen (2004). Virtanen et al. (2010) found that secondary organic aerosol (SOA) particles bounced in an ELPI. They defined a bounce factor by estimating the relative amount of extra current measured at the filter stage and the lowest impactor stage. The same method was applied by Virtanen et al. (2011) for particles below 30 nm by using only the current of the filter stage. The problem in the quantitative use of the bounce factor analysis was that it disregarded the effect of possible charge transfer during rebound on the current signal.

In **Paper I**, an ELPI, equipped with a filter stage and an additional impactor stage, was used to characterize particle rebound and charge transfer. Polydisperse aerosols were measured both with the corona charger and without the charger. With this procedure, we were able to distinguish the phenomena of rebound and charge transfer from each other. By connecting the experimental data to a response model described later in this chapter, the bounce and charge transfer properties could be defined for the measured particles. Individually calibrated collection efficiencies for the impactor were used as an input for the response model. Furthermore, the charging efficiency of the corona charger was given by (Marjamäki et al., 2002)

$$Pn = \begin{cases} 222.49 \cdot d_p^{1.3637}, & d_p \leq 0.023 \mu\text{m} \\ 68.12 \cdot d_p^{1.32}, & d_p > 0.023 \mu\text{m} \end{cases} \quad (3.1)$$

where d_p is the particle mobility diameter, P is the particle penetration through the charger, and n is the average number of charges per particle. Because the charging efficiency is dependent on the particle diameter d_p (mobility diameter) and the collection efficiencies are dependent on the aerodynamic diameter d_a , a conversion between these two was required. It can be written as

$$\rho_{\text{eff}} C_C(d_p) d_p^2 = \rho_0 C_C(d_a) d_a^2 \quad (3.2)$$

where ρ_{eff} is the effective density and C_C is the slip correction factor. This equation was also used in **Paper I** to convert the mobility size distribution measured by an SMPS to an aerodynamic size distribution.

Variable nozzle area impactor

A variable nozzle area impactor (VNAI) is a new type of an impactor introduced in **Paper II**. It was developed to measure the critical velocity of rebound and characterize other particle–surface interaction phenomena as a function of the particle impact velocity together with numerical simulations. Figure 3.2 shows a schematic of the VNAI. It consists of a narrow slit with a short nozzle throat length. The nozzle area of the impactor can be varied by sliding an adjustable cover and changing the slit length. In addition to **Paper II**, the VNAI was used in **Paper III** and **IV** to determine the critical velocity of rebound. During the measurements of **Paper II** and **Paper IV**, the nozzle width (0.3 mm) and the jet-to-plate distance (0.5 mm) of the impactor were constant, and the material of the impaction substrate was aluminum. In **Paper III**, the nozzle width and the jet-to-plate distance varied from 0.1 to 2.0 mm and 0.5 to 2.0 mm, respectively. The materials used in **Paper III** as an impaction substrate were steel, aluminum, molybdenum, and Tedlar® (polyvinyl fluoride). The metal substrates were equally machined and, in the case of **Paper III**, finally polished. The Tedlar substrate was compiled from a steel substrate that was covered with a layer of commercial adhesive tape with a Tedlar backing. In addition to these plain substrates, a substrate greased with Apiezon-L vacuum grease was used for reference measurements. Before the experiments, the plain substrates were flushed with isopropanol, distilled water and clean pressurized air, respectively.

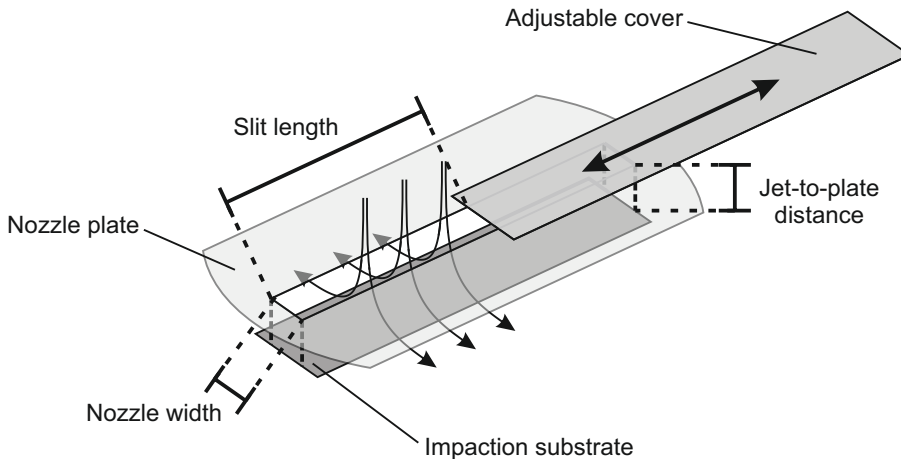


Figure 3.2: A schematic of the variable nozzle area impactor (VNAI). The nozzle area can be varied by sliding the adjustable cover. (Adapted from **Paper II**.)

The conditions and detection methods of the VNAI were changed in order to cover different particle size ranges, impact velocity ranges, materials, and oblique impacts. In addition to the impactor dimensions and substrate materials presented above, the main parameters in the experiments were the flow through the impactor and the impactor pressure. The impactor pressure was controlled with a vacuum pump and a critical orifice inlet in **Paper II** to create low-pressure conditions (106–256 mbar) and an appropriate volumetric flow (1.18 lpm) for the silver particles below 200 nm. In this setup, the particles were measured using electrical detection in which the impaction substrate and a filter downstream were connected to electrometers. The particles larger than 400 nm were measured in ambient pressure using optical detection and the impactor flow varied from 1.0 to 4.8 lpm. The instruments measuring the particle concentration before and after

the impactor were an OPS in **Paper II**, a LAS-X in **Paper IV**, and an UV-APS in **Paper III**. The collection efficiency of the VNAI was determined from the relation of the electrical signals or particle concentrations.

Figure 3.3 shows two examples of the collection efficiency of the VNAI for 82 nm silver particles measured using electrical detection and for 3.4 μm ammonium fluorescein particles measured using optical detection. In the measurement procedure, the slit was fully open in the beginning (30 mm) and it was gradually shortened at intervals of 1 mm down to 3 mm. At longer slit lengths, most of the particles were not collected, but the collection efficiency increased with the decreasing slit length reaching approximately 100% with the greased impaction substrates. With the plain substrates, the collection efficiency differed from the greased curve at the critical slit length L_{cr} and critical collection efficiency η_{cr} showing the onset of rebound. The exact value for the critical slit length was searched by observing the difference of the plain collection efficiency and the fitted curve of the greased collection efficiency. An uncertainty of ± 1 mm was estimated to represent the accuracy of the procedure. The critical slit length and critical collection efficiency obtained from the measurement were used in the simulation to determine the critical velocity of rebound as described later. As seen in Figure 3.3, the electrical and optical detection behaved similarly with respect to the determination of the critical slit length.

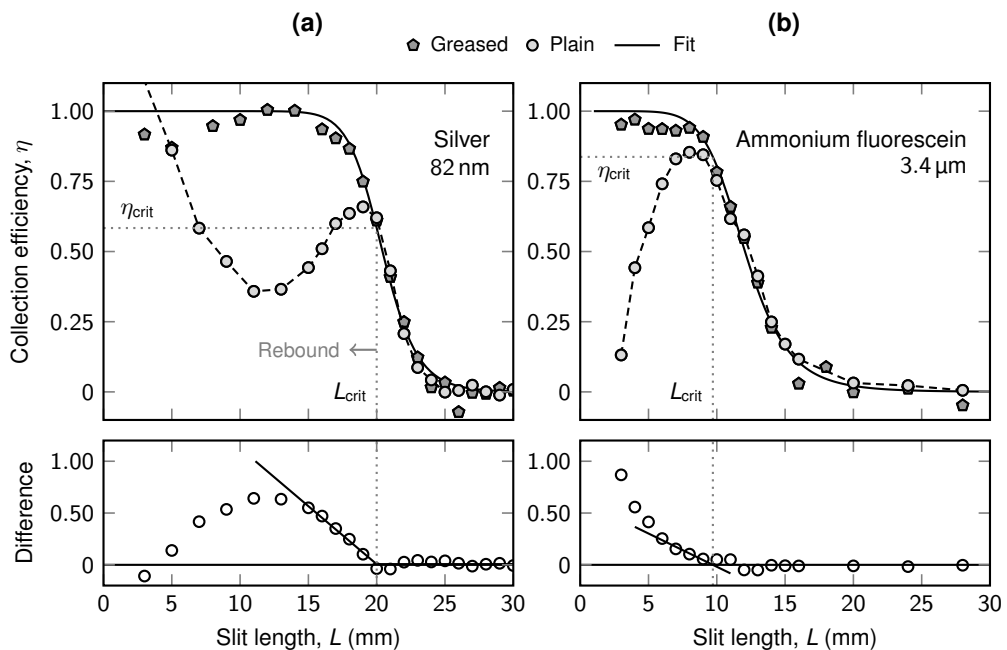


Figure 3.3: Examples of the collection efficiency of a variable nozzle area impactor (VNAI) as a function of the slit length for (a) silver (**Paper II**) and (b) ammonium fluorescein particles (**Paper III**) measured using electrical and optical detection, respectively. The onset of rebound was determined from the difference of the plain collection efficiency and the fitted curve of the greased collection efficiency. The critical slit length L_{cr} and the critical collection efficiency η_{cr} correspond to the onset of rebound.

3.2 Numerical simulation and analysis

Computational fluid dynamics

Computational fluid dynamics (CFD) can be used to solve problems involving fluid flows, based on the numerical solutions of the Navier–Stokes equations. CFD simulations were used in all of the publications of this thesis to design appropriate experimental impactor setups and calculate the impact velocities of particles. The work was based on two previous studies that presented a numerical model for an ELPI (Arffman et al., 2011) and revealed the advantages of a slit type impactor with a short nozzle throat length (Arffman et al., 2012). Recently, CFD simulations have also been used elsewhere to calculate impact velocities (Ihalainen et al., 2014; Rennecke and Weber, 2013b) and to optimize the performance of new instruments, such as a high-resolution low-pressure impactor (HR-LPI) (Arffman et al., 2014) and a real-time effective density monitor (DENSMO) (Juuti et al., 2016).

In this thesis, CFD simulations were conducted for an ELPI in **Paper I** and for a VNAI in **Paper II, III, and IV**. All of the simulations were carried out in two steps. The flow field was first simulated with ANSYS Fluent software by using the mass flow rate through the impactor and the static pressure at the outlet as boundary conditions. Then, the particle trajectories were solved using a Lagrangian particle tracking method. Figure 3.4 shows an example of the simulated flow field for the VNAI. In this case, the simulation of the slit type impactor and the variable nozzle area could be reduced to two dimensions by using the mass flow rate divided by the slit length as a boundary condition.

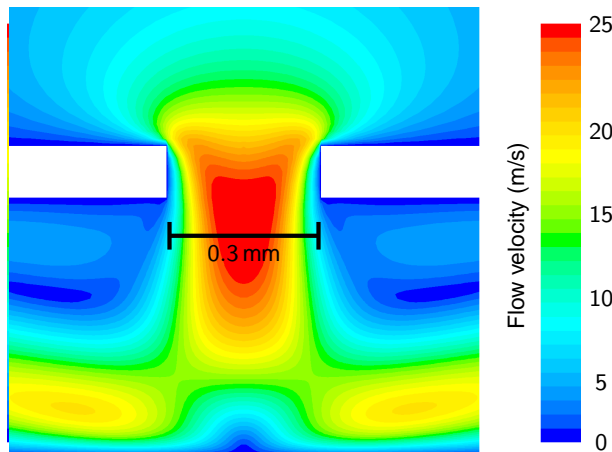


Figure 3.4: An example of the velocity field of a variable nozzle area impactor (VNAI) obtained using computational fluid dynamics (CFD) simulations. The bar shows the dimension of the jet flow and the impactor nozzle width (0.3 mm).

Impact velocity and collection efficiency

From the particle tracking data, we were able to determine the fraction of impacted particles and the impact velocities. Figure 3.5 shows examples of the simulated normal components of the impact velocity as a function of the normalized initial position of the particles in the impactor nozzle. The impact velocities for different particle sizes were used to build up the instrument response model in **Paper I**. The example in Figure 3.5a presents the impact velocities for the second stage of an ELPI. In **Paper II, III, and IV**, the critical velocity of rebound was determined by searching the impact velocity corresponding to the measured critical slit length. The example in Figure 3.5b illustrates the impact velocities in a VNAI with different slit lengths. The deviation in the impact velocities as a function of the initial position is small, which can be considered as an advantage for slit type impactors with a short nozzle throat length.

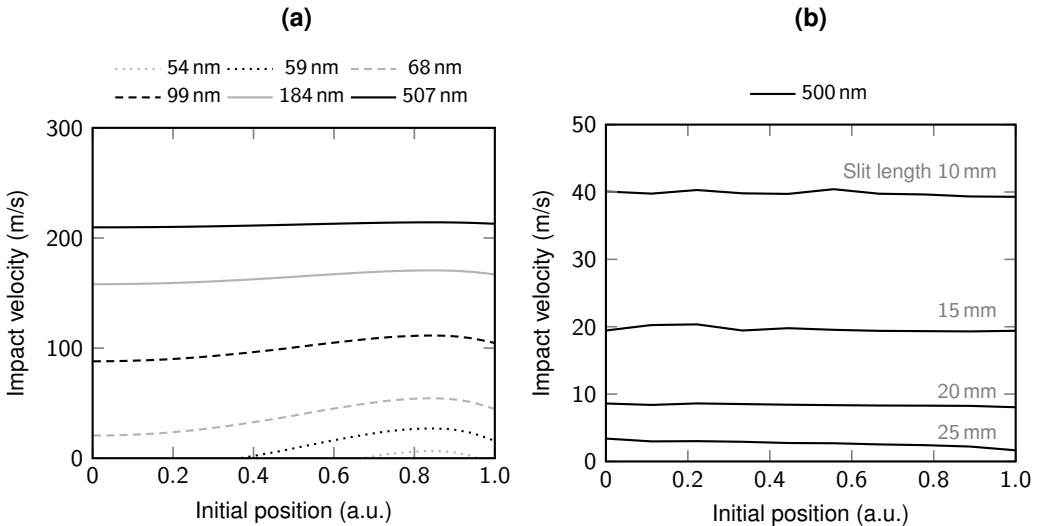


Figure 3.5: The normal component of the impact velocity as a function of the initial position of the particles (a) for different particle sizes at the second stage of an electrical low pressure impactor (ELPI) (**Paper I**) and (b) for 500 nm particles in a variable nozzle area impactor (VNAI) with different slit lengths (**Paper II**).

The methods used in this thesis work in the interface of experiments and simulations. A common problem is that the simulated collection efficiency of an impactor may not correspond to the experimental collection efficiency. Figure 3.6 shows two procedures for combining the simulated and experimental collection efficiencies. In **Paper I**, the simulated collection efficiencies, shown in Figure 3.6a for the first stage of an ELPI, was combined with the measured curves by generating random noise to the impact velocities and adjusting the cut-off size d_{50} . The random noise could be regarded as a means to take into account the turbulent diffusion and other factors not included in the simulated impact velocities (Figure 3.5a). As a result, the impact velocities corresponding to the experimental collection efficiency curves could be used in the response model. Figure 3.6b shows a schematic example of the measured and simulated collection efficiency curves of a variable nozzle area impactor (VNAI) as a function of the slit length adapted from **Paper II**. Two different methods were used to define the critical slit length. In the first method (1), the critical slit length $L_{\text{crit},1}$ was obtained straightforwardly from the measured curve

corresponding to the onset of rebound. The problem with this method was that it could result in too low impact velocities or even non-impacting particles with the collection efficiencies below 50 % arising from the difference of the simulated and measured curve. The solution was the second method (2) in which we took the critical collection efficiency $\eta_{\text{crit},2}$ corresponding to the onset of the rebound and obtained the critical slit length $L'_{\text{crit},2}$ from the simulated curve. The first method was used for the collection efficiencies above 50 % and the second method for the collection efficiencies below 50 %.

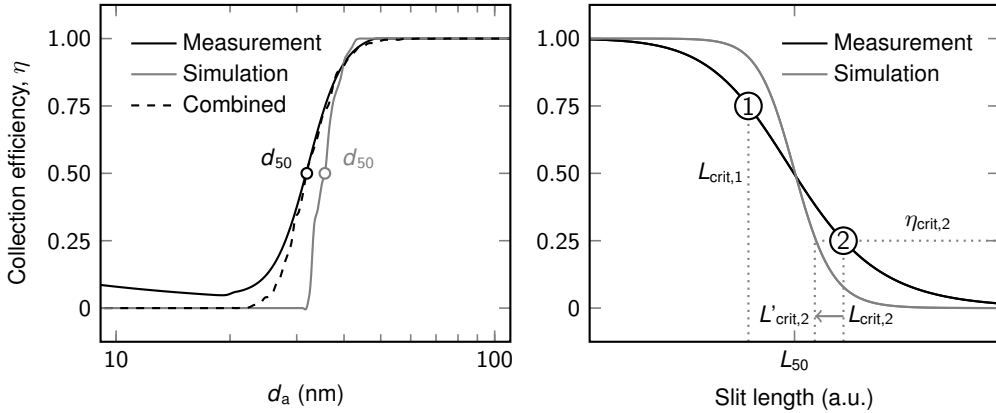


Figure 3.6: Two procedures for combining the simulated and experimental data. (a) The collection efficiency of the first stage of an electrical low pressure impactor (ELPI) as a function of the aerodynamic particle size (**Paper I**). The simulated curve was combined with the measured curve by generating random noise to the impact velocities and adjusting the cut-off size d_{50} . (b) A schematic example of the measured and simulated collection efficiency curves of a variable nozzle area impactor (VNAI) as a function of the slit length (**Paper II**). Two different methods for defining the critical slit length were used.

Instrument response model

A response model for the ELPI was built up in order to characterize particle rebound and charge transfer. The main idea in the model was to simulate the instrument response by using the mobility size distribution and three free parameters as inputs. The parameters were the effective density ρ_{eff} , the material coefficient of rebound α and the contact charge q_c corresponding to the particle size of 100 nm and the impact velocity of 100 m/s. The precharge sensitivity of charge transfer, namely β in Equation (2.7), was approximated to be zero. In the response model, two different cases were simulated, including the current measured with the charger and without the charger. The average charge of particles as a function of the particle mobility size was set to be equal to Pn given by Equation (3.1) in the first case and equal to zero in the latter.

At each impactor stage of the ELPI, the impacted and bounced fractions of the mobility size distribution were calculated by using the measured collection efficiency, the impact velocities obtained from the simulation, the effective density and the material coefficient of rebound. The impacted fraction generated an electric current that was calculated by multiplying the average charge distribution with the number size distribution of the impacted particles and with the volumetric flow. Furthermore, also the bounced particles generated a current. It was calculated by using the contact charge parameter. Finally,

the sum of these two currents represented the current signal of the impactor stage. In the step-by-step process, the complement of the impacted particle fraction and the bounced fraction continued to the next impactor stage. The average charge distribution of the particles entering the next stage was affected by the charge transfer of the bounced particle fraction.

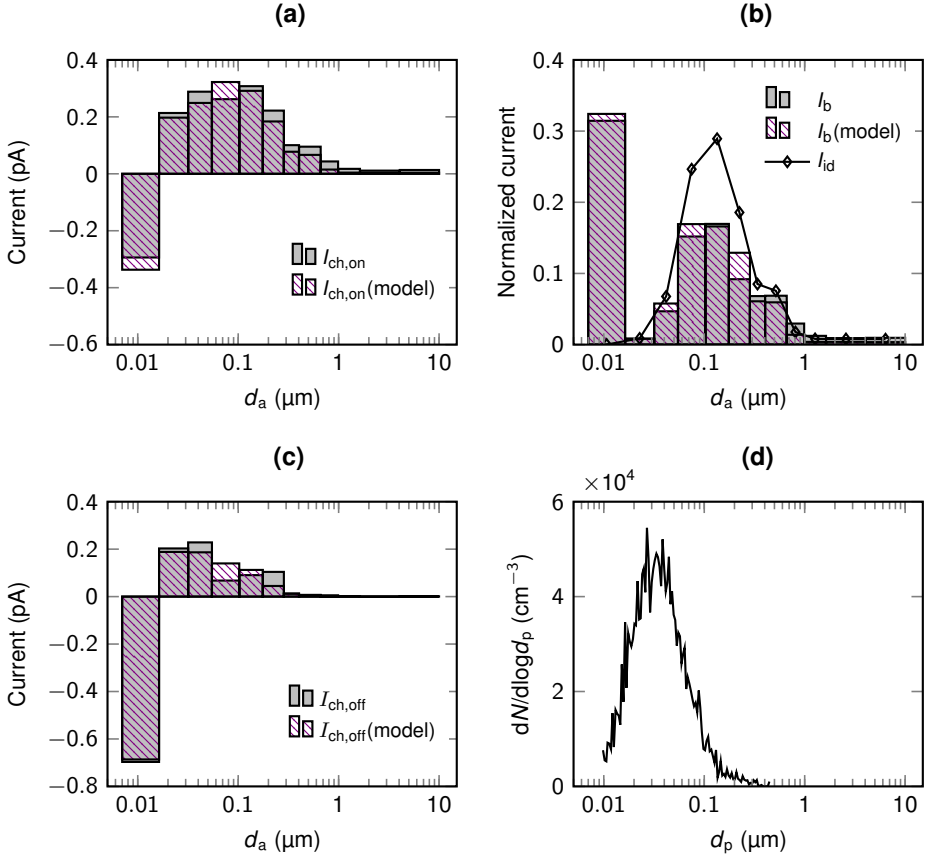


Figure 3.7: An example of the electrical low pressure impactor (ELPI) response model fitted to experimental data. The currents measured by an ELPI (a) with the charger $I_{\text{ch,on}}$ and (b) without the charger $I_{\text{ch,off}}$ as well as (c) the normalized bounce current I_b are drawn in gray. Bars with a line pattern represent the modeled currents and the solid line the ideal current I_{id} , which were calculated from (d) a mobility size distribution measured by a scanning mobility particle sizer (SMPS). (Adapted from **Paper I**.)

Figure 3.7 shows an example of the response model fitted to experimental data measured for sodium chloride particles. In order to distinguish the phenomenon of particle rebound and charge transfer also during the fitting process, a concept of a bounce current was defined and the fitting process was divided into two steps. The bounce current I_b could be written as a difference

$$I_b = I_{\text{ch,on}} - I_{\text{ch,off}} \quad (3.3)$$

where $I_{\text{ch,on}}$ is the current measured with the charger and $I_{\text{ch,off}}$ is the current measured without the charger. The bounce current represented the current measured for bouncing particles without the effect of charge transfer. In the first step of the fitting process, the

modeled bounce current was fitted to the measured current by using the effective density and the material coefficient of rebound as fitting parameters (Figure 3.7b). The second step consisted of fitting the currents without the charger by using the contact charge as a fitting parameter (Figure 3.7c). The results of fitting the response model to experimental data for each particle size distribution were the parameters: the effective density, the material coefficient of rebound, and the contact charge.

3.3 Generation of particles

Particles generated with an atomizer

Aerosol particles can be generated from liquid precursors with an atomizer. It consists of an air flow nozzle and a vertical tube above a liquid reservoir. The air flow nozzle causes a lower pressure, and the liquid is drawn upward in the tube and aerosolized in the nozzle. In this thesis, an atomizer aerosol generator (Topas ATM 220) was used in three publications. In order to generate solid particles, two different methods were used to dry the aerosol after the atomizer, including a silica gel dryer and dry dilution air (Figure 3.8a). Sodium chloride and levoglucosan particles were produced in **Paper I** from aqueous solutions. The polydisperse aerosols with a geometric mean diameter of 35–75 nm were introduced directly to the instrument. In **Paper II**, monodisperse silver particles from 0.4 μm to 1.0 μm were generated with the atomizer by using commercial silver powder dispersed in water and a DMA after the atomizer. Figure 3.9c shows a scanning electron microscope (SEM) micrograph of these particles. The generation of monodisperse ammonium fluorescein particles of 0.4–0.9 μm was also carried out using the atomizer and a DMA in **Paper III**. Ammonium fluorescein was dissolved in water. An example of the ammonium fluorescein particles generated with the atomizer can be seen in an SEM micrograph in Figure 3.9a. In order to prevent too fast drying of the droplets, the relative humidity (RH) of the dilution air was adjusted to 30%.

Evaporation–condensation method

A common method for nanoparticle production is to use evaporation and condensation (Harra et al., 2012; Scheibel and Porstendörfer, 1983). In **Paper II** of this thesis, the evaporation–condensation method was used to generate spherical silver particles in the size range of 20–200 nm. The experimental setup is illustrated in Figure 3.8b. Silver was evaporated from a small amount of bulk material in a tube furnace at temperatures of 1200–1500 $^{\circ}\text{C}$, depending on the desired particle size. The metal vapor was first carried out of the furnace and then diluted using nitrogen as a carrier gas. The silver particles, formed by condensation after cooling, were passed through a coagulation chamber before sintering. Two subsequent furnaces were used in the sintering step. The function of the latter furnace (400 $^{\circ}\text{C}$) was to smooth the particle surfaces from bumps caused by the partial evaporation and the formation of smaller particles near the bulk melting point in the first sintering furnace (600–800 $^{\circ}\text{C}$). Depending on the particle size, the flow rate through the furnaces was 0.3–1.0 lpm. The silver particles generated with the evaporation–condensation method were size-classified with a DMA before entering the VNAI. At some cases, the particles were also charged with a corona charger after the DMA in order to improve the sensitivity of the electrical detection. An example of the silver particles generated with the evaporation–condensation method can be seen in an SEM micrograph in Figure 3.9d. The sample for the micrograph was taken from the polydisperse aerosol before the DMA.

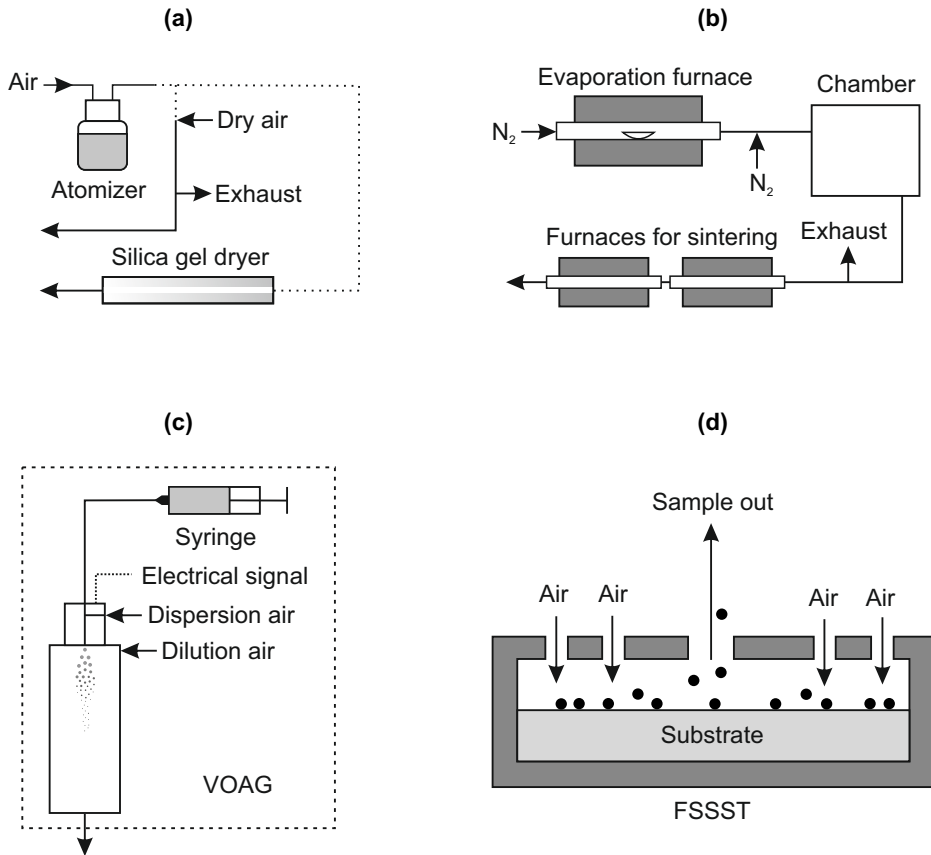


Figure 3.8: The particle generation methods used in the experiments. (a) An atomizer was used in **Paper I, II, and III** with two optional drying methods for sodium chloride, levoglucosan, silver and ammonium fluorescein particles. (b) Silver particles were generated with the evaporation–condensation method in **Paper II**. (c) A vibrating orifice aerosol generator (VOAG) was used in **Paper III** for ammonium fluorescein particles. (d) Fungal spores, silicon carbide particles and silver particles were generated with a fungal spore source strength tester (FSSST) in **Paper IV**.

Vibrating orifice aerosol generator

Test aerosols with spherical shape and exact size above one micron can be produced with a vibrating orifice aerosol generator (VOAG). The generation system was introduced by Berglund and Liu (1973) and it has been widely used e.g. in the calibration of impactor collection efficiencies (Järvinen et al., 2014; Marjamäki et al., 2000). In the VOAG, a liquid solution is fed using a syringe pump into a vibrating orifice controlled by an electric signal (Figure 3.8c). Highly monodisperse liquid droplets are formed in the orifice. Then the droplets are dispersed and dried in order to generate a monodisperse aerosol of desired material and particle size. The diameter of the liquid droplet can be calculated from the volumetric liquid feed flow and the frequency of the disturbance in the vibrating orifice (Berglund and Liu, 1973). The final particle diameter is a function of the droplet diameter and the volumetric concentration of a nonvolatile solute in a volatile solvent. In **Paper III** of this thesis, solutions of ammonium fluorescein were prepared by dissolving fluorescein powder ($C_{20}H_{12}O_5$) in aqueous ammonia (NH_4OH) as described by

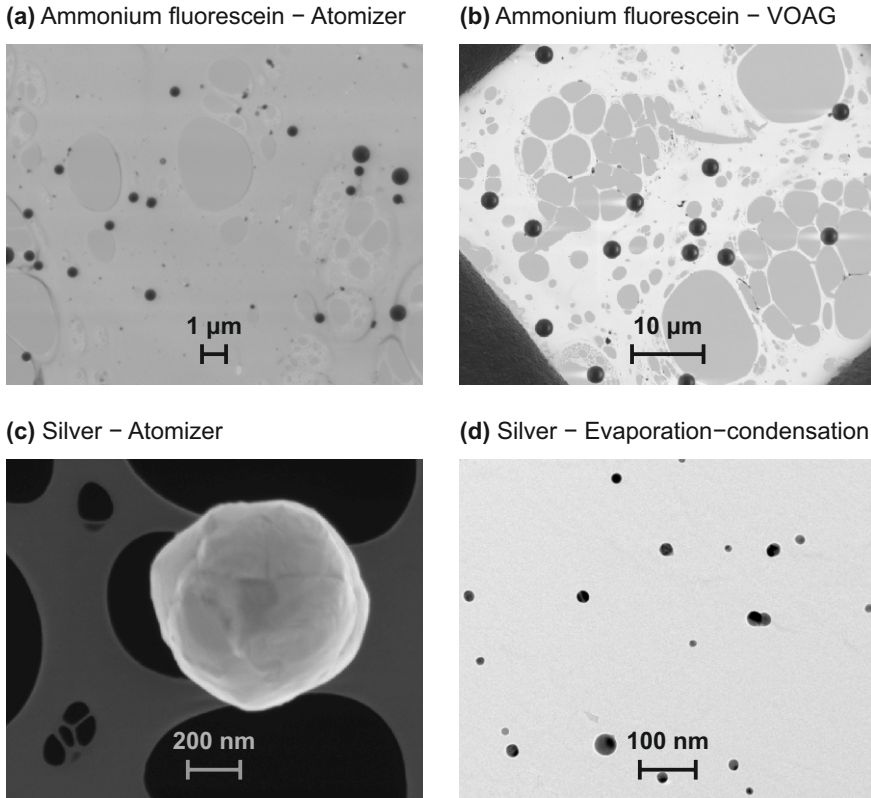


Figure 3.9: Examples of (a–c) scanning electron microscope (SEM) and (d) transmission electron microscope (TEM) micrographs showing the morphology of the generated particles. Ammonium fluorescein particles were generated (a) with an atomizer and (b) with a vibrating orifice aerosol generator (VOAG) in **Paper III**. Silver particles were generated using (c) an atomizer and (d) an evaporation–condensation method in **Paper II**.

Vanderpool and Rubow (1988). In the aqueous solutions, the concentration of ammonium fluorescein varied from 0.08 to 2.2 g/m³. The frequency of the disturbance was 33 or 60 Hz, the liquid feed flow was 10 ml/h and the diameter of the orifice was 20 µm. The relative humidity (RH) of the dispersion and dilution air was adjusted to 30%. After the VOAG, the particles were neutralized with a radioactive source before entering the VNAI. An example of the spherical ammonium fluorescein particles generated with the VOAG is seen in an SEM micrograph in Figure 3.9b.

Aerosolization through resuspension

Relatively large solid particles, such as powders and dusts, can be aerosolized through resuspension. For instance, an instrument called a fungal spore source strength tester (FSSST) can be used to aerosolize fungal spores and other solid particles. The tester was introduced by Sivasubramani et al. (2004) and it has been used in several other studies. In the FSSST, a generation substrate covered with particles is placed below a multiple-nozzle plate. When an air stream is driven through the nozzles, the particles are blown off and aerosolized. A schematic of the instrument is illustrated in Figure 3.8d. In **Paper IV** of

this thesis, the FSSST was used to generate fungal spores and reference materials with a total flow of 25 lpm. Spores of three different fungal species used in the experiments were *Aspergillus versicolor* (*A.v.*), *Cladosporium cladosporioides* (*C.c.*), and *Penicillium brevicompactum* (*P.b.*). A detailed description of the fungal spore sample preparation can be found in a previous study (Saari et al., 2015). Briefly, fungal spore suspensions were inoculated on agar plates and incubated in a conditioned chamber for a growth period of one month. The chamber was exposed to daylight and darkness throughout the growth period. Before the aerosolization, the samples were dried in a laminar flow hood overnight to improve the release of spores. In addition to the fungal spores, silicon carbide (SiC) standard test dust and commercial silver powder were used as reference materials. Figure 3.10 shows the number size distributions of the different species of fungal spores and the reference materials generated with the FSSST and measured with an OPS. The optical size of the silver particles was smaller than for other materials, but aerodynamically they were comparable because of the relatively high density of silver.

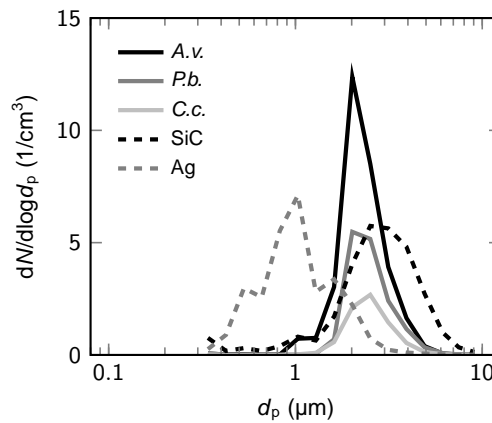


Figure 3.10: The number size distributions of different particles generated with a fungal spore source strength tester (FSSST). *A.v.*, *P.b.*, and *C.c.* are abbreviations for fungal species *Aspergillus versicolor*, *Penicillium brevicompactum*, and *Cladosporium cladosporioides*, respectively. Silver (Ag) and silicon carbide (SiC) were used as reference materials. (Adapted from **Paper IV**.)

The samples aerosolized with the FSSST were brief bursts that were introduced to resuspension tests and a rebound impactor which was a single stage of an ELPI (stage number 8, cut-off $0.92 \mu\text{m}$). Five different substrate materials, used in the impactor, were steel, glass, polystyrene, paper, and polytetrafluoroethylene (PTFE). The particle concentration was measured upstream of the impactor with an OPS, and electrometers were connected to the impactor stage and a filter stage placed downstream of the impactor. All the measurements were averaged over the sample length which was usually about two minutes. The preliminary and transferred charges were calculated from the current signals and particle concentration. Particles were either led after the FSSST directly to the impactor or charged with a corona charger before the impactor, in order to cover a wide range of pre-existing charges.

The FSSST was also directly used to study the resuspension from different surfaces. The fungal spores were generated either from the agar growth plates or from substrates with different materials, including steel, glass, polystyrene, paper, and PTFE. The fungal spores were moved from the growth plates onto the different substrates by using small

glass beads. The reference materials, silicon carbide and silver, were also generated using the FSSST and different substrate materials. In order to test the effect of different deposition mechanisms on the triboelectric charging during resuspension, the resuspension experiments were repeated with an impactor. A single ELPI impactor stage (stage number 9, cut-off $1.6 \mu\text{m}$) was used for the deposition on the substrates of different materials with an aerosol flow of 10 lpm. Upstream of the impactor, a radioactive source was used to neutralize the particles and collected sample. This deposition process was assumed to be more sophisticated than the FSSST method for studying the triboelectric charging during rebound and the effect of different material pairs. In the last step of the experiment, a flow of 25 lpm was led through the impactor causing the resuspension of particles. The particles were detected downstream of the impactor by using both electrical (FCE) and optical detection (OPS) in order to determine the charging state of the particles.

4 Results and discussion

An overview of the results presented in the publications of this thesis is given here. The new methods, including the use of an ELPI combined to the response model in **Paper I** and the VNAI in **Paper II**, can also be considered as significant results in these publications. However, since the methods have been thoroughly introduced in the previous chapter, the discussion in this chapter is focused on the fundamental phenomena. At first, the results obtained for the critical velocity of rebound are analyzed with respect to the obliquity of the impact, materials, and previous studies. Also the role of different methods is discussed. Secondly, the results considering the triboelectric charging of particles during resuspension and rebound are reviewed.

4.1 Critical velocity of rebound

The effect of the obliquity of impact on the critical velocity was studied in **Paper III**. In order to characterize the obliquity, the maximum tangential ($v_{t,\max}$) and normal ($v_{n,\max}$) velocities corresponding to the onset of rebound and the critical slit length in the VNAI were determined from the simulation. The maximum normal velocity was used as an estimate for the critical velocity of rebound, and the ratio of the maximum tangential and normal velocities was used to describe the obliquity of the impact. According to previous studies, the presence of the tangential velocity component may lower the critical normal velocity required for the rebound (Brach et al., 2000; Wang and John, 1988). Because of the variety of the velocity components for different particles impacting at different locations of the impaction substrate, the rebound can start at a certain location from the particles having a lower normal velocity and higher tangential velocity compared to the particles impacting with the maximum normal velocity. The exact velocity components involved in the onset of rebound cannot be distinguished. The maximum normal velocity forms an upper limit for the critical velocity of rebound and the lower limit is the normal velocity component for the particles impacting with the maximum tangential velocity. For the experiments of **Paper III**, the lower limit was calculated to be close to the upper limit and approximately 40% of the upper limit even in the worst case.

Figure 4.1a shows the critical velocity of rebound as a function of the particle size determined for ammonium fluorescein particles in **Paper III**. The significant deviation, seen in the critical velocities, was initially connected to the change of impactor parameters and impaction conditions. In the further analysis, the results were divided into three different groups emphasized by the theoretical fits based on Equation (2.4). Quantitatively, these groups were defined according to the ratio of the maximum tangential and normal velocities corresponding to the obliquity of the impact. In Figure 4.1b, the critical velocity normalized with an arbitrary theoretical critical velocity (v_{theor}) is presented as a function of the velocity ratio. It can be seen that this size-independent quantity for the critical

velocity strongly decreased with the increasing obliquity and three different groups were distinguished. The first group was formed for close-to-normal impacts with the velocity ratio below 1.5 and the second group for higher obliquity with the velocity ratios between 2 and 4. In the third group, the impacts were extremely oblique with the velocity ratio above 9. As shown in Figure 4.1a, the obliquity seemed to affect significantly the critical velocity of rebound. Based on the comparison of the theoretical fits, the critical velocity values for velocity ratios of 2–4 differed from the values for the close-to-normal impacts (ratio < 1.5) by a factor of 4. The critical velocities for the most oblique impacts with the velocity ratio above 9 were more than a magnitude lower than the critical velocities for the close-to-normal impacts. These results are in line with the observations of previous studies (Brach et al., 2000; Chen et al., 2015; Wang and John, 1988), and they provide a means to estimate quantitatively the effect of the obliquity on the critical velocity of rebound in impactors.

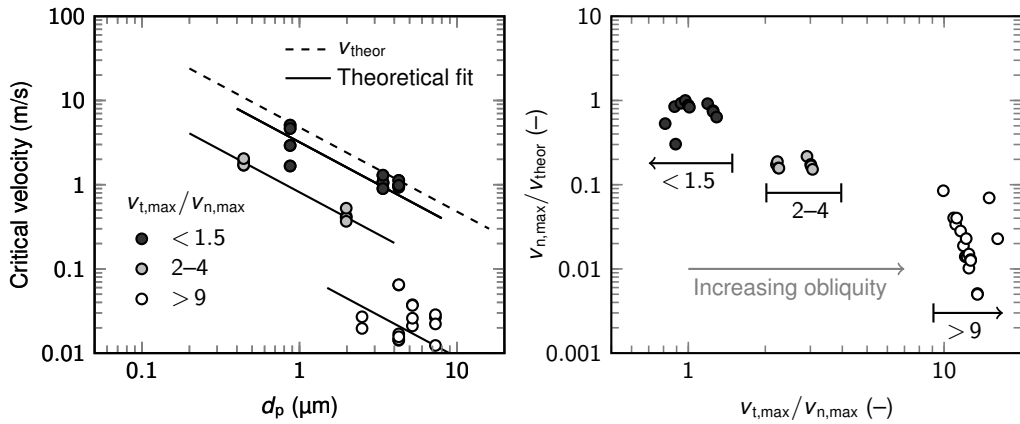


Figure 4.1: (a) The critical velocity of rebound as a function of the particle size for ammonium fluorescein particles with respect to the obliquity of the impact. (b) The critical velocity normalized with an arbitrary theoretical critical velocity (v_{theor}) as a function of the ratio of the maximum tangential ($v_{t,\text{max}}$) and normal ($v_{n,\text{max}}$) velocities. The ratio of the maximum tangential and normal velocities corresponds to the obliquity of the impact. Three different groups of data can be seen. (Adapted from **Paper III**.)

The critical velocities determined during the research of this thesis are presented as a function of the particle size in Figure 4.2. Also the results from previous studies, introduced in Figure 2.3, are shown. The results for sodium chloride (NaCl) and levoglucosan particles on a steel substrate were reproduced from the material coefficient values reported in **Paper I**. These critical velocities were calculated using Equation (2.5), the material coefficient values, and the geometric mean diameter of the polydisperse size distributions. In **Paper II**, the critical velocity of rebound was determined in a wide sub-micron size range for silver (Ag) particles on an aluminum substrate. The results for ammonium fluorescein (AF) particles with different surface materials, including the critical velocities of the close-to-normal impacts from **Paper III**, were used for a further analysis. **Paper IV** provided the critical velocities for fungal spores (*Aspergillus versicolor*) and silicon carbide (SiC) on an aluminum substrate. The main results for silver and ammonium fluorescein were checked to be comparable with respect to the obliquity of the impact.

As seen in Figure 4.2, the results of this thesis significantly contributed to the present knowledge of the critical velocity of rebound. The results for silver particles filled the gap

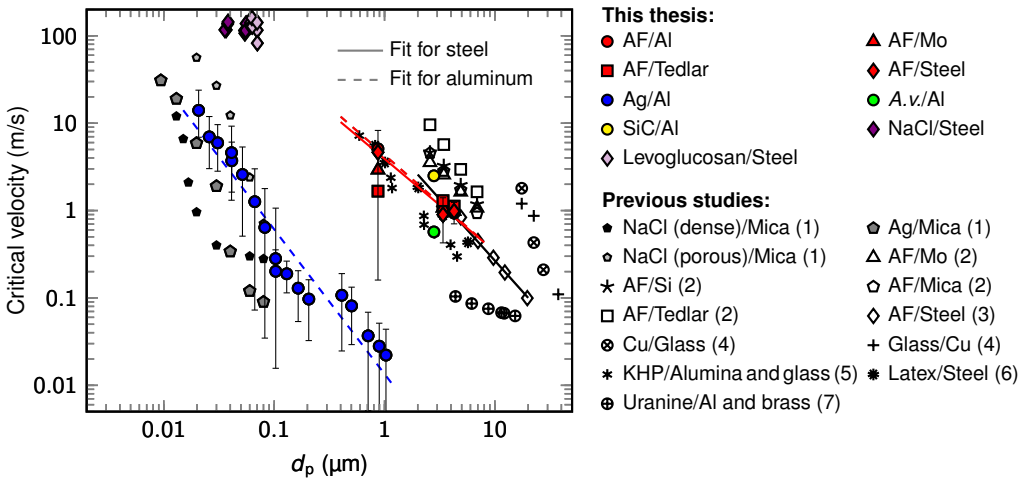


Figure 4.2: The critical velocity of rebound as a function of the particle size. All the results of this thesis are presented with respect to the previous studies of (1) Rennecke and Weber (2013a), (2) Wall et al. (1990), (3) Wang and John (1988), (4) Rogers and Reed (1984), (5) D’Ottavio and Goren (1982), (6) Cheng and Yeh (1979), and (7) Esmen et al. (1978). The legend shows the material of the particle/surface. The values for sodium chloride (NaCl) and levoglucosan particles were reproduced from the results of **Paper I**. The critical velocity for silver particles was determined in **Paper II**, for ammonium fluorescein (AF) in **Paper III**, and for *Aspergillus versicolor* (*A.v.*) fungal spores and silicon carbide (SiC) in **Paper IV**. The dashed and solid lines are fits for aluminum and steel substrates, respectively, and the error bars represent the uncertainty of the method for two material pairs (Ag/Al and AF/Steel).

between micron-sized particles and nanoparticles in a previously unexplored sub-micron size range. Furthermore, because of the wide size range and large number of data points, reliable information on the particle size dependency was obtained. The critical velocity of rebound was found to be dependent on the power of -1.6 of the particle size with a coefficient of determination (R^2) of 0.924 obtained for the fit. The exponent value was in line with the previous studies for micron-sized particles but differed from the theoretical value which is -1 . Within the accuracy of the method, the same size dependency covered the whole size range observed for silver particles and no clear change of the slope was seen. According to the theoretical knowledge, this would indicate a size dependency in the Hamaker constant or in the coefficient of restitution defined by Equation (2.6). The size dependency for ammonium fluorescein particles was found to be closer to the theoretical dependency but the observation was not as reliable because of a small amount of data as a function of the particle size. With the method used for sodium chloride and levoglucosan particles, the size dependency could not be analyzed. The error bars in Figure 4.2 represent the uncertainty of the critical velocity values determined with the VNAI for silver particles and for ammonium fluorescein on a steel substrate, and they were determined by simulating the impact velocities with an accuracy of ± 1 mm in the critical slit length. Unfortunately, there seemed to be a high variation in the accuracy of the critical velocity values arising from the variation of the impactor parameters and impaction conditions. However, in most of the previous studies, the accuracy of the results have not been estimated at all.

According to our results, the particle material can significantly affect the value of the

critical velocity. The fits in Figure 4.2 for aluminum and steel as a surface material ease the comparison between different particle materials. The difference between the results for silver particles with an aluminum substrate and the results for ammonium fluorescein with the same substrate was substantial. At the particle size of one micron, the difference in the critical velocity was approximately two orders of magnitude. On the other hand, our results for ammonium fluorescein on a steel substrate agreed well with the results of Wang and John (1988) for the same materials, but there was a difference between our results and the results of Wall et al. (1990) for ammonium fluorescein on molybdenum, and Tedlar substrates. This difference was most likely due to the different methods used in these studies. The critical velocities for ammonium fluorescein were determined in this thesis by using a combination of impactor measurements and numerical simulations, whereas the results of Wall et al. (1990) were based on the direct measurement of the coefficient of restitution. Even though the impacts were found to be close-to-normal in the impactor, the direct measurement enables more accurately controlled normal impacts. This issue was already raised by Wang and John (1988). The critical velocities for sodium chloride and levoglucosan were found to be much higher than the critical velocities for silver in the same size range. In these results, the morphology of the particles, connected to the different generation methods, may play an important role. Rennecke and Weber (2013a) already showed that the critical velocity of porous and dense sodium chloride particles differed significantly from each other. In our measurements, the sodium chloride and levoglucosan particles were not spherical and the inner structure was not analyzed. In addition, the uncertainty related to the used method for polydisperse particles was significant. Because the particles bounce on several stages in the cascade impactor, this method can possibly emphasize the accurately normal impacts at the lower impactor stages more than the method based on single stage impactor measurements, which may also result in higher critical velocities. The fungal spores were found to rebound from an aluminum substrate more easily than silicon carbide or ammonium fluorescein. This can be relevant from the perspective of indoor aerosols and ventilation systems.

The role of the surface material could also be estimated based on the results shown in Figure 4.2. Within the accuracy of the method, different surface materials, including steel, aluminum, molybdenum, and Tedlar, seemed to have only a minor effect on the critical velocity of rebound for ammonium fluorescein particles. This observation was consistent with the results of Wall et al. (1990), although the direct measurement of the coefficient of restitution enabled to distinguish relatively small differences between Tedlar and other materials. The comparison of the results for silver particles on an aluminum substrate determined in this thesis and the results for silver particles on a mica substrate determined by Rennecke and Weber (2013a) also showed a similar tendency. With small particle sizes, the critical velocities were almost the same and the difference slightly increased with the increasing particle size. All in all, the effect of the surface material on the critical velocity was found to be small compared to the effect of the particle material. This indicates that the mechanical properties of particles affect the critical velocity much more than the adhesion between the particle and surface materials. All of the studied surface materials were hard materials, and the situation would be different with soft materials or materials covered with grease or liquid layer, leading to dissipative processes and energy losses in the surface.

4.2 Triboelectric charging

The transferred charge during rebound was measured in **Paper IV** as a function of the pre-existing charge. Spores of three different fungal species (*Aspergillus versicolor*, *Penicillium brevicompactum*, *Cladosporium cladosporioides*), two reference particle materials (silver, silicon carbide) and five different surface materials (steel, glass, polystyrene, paper, PTFE) formed the matrix of different particle–surface combinations. For each combination, the transferred charge was measured several times with different pre-existing charges. Linear functions, corresponding Equation (2.7), were fitted to the measurements, and the charge transfer parameters, q_c and β , were obtained. The β -parameter was the slope of the fit and the contact charge represented the transferred charge for a previously neutral particle. The correspondence between the theoretical fits and experimental data was good, except in a few cases for steel and glass substrates. This was confirmed statistically by the 95 % confidence limits obtained for the fitting parameters. The β -values were mainly between 0.2 and 0.7. Based on our results, β seemed to depend on the surface material. The highest values were obtained for PTFE (average with a standard deviation 0.63 ± 0.08) and glass (0.51 ± 0.18), and the lowest values for paper (0.28 ± 0.15) and steel (0.29 ± 0.24). The contact charge (q_c) values varied from -830 to $+710$ elementary charges which are in the same order of magnitude than the values previously published by John et al. (1980) for different material pairs. For the fungal spores, the contact charge values with a steel substrate were negative and close to each other, but a substantial variation was found with a glass substrate, including both positive and negative values.

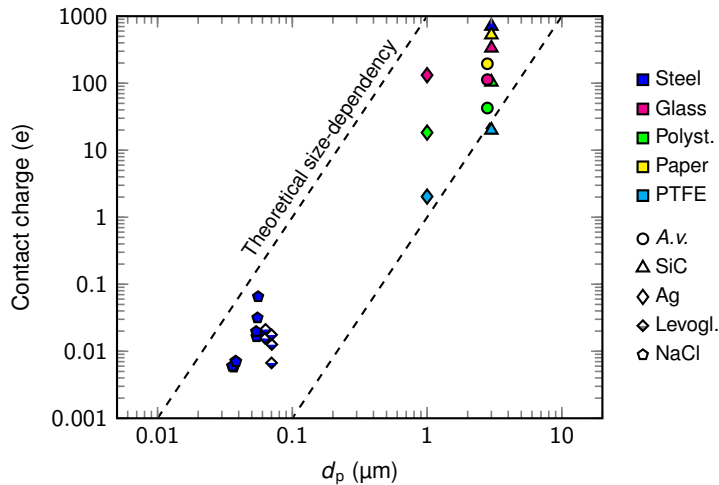


Figure 4.3: The contact charge as a function of the particle size. The color and marker shape represent the surface and particle material, respectively. The contact charge values for sodium chloride (NaCl) and levoglucosan were reproduced from the results of **Paper I**. The values for silicon carbide (SiC), silver (Ag), and *Aspergillus versicolor* (*A.v.*) fungal spores were adapted from **Paper IV**.

The contact charge values were also determined for sodium chloride and levoglucosan nanoparticles on a steel substrate in **Paper I**. The output parameters from the response model, i.e. the contact charges corresponding the particle size of 100 nm and the impact velocity of 100 m/s, were positive and on average $0.49(\pm 0.15)$ and $0.22(\pm 0.14)$ elementary charges per particle for sodium chloride and levoglucosan, respectively. These values were

converted to the contact charges corresponding to the geometric mean diameter of the polydisperse size distributions and the impact velocity of 25 m/s by using the theoretical dependency of the contact charge on the cube of the particle diameter and on the impact velocity. The impact velocities in **Paper IV** were calculated to be approximately 25 m/s. Consequently, Figure 4.3 shows the positive contact charge values obtained from **Paper I** and **IV** as a function of the particle size. Despite the variety of different particle and surface materials, the data seemed to obey approximately the theoretical size dependency. The highest contact charge values were measured for steel as a surface material and the lowest values for PTFE. Interestingly, also negative contact charge values were measured for steel with some particle materials, such as fungal spores. Table 4.1 shows a quantified triboelectric series for glass, polystyrene and PTFE based on the contact charging with *A.v.* fungal spores, silver and silicon carbide. All of these three series, based on three different surface materials, behaved consistently with each other and were also comparable with a reference adapted from a contact charge measurement between macroscopic objects (Diaz and Felix-Navarro, 2004).

Table 4.1: Quantified triboelectric series for three different surface materials based on the contact charging with *Aspergillus versicolor* (*A.v.*) fungal spores, silver (Ag), and silicon carbide (SiC) particles. A reference (q_{ref}) from the study of Diaz and Felix-Navarro (2004) is based on the contact charging with a macroscopic object made of gold. PTFE refers to polytetrafluoroethylene. (Adapted from **Paper IV**.)

	Gold*	<i>A.v.</i>	Ag	SiC
	q_{ref} (nC)	q_c (e)	q_c (e)	q_c (e)
Glass	1.3	113	132	335
Polystyrene	0	43	18	104
PTFE	-2.8	-37	2	20

* Diaz and Felix-Navarro (2004)

Two different experiments were conducted in **Paper IV** to study the contact charging during resuspension, and the net charges were measured with the same materials used in the rebound experiment. A comparison between the results from these two experiments showed no correlation. The net charge from the FSSST varied from -747 to $+48$ elementary charges, and it was found to be negative or close to zero for all the material pairs. Also the fungal spores generated directly from an agar substrate obtained a negative net charge. On the contrary, the net charge from the impactor resuspension ranged from -210 to $+310$ elementary charges and both polarities were represented. The impactor resuspension with a more sophisticated particle deposition process seemed to better describe the contact charging during resuspension from different surfaces. Most likely, the charging state of particles measured directly from the FSSST poorly represented the charging state from fundamental resuspension, but it was a product of the sample preparation process, multilayer deposits, and collisions after the re-entrainment. Nevertheless, the results reported in this thesis are important for the characterization of the FSSST as a generation method widely used for fungal spores.

Figure 4.4a shows the contact charge obtained from the rebound experiment as a function of the net charge from the impactor resuspension for different particle and surface materials. In spite of the wide variation, a negative correlation between these two quantities can be seen. This is reasonable because the contact charge was defined as the

transferred charge from a neutral particle to a surface, and the charge from the impactor resuspension was the charge obtained by the particle. The correlation indicated that the triboelectric charging of particles during rebound correlated with the triboelectric charging of particles during resuspension. The similarity of these two phenomena is schematically illustrated in Figure 4.4b. Consequently, by investigating the charging properties of particles in a rebound test, it is also possible to predict their behavior during resuspension. This is especially important in indoor environments where the resuspension of fungal spores and other particles from surfaces of different materials can significantly affect the charge and dynamics of the particles, but the challenges related to the experimental characterization of resuspension restrain the characterization. However, the connection of the charging behavior during resuspension and rebound found in this thesis should be further studied with different materials and different experimental setups relevant for real-world environments.

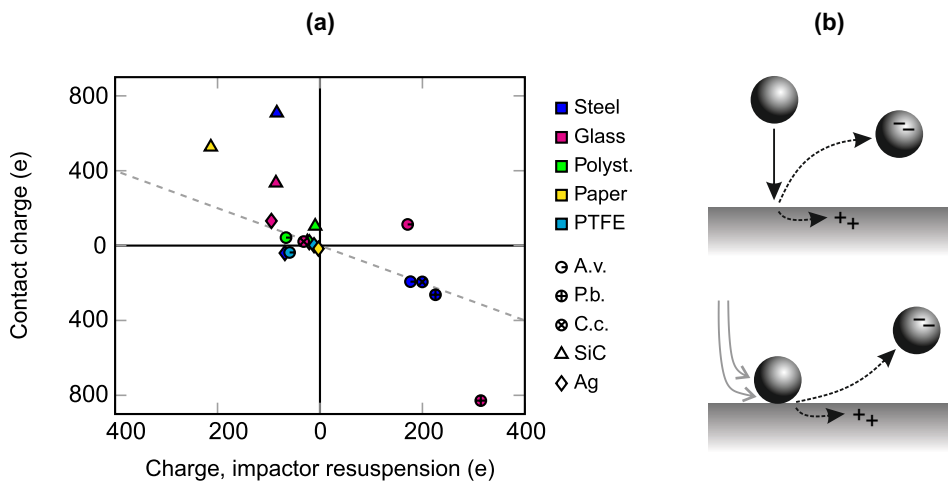


Figure 4.4: (a) The contact charge measured during rebound as a function of the charge from the impactor resuspension experiment. The color and marker shape represent the surface and particle material, respectively. A dashed line represents the negative one-to-one correlation line. *A.v.*, *P.b.*, and *C.c.* are abbreviations for fungal species *Aspergillus versicolor*, *Penicillium brevicompactum*, and *Cladosporium cladosporioides*, respectively. PTFE refers to polytetrafluoroethylene, SiC to silicon carbide, and Ag to silver. (b) A schematic illustrates the similarity of the charge transfer during rebound and resuspension. (Adapted from **Paper IV**.)

5 Conclusions

The interaction between particles and surfaces is a fundamental issue in aerosol physics. The scientific knowledge of this interaction has previously provided a basis for many innovations and improvements in aerosol instrumentation and applications. In addition, the research of surface interaction phenomena has been found to characterize important structural properties of particles, for example, in the field of atmospheric aerosols and engineered nanoparticles. The ever-increasing number of applications and the need of detailed information on the structural properties requires more profound knowledge of the surface interaction phenomena. In this thesis, the rebound of particles from a surface and the electrical charge transfer taking place during rebound and resuspension were studied.

New methods for investigating particle rebound and charge transfer were developed and introduced. The response model connected to the certain measurement procedure with an electrical low pressure impactor (ELPI) provided a simple method for characterizing the rebound and charge transfer of polydisperse nanoparticles. On the other hand, the method can generally be used as a tool to recognize unwanted rebound and charge transfer in cascade impactors. The main instrument, developed during the research of this thesis and used in the experiments, was the variable nozzle area impactor (VNAI). It is a new type of an impactor that can be applied to study different surface interaction phenomena as a function of the particle impact velocity. In this thesis, the VNAI was used to determine the critical velocity of rebound. The advantage of the VNAI is that it covers a wide size range from nanoparticles to micron-sized particles and the impaction conditions are well controlled. As a slit type impactor, it provides uniform impact velocities, and different phenomena, such as the obliquity of impacts, can also be studied by modifying the impactor width and the volumetric flow through the impactor. In addition to the development of the rebound experiments, the thesis also included characterization of the resuspension test systems, such as the fungal spore source strength tester (FSSST) and a single stage impactor, with respect to the triboelectric charging.

The critical velocity of rebound was determined for different particle and surface materials in a wide particle size range. The size range also included a previously unexplored region, and the results of this thesis filled the gap between the previous results for nanoparticles and micron-sized particles. Within the accuracy of our method and explored materials, the particle material was found to have a substantial effect on the value of the critical velocity but the effect of the surface material was insignificant. The critical velocity for ammonium fluorescein particles was approximately two orders of magnitude higher than the critical velocity for silver particles at the particle size of one micron. The tested hard surface materials, including steel, aluminum, molybdenum, and Tedlar, differed only slightly from each other. However, the relatively great amount of different materials enabled a comprehensive comparison to previous studies. It was found that the methods based on impactor measurements agreed with each other but the methods based on the

direct measurement of the particle velocity provided slightly higher critical velocities. This observation was in line with the fact that the increasing obliquity of the impact was shown to substantially decrease the critical velocity of rebound. Consequently, the obliquity of the impact should be taken into account in designing instruments and applications possibly dealing with particle rebound.

The parameters of triboelectric charge transfer were measured for nanoparticles, fungal spores and micron-sized test dusts. In the nanoparticle size range, the contact charge values of sodium chloride and levoglucosan were determined in an ELPI for bouncing particles. For fungal spores and test dusts, the triboelectric charging during rebound was found to correlate with the triboelectric charging during resuspension. This is an important result connecting these two mechanically very different phenomena from the point of view of charge transfer. The observation increases the understanding of triboelectric charge transfer and provides new possibilities for the experimental characterization of the phenomena, as well as for different applications. However, a need for further experiments still exists to truly understand the fundamental connection and show the relevance of this observation in real-world environments.

Spores of different fungal species were found to charge both positively and negatively during resuspension and rebound with different surface materials. The surface interaction of fungal spores is of great interest in indoor environments, because of their adverse health effects and the dynamics typical for micron-sized aerosol particles. The deposition of fungal spores is relatively fast and they may also be resuspended easily. In ventilation and filtration systems, they may impact on fibers and walls. In addition to the charge transfer properties, also the critical velocity of rebound was determined for fungal spores in this thesis and found to be relatively low compared to other particle materials. All in all, the results of this thesis provide a means to predict the charging and dynamics of fungal spores in indoor environments, as well as to enhance the development of monitoring and sampling methods for bioaerosols.

Bibliography

- Arffman, A., Marjamäki, M., and Keskinen, J., “Simulation of low pressure impactor collection efficiency curves,” *Journal of Aerosol Science*, vol. 42, no. 5, pp. 329–340, 2011.
- Arffman, A., Yli-Ojanperä, J., and Keskinen, J., “The influence of nozzle throat length on the resolution of a low pressure impactor – An experimental and numerical study,” *Journal of Aerosol Science*, vol. 53, pp. 76–84, 2012.
- Arffman, A., Yli-Ojanperä, J., Kalliokoski, J., Harra, J., Pirjola, L., Karjalainen, P., Rönkkö, T., and Keskinen, J., “High-resolution low-pressure cascade impactor,” *Journal of Aerosol Science*, vol. 78, pp. 97–109, 2014.
- Bateman, A., Belassein, H., and Martin, S., “Impactor apparatus for the study of particle rebound: Relative humidity and capillary forces,” *Aerosol Science and Technology*, vol. 48, no. 1, pp. 42–52, 2014.
- Berglund, R. and Liu, B., “Generation of monodisperse aerosol standards,” *Environmental Science and Technology*, vol. 7, no. 2, pp. 147–153, 1973.
- Bergström, L., “Hamaker constants of inorganic materials,” *Advances in Colloid and Interface Science*, vol. 70, no. 1–3, pp. 125–169, 1997.
- Boor, B., Siegel, J., and Novoselac, A., “Monolayer and multilayer particle deposits on hard surfaces: Literature review and implications for particle resuspension in the indoor environment,” *Aerosol Science and Technology*, vol. 47, no. 8, pp. 831–847, 2013.
- Brach, R., Dunn, P., and Li, X., “Experiments and engineering models of microparticle impact and deposition,” *Journal of Adhesion*, vol. 74, no. 1–4, pp. 227–282, 2000.
- Castle, G., “Contact charging between insulators,” *Journal of Electrostatics*, vol. 40–41, pp. 13–20, 1997.
- Chang, M., Seongheon, K., and Sioutas, C., “Experimental studies on particle impaction and bounce: Effects of substrate design and material,” *Atmospheric Environment*, vol. 33, no. 15, pp. 2313–2322, 1999.
- Chen, S., Li, S., and Yang, M., “Sticking/rebound criterion for collisions of small adhesive particles: Effects of impact parameter and particle size,” *Powder Technology*, vol. 274, pp. 431–440, 2015.
- Cheng, Y. S. and Yeh, H. C., “Particle bounce in cascade impactors,” *Environmental Science and Technology*, vol. 13, no. 11, pp. 1392–1396, 1979.

- Dahneke, B., "The capture of aerosol particles by surfaces," *Journal of Colloid and Interface Science*, vol. 37, no. 2, pp. 342–353, 1971.
- — —, "Further measurements of the bouncing of small latex spheres," *Journal of Colloid and Interface Science*, vol. 51, no. 1, pp. 58–65, 1975.
- Diaz, A. and Felix-Navarro, R., "A semi-quantitative tribo-electric series for polymeric materials: The influence of chemical structure and properties," *Journal of Electrostatics*, vol. 62, no. 4, pp. 277–290, 2004.
- D'Ottavio, T. and Goren, S. L., "Aerosol capture in granular beds in the impaction dominated regime," *Aerosol Science and Technology*, vol. 2, no. 2, pp. 91–108, 1982.
- Douwes, J., Thorne, P., Pearce, N., and Heederik, D., "Bioaerosol health effects and exposure assessment: Progress and prospects," *Annals of Occupational Hygiene*, vol. 47, no. 3, pp. 187–200, 2003.
- Dzubay, T. G., Hines, L. E., and Stevens, R. K., "Particle bounce errors in cascade impactors," *Atmospheric Environment*, vol. 10, no. 3, pp. 229–234, 1976.
- Dzubay, T. and Barbour, R., "A method to improve the adhesion of aerosol particles on teflon filters," *Journal of the Air Pollution Control Association*, vol. 33, no. 7, pp. 692–695, 1983.
- Ebnesajjad, S., *Surface Treatment of Materials for Adhesion Bonding*. William Andrew Publishing, 2006.
- Esmen, N. A., Ziegler, P., and Whitfield, R., "The adhesion of particles upon impaction," *Journal of Aerosol Science*, vol. 9, no. 6, pp. 547–556, 1978.
- Froeschke, S., Kohler, S., Weber, A. P., and Kasper, G., "Impact fragmentation of nanoparticle agglomerates," *Journal of Aerosol Science*, vol. 34, no. 3, pp. 275–287, 2003.
- Gomes, C., Freihaut, J., and Bahnfleth, W., "Resuspension of allergen-containing particles under mechanical and aerodynamic disturbances from human walking," *Atmospheric Environment*, vol. 41, no. 25, pp. 5257–5270, 2007.
- Hamaker, H. C., "The London–van der Waals attraction between spherical particles," *Physica*, vol. 4, pp. 1058–1072, 1937.
- Harra, J., Mäkitalo, J., Siikanen, R., Virkki, M., Genty, G., Kobayashi, T., Kauranen, M., and Mäkelä, J. M., "Size-controlled aerosol synthesis of silver nanoparticles for plasmonic materials," *Journal of Nanoparticle Research*, vol. 14, no. 6, p. 870, 2012.
- Heim, M., Mullins, B., Wild, M., Meyer, J., and Kasper, G., "Filtration efficiency of aerosol particles below 20 nanometers," *Aerosol Science and Technology*, vol. 39, no. 8, pp. 782–789, 2005.
- Hinds, W. C., *Aerosol Technology: Properties, Behavior, and Measurement of Airborne Particles*, 2nd ed. John Wiley & Sons, 1999.
- Hubbard, J., Salazar, K., Crown, K., and Servantes, B., "High-volume aerosol filtration and mitigation of inertial particle rebound," *Aerosol Science and Technology*, vol. 48, no. 5, pp. 530–540, 2014.

- Ihalainen, M., Lind, T., Arffman, A., Torvela, T., and Jokiniemi, J., “Break-up and bounce of TiO₂ agglomerates by impaction,” *Aerosol Science and Technology*, vol. 48, no. 1, pp. 31–41, 2014.
- Ireland, P., “Contact charge accumulation and separation discharge,” *Journal of Electrostatics*, vol. 67, no. 2–3, pp. 462–467, 2009.
- Järvinen, A., Aitomaa, M., Rostedt, A., Keskinen, J., and Yli-Ojanperä, J., “Calibration of the new electrical low pressure impactor (ELPI+),” *Journal of Aerosol Science*, vol. 69, pp. 150–159, 2014.
- John, W., Reischl, G., and Devor, W., “Charge transfer to metal surfaces from bouncing aerosol particles,” *Journal of Aerosol Science*, vol. 11, no. 2, pp. 115–138, 1980.
- Juuti, P., Arffman, A., Rostedt, A., Harra, J., Mäkelä, J., and Keskinen, J., “Real-time effective density monitor (DENSMO) for aerosol nanoparticle production,” *Aerosol Science and Technology*, vol. 50, no. 5, pp. 487–496, 2016.
- Kang, M., Cho, H.-J., Kwak, H., and Park, K., “Evaluation of particle bounce in various collection substrates to be used as vaporizer in aerosol mass spectrometer,” *Aerosol Science and Technology*, vol. 49, no. 5, pp. 332–339, 2015.
- Keskinen, J., Pietarinen, K., and Lehtimäki, M., “Electrical low pressure impactor,” *Journal of Aerosol Science*, vol. 23, no. 4, pp. 353–360, 1992.
- Kleman, M. and Lavrentovich, O., *Soft Matter Physics: An Introduction*. Springer, 2003.
- Lee, S.-A., Willeke, K., Mainelis, G., Adhikari, A., Wang, H., Reponen, T., and Grinshpun, S., “Assessment of electrical charge on airborne microorganisms by a new bioaerosol sampling method,” *Journal of Occupational and Environmental Hygiene*, vol. 1, no. 3, pp. 127–138, 2004.
- Lowell, J. and Rose-Innes, A., “Contact electrification,” *Advances in Physics*, vol. 29, no. 6, pp. 947–1023, 1980.
- Mainelis, G., Willeke, K., Baron, P., Reponen, T., Grinshpun, S., Górný, R., and Trakumas, S., “Electrical charges on airborne microorganisms,” *Journal of Aerosol Science*, vol. 32, no. 9, pp. 1087–1110, 2001.
- Marjamäki, M. and Keskinen, J., “Effect of impaction plate roughness and porosity on collection efficiency,” *Journal of Aerosol Science*, vol. 35, no. 3, pp. 301–308, 3 2004.
- Marjamäki, M., Keskinen, J., Chen, D.-R., and Pui, D. Y. H., “Performance evaluation of the electrical low-pressure impactor (ELPI),” *Journal of Aerosol Science*, vol. 31, no. 2, pp. 249–261, 2000.
- Marjamäki, M., Ntziachristos, L., Virtanen, A., Ristimäki, J., Keskinen, J., Moisio, M., Palonen, M., and Lappi, M., “Electrical filter stage for the ELPI,” in *Society of Automotive Engineers (SAE) Technical paper series 2002-01-0055*, 2002.
- Matusaka, S., Maruyama, H., Matsuyama, T., and Ghadiri, M., “Triboelectric charging of powders: A review,” *Chemical Engineering Science*, vol. 65, no. 22, pp. 5781–5807, 2010.

- Mendell, M., Mirer, A., Cheung, K., Tong, M., and Douwes, J., “Respiratory and allergic health effects of dampness, mold, and dampness-related agents: A review of the epidemiologic evidence,” *Environmental Health Perspectives*, vol. 119, no. 6, pp. 748–756, 2011.
- Miaskiewicz-Peska, E. and Lebkowska, M., “Comparison of aerosol and bioaerosol collection on air filters,” *Aerobiologia*, vol. 28, no. 2, pp. 185–193, 2012.
- Mittal, K. L., “Adhesion measurement of thin films,” *Electrocomponent Science and Technology*, vol. 3, pp. 21–42, 1975.
- Nicholson, K. W., “Wind tunnel experiments on the resuspension of particulate material,” *Atmospheric Environment*, vol. 27, no. 2, pp. 181–188, 1993.
- Pajunoja, A., Lambe, A., Hakala, J., Rastak, N., Cummings, M., Brogan, J., Hao, L., Paramonov, M., Hong, J., Prisle, N., Malila, J., Romakkaniemi, S., Lehtinen, K., Laaksonen, A., Kulmala, M., Massoli, P., Onasch, T., Donahue, N., Riipinen, I., Davidovits, P., Worsnop, D., Petäjä, T., and Virtanen, A., “Adsorptive uptake of water by semisolid secondary organic aerosols,” *Geophysical Research Letters*, vol. 42, no. 8, pp. 3063–3068, 2015.
- Park, C., Park, J., Jeon, H., and Chun, B., “Triboelectric series and charging properties of plastics using the designed vertical-reciprocation charger,” *Journal of Electrostatics*, vol. 66, no. 11–12, pp. 578–583, 2008.
- Reeks, M. and Hall, D., “Kinetic models for particle resuspension in turbulent flows: Theory and measurement,” *Journal of Aerosol Science*, vol. 32, no. 1, pp. 1–31, 2001.
- Rennecke, S. and Weber, A. P., “The critical velocity for nanoparticle rebound measured in a low pressure impactor,” *Journal of Aerosol Science*, vol. 58, pp. 135–147, 2013.
- — —, “A novel model for the determination of nanoparticle impact velocity in low pressure impactors,” *Journal of Aerosol Science*, vol. 55, pp. 89–103, 2013.
- — —, “Charge transfer to metal nanoparticles bouncing from conductive surfaces,” *Aerosol Science and Technology*, vol. 48, no. 10, pp. 1059–1069, 2014.
- Reponen, T., Lehtonen, M., Raunemaa, T., and Nevalainen, A., “Effect of indoor sources on fungal spore concentrations and size distributions,” *Journal of Aerosol Science*, vol. 23, no. 1, pp. 663–666, 1992.
- Rogers, L. N. and Reed, J., “The adhesion of particles undergoing an elastic-plastic impact with a surface,” *Journal of Physics D: Applied Physics*, vol. 17, no. 4, pp. 677–689, 1984.
- Saari, S., Mensah-Attipoe, J., Reponen, T., Veijalainen, A. M., Salmela, A., Pasanen, P., and Keskinen, J., “Effects of fungal species, cultivation time, growth substrate, and air exposure velocity on the fluorescence properties of airborne fungal spores,” *Indoor Air*, vol. 25, no. 6, pp. 653–661, 2015.
- Saukko, E., Kuuluvainen, H., and Virtanen, A., “A method to resolve the phase state of aerosol particles,” *Atmospheric Measurement Techniques*, vol. 5, no. 1, pp. 259–265, 2012.

- Scheibel, H. G. and Porstendörfer, J., "Generation of monodisperse Ag- and NaCl-aerosols with particle diameters between 2 and 300 nm," *Journal of Aerosol Science*, vol. 14, no. 2, pp. 113–126, 1983.
- Schöner, C., Rennecke, S., Weber, A. P., and Pöschel, T., "Introduction of a new technique to measure the coefficient of restitution for nanoparticles," *Chemie Ingenieur Technik*, vol. 86, no. 3, pp. 365–374, 2014.
- Seipenbusch, M., Toneva, P., Peukert, W., and Weber, A. P., "Impact fragmentation of metal nanoparticle agglomerates," *Particle and Particle Systems Characterization*, vol. 24, no. 3, pp. 193–200, 2007.
- Sivasubramani, S., Niemeier, R., Reponen, T., and Grinshpun, S., "Fungal spore source strength tester: Laboratory evaluation of a new concept," *Science of the Total Environment*, vol. 329, no. 1–3, pp. 75–86, 2004.
- Stepien, M., Saarinen, J. J., Teisala, H., Tuominen, M., Aromaa, M., Kuusipalo, J., Mäkelä, J. M., and Toivakka, M., "Adjustable wettability of paperboard by liquid flame spray nanoparticle deposition," *Applied Surface Science*, vol. 257, no. 6, pp. 1911–1917, 2011.
- Thatcher, T. L. and Layton, D. W., "Deposition, resuspension, and penetration of particles within a residence," *Atmospheric Environment*, vol. 29, no. 13, pp. 1487–1497, 1995.
- Tsai, C.-J., Pui, D. Y., and Liu, B. Y., "Capture and rebound of small particles upon impact with solid surfaces," *Aerosol Science and Technology*, vol. 12, no. 3, pp. 496–507, 1990.
- Vanderpool, R. and Rubow, K., "Generation of large, solid, monodisperse calibration aerosols," *Aerosol Science and Technology*, vol. 9, no. 1, pp. 65–69, 1988.
- Virtanen, A., Kannosto, J., Kuuluvainen, H., Arffman, A., Joutsensaari, J., Saukko, E., Hao, L., Yli-Pirilä, P., Tiitta, P., Holopainen, J. K., Keskinen, J., Worsnop, D. R., Smith, J. N., and Laaksonen, A., "Bounce behavior of freshly nucleated biogenic secondary organic aerosol particles," *Atmospheric Chemistry and Physics*, vol. 11, no. 16, pp. 8759–8766, 2011.
- Virtanen, A., Joutsensaari, J., Koop, T., Kannosto, J., Yli-Pirilä, P., Leskinen, J., Mäkelä, J. M., Holopainen, J. K., Pöschl, U., Kulmala, M., Worsnop, D. R., and Laaksonen, A., "An amorphous solid state of biogenic secondary organic aerosol particles," *Nature*, vol. 467, no. 7317, pp. 824–827, 2010.
- Wall, S., John, W., and Wang, H.-C., "Measurements of kinetic energy loss for particles impacting surfaces," *Aerosol Science and Technology*, vol. 12, no. 4, pp. 926–946, 1990.
- Wang, H.-C. and John, W., "Dynamic contact charge transfer considering plastic deformation," *Journal of Aerosol Science*, vol. 19, no. 4, pp. 399–411, 1988.
- Wang, H.-C. and Kasper, G., "Filtration efficiency of nanometer-size aerosol particles," *Journal of Aerosol Science*, vol. 22, no. 1, pp. 31–41, 1991.
- Watanabe, H., Ghadiri, M., Matsuyama, T., Ding, Y. L., Pitt, K. G., Maruyama, H., Matsusaka, S., and Masuda, H., "Triboelectrification of pharmaceutical powders by particle impact," *International Journal of Pharmaceutics*, vol. 334, no. 1–2, pp. 149–155, 2007.

- Weber, A. P. and Wu, T., “Kontaktauflaug von Nanopartikeln bei Impaktion,” *Chemie Ingenieur Technik*, vol. 81, no. 6, pp. 791–795, 2009.
- Weir, G. and McGavin, P., “The coefficient of restitution for the idealized impact of a spherical, nano-scale particle on a rigid plane,” *Proceedings of the Royal Society A: Mathematical, Physical and Engineering Sciences*, vol. 464, no. 2093, pp. 1295–1307, 2008.
- Yamamoto, H. and Scarlett, B., “Triboelectric charging of polymer particles by impact,” *Particle Characterization*, vol. 3, no. 3, pp. 117–121, 1986.
- Yli-Ojanperä, J., Kannosto, J., Marjamäki, M., and Keskinen, J., “Improving the nanoparticle resolution of the ELPI,” *Aerosol and Air Quality Research*, vol. 10, no. 4, pp. 360–366, 2010.

Publications

Paper I

Heino Kuuluvainen, Anssi Arffman, Erkka Saukko, Annele Virtanen, and Jorma Keskinen

“A new method for characterizing the bounce and charge transfer properties of nanoparticles”

Journal of Aerosol Science, vol. 55, pp. 104-115, 2013

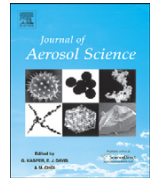
doi: 10.1016/j.jaerosci.2012.08.007

© Elsevier B.V.



Contents lists available at SciVerse ScienceDirect

Journal of Aerosol Science

journal homepage: www.elsevier.com/locate/jaerosci

I



A new method for characterizing the bounce and charge transfer properties of nanoparticles

Heino Kuuluvainen^{a,*}, Anssi Arffman^a, Erkka Saukko^a, Annele Virtanen^b,
Jorma Keskinen^a

^a *Aerosol Physics Laboratory, Department of Physics, Tampere University of Technology, Tampere, Finland*

^b *Department of Applied Physics, University of Eastern Finland, Kuopio, Finland*

ARTICLE INFO

Article history:

Received 14 June 2012

Received in revised form

28 August 2012

Accepted 28 August 2012

Available online 3 September 2012

Keywords:

Bouncing

Charge transfer

Nanoparticle

Impactor

ELPI

ABSTRACT

Bouncing and charge transfer between a particle and a surface are fundamental phenomena in aerosol physics. In this study, a new method is presented for characterizing these phenomena in the nanometer size range. The method is based on electrical detection of particles and on a new manner to exploit an electrical low pressure impactor (ELPI). By measuring particles with and without the charger, bouncing and charge transfer can be distinguished. To connect the measurement with the existing theoretical knowledge, a new model describing the bouncing and charge transfer behavior in a cascade impactor is presented. The model is linked to measurements through a fitting process which provides theoretical parameters for polydisperse nanoparticles. With this method, the bouncing and charge transfer of nanoparticles can be described by the existing theory of micrometer-sized particles. To demonstrate the performance of the method in practice, measurements were carried out to define the parameters for sodium chloride and levoglucosan particles.

© 2012 Elsevier Ltd. All rights reserved.

1. Introduction

Nanoparticles are of interest in many fields of aerosol physics. Present research of aerosol synthesis, atmospheric aerosols, traffic related aerosols and their health effects is focused on ultrafine particles, i.e. particles below 100 nm (Kittelson et al., 2004; Kruis et al., 1998; Kulmala et al., 2004). It is well known that the properties of nanoparticles can differ significantly from those of larger aerosol particles and, in general, all the knowledge should be confirmed before applying it to nanoscale. In that sense, the interaction between a nanoparticle and a surface is rather poorly understood, especially considering the phenomena of particle bouncing and charge transfer.

Motivation to study the bouncing of aerosol particles has often been in means to prevent or reduce it. There are several studies focused on impactors and filters where particle bouncing is an undesirable phenomenon (e.g. Chang et al., 1999; Fujitani et al., 2006; Mullins et al., 2003). Charge transfer is a side effect of bouncing when a particle is in a contact with different surface material. Charge transfer has been studied as a fundamental phenomenon (John, 1995; John et al., 1980) and within some medical inhalator applications, in which the role of contact charging is significant (Matsusaka et al., 2010; Watanabe et al., 2007). Common for both bouncing and charge transfer is that experimental studies are practically restricted to particle sizes over one micrometer. In spite of the experimental challenges and the lack of interest from the perspective of medical inhalators in the nanometer size range, a few studies have recently been published related to

* Corresponding author.

E-mail address: heino.kuuluvainen@tut.fi (H. Kuuluvainen).

the bouncing and charge transfer of nanometer-sized particles. Weber & Wu (2009) defined yield points for particle materials by measuring the charge transfer of spherical metal nanoparticles. Furthermore, recent fragmentation studies of nanoparticle agglomerates are closely related to particle bouncing (Froeschke et al., 2003; Seipenbusch et al., 2007).

Recently, an electrical low pressure impactor (ELPI) was used in a totally new manner to indicate an amorphous solid state of secondary organic aerosol particles (Virtanen et al., 2010). The method was based on particle bouncing in the impactor. The ELPI, originally developed by Keskinen et al. (1992), is a commercially available measuring device, in which particles are charged in a corona charger and led to a cascade impactor. The device is capable of measuring an aerosol size distribution in the size range of 7 nm to 10 μm . In the normal operation of an ELPI, particles are collected on impactor substrates and a current signal is measured at each impactor stage connected to an electrometer. However, if particles are bouncing in the impactor, apparent changes can be observed in the measured current distribution compared to the ideal case of non-bouncing particles.

A concept of bounce factor was defined to quantify the amount of bounce in an ELPI (Virtanen et al., 2010, 2011). The factor is calculated simply from the extra current measured at the lowest impactor stage or filter stage, and it should represent the ratio of the current transferred by bounced particles to the ideal current of non-bouncing particles. However, the problem is that the factor does not take into account possible charge transfer nor the precise characteristics of a low pressure cascade impactor. More recently, Kannosto et al. (accepted) were able to define a lower limit for the bouncing probability of particles by taking into account possible charge transfer in a simplified manner. Although the procedure was based only on the measurements of secondary organic aerosol particles with an ELPI equipped with greased substrates, the bounce probability represented the real fraction of bounced particles at a single impactor stage. However, in this respect, it is more accurate and more applicable to use a single stage impactor and an optical measurement of particle concentration. Saukko et al. (2012) introduced a method of this kind, naming the corresponding bounce probability as bounced fraction. Principally, this method is a very good means to measure particle bounce with similar conditions for all particles, but it practically requires a monodisperse aerosol sample. In this work, the analysis of bouncing and charge transfer rests upon previous theoretical knowledge. The theoretical knowledge of particles over one micrometer is applied in the nanometer size range. The contact charge in charge transfer and the capture limit velocity of bouncing are even more profound concepts than bounce probability in the case of a single stage impactor. Through a new model and a principle of measurement introduced in this work, the measurement of a polydisperse aerosol sample with an ELPI can be connected to these concepts.

Using an ELPI or another instrument based on electrical measurement of particles in bouncing and charge transfer measurements, there is especially one question that should be settled. That is how to distinguish the phenomena of bouncing and charge transfer from each other. In this work, the key to the solution is that particles are measured with two different preliminary states of charge. Simply by calculating the difference of the two measured currents, the fraction of bounced particles can be seen. This simple principle of measurement is the basis of this study but it will also be accompanied with a fundamental theoretical analysis and modeling of the instrument behavior.

For the further analysis, a new model for bouncing particles and charge transfer in an ELPI is presented. The model is based on previous theories of bouncing and charge transfer (Dahneke, 1971; John et al., 1980) and on a recent flow field model of a low pressure impactor (Arffman et al., 2011). The aim of the bouncing and charge transfer model is to calculate the theoretical output of the instrument starting from an aerosol size distribution and parameters describing the bounce and charge transfer properties of particles. Finally, when measurements with an ELPI and with a scanning mobility particle sizer (SMPS) are performed simultaneously, the bounce and charge transfer properties of nanoparticles can be defined by fitting the modeled currents to the measured ELPI currents.

2. Theoretical background

2.1. Bouncing

There are three elements that affect the process when an aerosol particle collides with a surface. Those three elements are adhesion, the initial velocity of the particle and energy loss mechanisms in the collision. Assuming a spherical particle and an infinite smooth surface, the adhesion energy between the particle and the surface can be written as (Dahneke, 1971)

$$E_{\text{adh}} = \frac{Ad_p}{12z_0}, \quad (1)$$

where d_p is the particle diameter, A is Hamaker constant and z_0 is the separation distance usually assumed to be 0.4 nm. Hamaker constant is dependent on both particle and surface materials. It arises from the van der Waals interaction of molecules and can be calculated theoretically using Lifshitz theory (Bergström, 1997).

The relation between the initial velocity of the particle v_i , perpendicular to the surface, and the rebound velocity of the particle v_r is called coefficient of restitution,

$$C_R = \frac{v_r}{v_i}, \quad (2)$$

and it represents the amount of energy losses in the collision. The smaller the value of C_R , the more energy is lost during the impact and rebound. In practice, there are several different energy loss mechanisms in the case of an aerosol particle and a firm surface, but the most important is the plastic deformation of the particle. Particle bouncing was studied in more detail from the aspect of plastic and elastic deformation by Rogers & Reed (1984).

Because of the energy losses and relatively large adhesion energies arising from the area-to-mass ratio, aerosol particles do not usually bounce after a contact to a surface but they tend to adhere. According to Hinds (1999), this is one of the characteristics that distinguishes aerosol particles from gas molecules. However, if the initial velocity of a particle is large enough, its kinetic energy after the contact may suffice to overcome the adhesion energy resulting particle bounce. For the initial velocity, there is a certain capture limit v_i^* , which can be derived from the Eqs. (1) and (2) by setting the rebound kinetic energy equal to the adhesion energy. This was done by Dahneke (1971) and the result is

$$v_i^* = \frac{\alpha}{d_p}, \quad (3)$$

where the material coefficient of bouncing

$$\alpha = \left(\frac{A(1-C_R^2)}{\pi z_0 \rho_p C_R^2} \right)^{1/2}, \quad (4)$$

is dependent on the coefficient of restitution, Hamaker constant and particle density ρ_p . Thus, according to the theory, the capture limit is inversely proportional to particle diameter. Note also the dependency on particle density: $\alpha \propto 1/\sqrt{\rho_p}$. John (1995) collected results from several experimental studies in the micrometer size range showing that the value of the product $v_i^* d_p$ spanned approximately an order of magnitude for different particle and surface materials, corresponding α values between 10^{-6} and 10^{-5} m²/s. Cheng & Yeh (1979) introduced a semi-empirical relationship for the capture limit in an impactor,

$$v_i^* d_p \sqrt{\frac{\rho_p}{\rho_0}} = B \times 10^{-6} \text{ m}^2/\text{s}, \quad (5)$$

where ρ_0 is the unit density and B ranges from 2.5 to 9.2 depending on the particle and surface materials and the type of the impactor. In this representation, material coefficient $\alpha = (B \times 10^{-6} \text{ m}^2/\text{s})/\sqrt{\rho_p/\rho_0}$.

2.2. Charge transfer

Charge transfer between a particle and a surface is a triboelectric phenomenon, in which electrons are transferred due to the properties of different materials. From the point of view of a particle, the process can also be called as contact charging or triboelectrification. The difference between these two terms may not always be recognized but, for example, Bailey (1984) considered the triboelectrification as more general than contact charging, because it includes sliding/frictional contact. A theoretical approach to the phenomenon, supported by extensive experimental data in the micrometer size range, was introduced by John et al. (1980). Starting from the elasticity theory of Hertz, they derived theoretical equations for a spherical particle and a smooth surface. The charge transfer process was divided into two parts, one depending on the material properties and particle size, and another depending on the particle precharge. As a result, the total charge transferred in the contact could be written as

$$q_{\text{tot}} = q_c + \beta q_0, \quad (6)$$

where q_c is the contact charge, q_0 is the precharge and β is a constant describing precharge sensitivity of the process. All the details of the theory are not presented here, but one equation is important related to this work. That is the final form of the equation of contact charge for insulating particle materials. According to John et al. (1980),

$$q_c = \frac{0.3675\pi V_c}{z_0 K Q} \left(\frac{5}{4} \pi^2 \rho_p (k_p + k_s) \right)^{4/5} v_i^{3/5} d_p^3, \quad (7)$$

where V_c is the contact potential between the particle and surface materials, K is the dielectric constant, Q is the resistivity, k_p is the elasticity parameter of particle material, k_s is the elasticity parameter of surface material and v_i is the impact velocity. Note that q_c is proportional to $\rho_p^{4/5}$.

The theoretical dependencies were confirmed and parameter values for different materials were defined in the experiments also performed by John et al. (1980). In the measurements, a single stage impactor and aerosol particles from 3 to 7 μm were used. They found that contact charge was dependent on substrate material but the substrate did not significantly affect the value of β . For methylene blue particles the average value of β was 0.043 ± 0.009 , for potassium biphthalate 0.036 ± 0.016 and for sodium chloride 0.42 ± 0.05 . Theoretically, contact charge is proportional to particle diameter raised to the power of two for conducting materials and raised to the power of three for insulating materials. As an example, John et al. (1980) measured for sodium chloride particles on a steel substrate a size dependency of $q_c = 124 \times d_p^{2.45}$, where d_p is in micrometers and the unit of the result is elementary charge. They used an impact velocity

of 50 m/s. In this work, the size dependency of contact charge is formulated as

$$q_c(d_p) = \frac{q_{c,0}}{d_{p,0}^{b_c}} \cdot d_p^{b_c}, \quad (8)$$

where b_c is the power of the dependency and $q_{c,0}$ is the contact charge for a certain particle size $d_{p,0}$. In addition to size dependency, contact charge is also dependent on impact velocity v_i . John et al. (1980) noticed in the experiments that contact charge is directly proportional to impact velocity, although the theory would predict q_c being proportional to $v_i^{3/5}$. In this work, for a certain particle size, the dependency is formulated as

$$q_c(v_i) = \frac{q_{c,0}}{v_{i,0}} v_i, \quad (9)$$

where $q_{c,0}$ is the contact charge for a certain impact velocity $v_{i,0}$.

2.3. Impaction velocities

In an experimental analysis of particle bouncing, it is essential to quantify the impaction velocities of particles. There are some methods based on direct measurement such as laser doppler velocimetry, which was used for example by Wall et al. (1990) for particles over one micrometer, and high speed cameras which can be used for macroscopic spheres. Nevertheless, none of these methods are directly applicable for nanometer-sized particles. First steps in applying optical velocity measurement for nanoparticles were taken by Reuter-Hack et al. (2007). They used “transparent” agglomerates of low fractal dimension, which have optical size adequate for optical detection but are aerodynamically much smaller.

Besides the challenging experimental methods, another means is to use flow field modeling. Impaction velocities can be defined by modeling the flow field in impactors and calculating the trajectories of particles. Recently, Arffman et al. (2011) published a flow field model of a low pressure impactor, in which the flow field was solved with a commercial CFD modeling software and particle trajectories were defined using Lagrangian methods. The study was focused on calculating the collection efficiency curves but the model is applicable also in predicting impaction velocities. When calculating collection efficiency curves, particles are considered to impact when they have a velocity component perpendicular to the surface close to the impaction plate.

In this work, the model of Arffman et al. (2011) for ELPI is exploited in quantifying impaction velocities with a semi-empirical approach. First of all, the impaction velocities were calculated with the model for several impactor stages and for several particle sizes. This information was combined with the known impactor pressures and the impaction velocity profiles, i.e. impaction velocities as a function of radial distance from the center of the jet, were defined for the cut-off particle sizes of all the impactor stages. The results of the model were also used to generate a functional form for the size dependency of impaction velocity. The final form is

$$v_{i,n}(d_a) = v_{j,n} - \frac{d_{50,n}(v_{j,n} - v_{50,n})}{d_a}, \quad (10)$$

where d_a is the aerodynamic particle diameter, $v_{j,n}$ is the jet velocity, $d_{50,n}$ is the cut-off size and $v_{50,n}$ is the velocity from the velocity profile of the cut-off size, all of which are defined for a stage n . The impaction velocities are seen in Fig. 1 as a function of radial distance from the center of the jet, r , and as a function of particle diameter for the 2nd impactor stage of an ELPI.

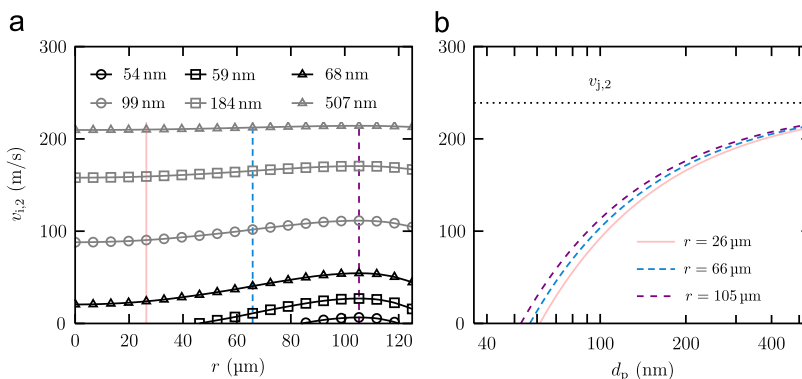


Fig. 1. Impaction velocities $v_{i,2}$ (a) for different particle sizes as a function of radial distance from the center of the impactor jet, r and (b) for three different radial distance as a function of particle size at the 2nd stage of an ELPI. The cut-off size of the stage is 55 nm, the radius of the jet 120 μm and the flow velocity in the jet 239 m/s.

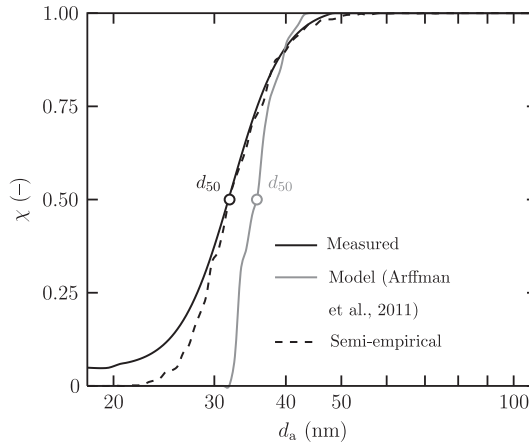


Fig. 2. Collection efficiency χ of the 1st stage of an ELPI as a function of aerodynamic particle size. The semi-empirical approach of adjusting the impaction velocities of the model provides a more realistic cut-off curve than the pure model.

The semi-empirical approach means that the impaction velocities were adjusted to correspond with the experimental collection efficiency curves by determining a certain cut-off size for each impactor stage and adding random noise to the velocities. The latter can also be justified physically because the pure model does not take account the effect of turbulent diffusion on impact velocities. Fig. 2 shows an example of this adjusting for the 1st impactor stage of an ELPI. The collection efficiency calculated by the model of Arffman et al. (2011) is sharper than the measured collection efficiency and the cut-off size is slightly different. In the semi-empirical approach, calculated impaction velocity profiles are moved either towards smaller or towards larger particle size, so that the cut-off size d_{50} matches with the experimental collection efficiency curve. Finally, random noise of 15% is added to the impaction velocity profiles in order to achieve more realistic shape for the collection efficiency curve. Because of the variation caused by the randomness, a set of 100 different cases and averaging are used.

3. Method description

Electrical detection of particles is problematic in measuring particle bouncing and charge transfer. For example, by measuring a current signal from a single impactor stage, it is practically impossible to distinguish the current caused by impacted particles from the current caused by bounced particles and charge transfer. In addition, if the amount of transferred charge is not known, the state of charge of bounced particles continuing to further measurements remains unknown. In this work, this problem is solved with a new approach, which includes a theoretical assumption and a principle of measurement. The theoretical assumption is that the parameter β can be approximated as zero, i.e. the amount of transferred charge is not dependent on the precharge of a particle. And further, the principle of measurement states that by measuring particles with two different preliminary states of charge, the fraction of bounced particles can be seen from the difference of the measured currents.

In practice, the experimental part of the method introduced in this work consists of two current distribution measurements with an ELPI. The first $I_{\text{ch,on}}$ is measured with the charger and the other $I_{\text{ch,off}}$ is measured without the charger. Thus, the initial charge distribution of the particles is described either by the charging efficiency curve of the ELPI charger or by the equilibrium charge distribution of net neutral particles. In both cases, it is enough to use the average number of charges per particle as an estimate of the charge distribution, which in the latter case is simply zero. Assuming $\beta \approx 0$, it is possible to eliminate the effect of charge transfer on the current distribution by calculating the difference of the two measured currents. In this study, so-called bounce current is defined

$$I_b = I_{\text{ch,on}} - I_{\text{ch,off}}, \quad (11)$$

which now represents the fraction of bounced particles, i.e. the current distribution in the case no charge transfer occurs.

Only by measuring $I_{\text{ch,on}}$ and $I_{\text{ch,off}}$ with an ELPI, the bounce current can be defined and analyzed further. For instance, the bounce factor analysis used by Virtanen et al. (2010, 2011) is now exploitable for a current distribution that is not disturbed by charge transfer. However, the bounce factor analysis still includes some problems such as changes in the particle size and density, which can affect the final bounce factor value even if the ability to bounce would stay unchanged. Another weakness of the bounce factor analysis is that it does not provide any absolute information comparable to fundamental theories or other studies. Consequently, this study focuses on a more profound method, but it is good to remember that the bounce factor analysis together with the defined bounce current provides a simple and approximate

on-line method for bouncing measurement. The more profound method introduced in this work is based on a size distribution measurement with an SMPS together with the ELPI measurement and calculation of bounce current. The idea is to simulate the measured ELPI current distributions starting from a size distribution by modeling the bounce and charge transfer behavior of incoming particles in an ELPI. The simulated current distributions are dependent on the theoretical parameters of bouncing and charge transfer and through a fitting process the values of these parameters can be defined.

4. Model

A new model describing the bounce and charge transfer behavior of nanoparticles in an ELPI is presented here. As an input for the model, there are incoming aerosol distribution in the form of mobility size distribution, effective density of the incoming particles and parameters of bouncing and charge transfer describing the particle–surface interaction. Effective density is required to convert particle mobility size to aerodynamic size and vice versa. The relation between these two size metrics is

$$\rho_{\text{eff}} C_C(d_b) d_b^2 = \rho_0 C_C(d_a) d_a^2, \tag{12}$$

where d_b is the mobility diameter, d_a the aerodynamic diameter, C_C the slip correction factor and ρ_{eff} the effective density. In this work, the mobility diameter d_b is identified with the particle diameter d_p used in the bouncing and charge transfer model. The output of the model is the same as the output of the instrument in measurements including current distributions with and without the charger, $I_{\text{ch,on}}$ and $I_{\text{ch,off}}$, respectively. In addition, the bounce current derived from these by Eq. (11) plays an important role in comparing the model and measurements.

To obtain an idea of the model and its operation, it is reasonable to explain the process at a single impactor stage in detail. There are a few factors that play an important role in the process. Those are the collection efficiency curve of the impactor stage, bouncing probability and the charge distribution of the incoming particles. As an example, the collection efficiency χ of the second stage of an ELPI and the corresponding bouncing probability $P_{b,2}$, calculated with the help of impaction velocities and Eq. (3), are illustrated in Fig. 3. When a particle distribution $f_n(d_b, \rho_{\text{eff}})$ with a certain particle density enters the stage n , it is straightforward to calculate the part of the distribution $f_{i,n}$ that impacts and another part $f_{b,n}$ that bounces after the impact, i.e. $f_{i,n} = \chi_n(d_a) f_n(d_b, \rho_{\text{eff}})$ and $f_{b,n} = P_{b,2}(d_b) f_{i,n}$ (or $f_{b,n} = P_{b,2}(d_p) f_{i,n}$). Finally, the part that remains at the impactor stage is

$$f_{f,n} = f_{i,n} - f_{b,n}, \tag{13}$$

and the part that continues to the next stage, f_{n-1} , is the complement of the latter.

The last procedure at a single stage is to calculate the output of the model, i.e. current signal caused by the impacted and bounced particles. The charge distribution of the incoming particles is an essential part of the preliminary information required in the procedure. As mentioned earlier, the charge distribution $g_n(d_b)$ entering the stage n is initially either zero or equal to the charging efficiency curve of the ELPI charger. Charging efficiency of the ELPI charger is often presented as a function of particle mobility size in the form (Marjamäki et al., 2002)

$$P_n = \begin{cases} 222.49 \times d_b^{1.3637}, & d_b \leq 0.023 \text{ } \mu\text{m}, \\ 68.12 \times d_b^{1.32}, & d_b > 0.023 \text{ } \mu\text{m}, \end{cases} \tag{14}$$

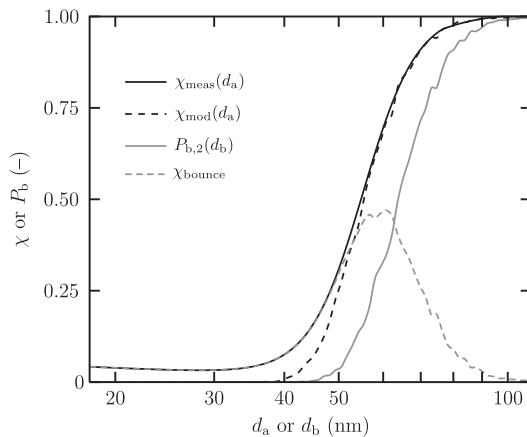


Fig. 3. Measured collection efficiency χ_{meas} , modeled collection efficiency χ_{mod} without diffusion losses and bounce probability $P_{b,2}$ as a function of particle size for the 2nd stage of an ELPI. In this figure, effective density is assumed to be one and thus $d_a = d_b$. In addition, collection efficiency χ_{bounce} when bouncing occurs and the illustrated bounce probability are shown.

where P is the particle penetration through the charger and n is the average number of charges per particle. Because the losses of the charger are mainly caused by the electric field in the charger, it is technically correct to include the penetration function to the initial charge distribution (i.e. $g_n = Pn$) when the charger is considered to be on but not when the charger is considered to be off. In the latter case, the charge distribution is initially zero.

At the stage n , the final current signal is caused by the particles $f_{i,n}$ and by the particles $f_{b,n}$ through charge transfer. The first part is calculated as

$$I'_n = eQ \int_0^\infty g_n(d_b) f_{i,n}(d_b) d \log d_b, \quad (15)$$

where e is the elementary charge and Q is the flow rate through the impactor. The current induced by the bounced particles and charge transfer can be calculated by integrating Eq. (6) over the distribution $f_{b,n}$ and multiplying it with the term eQ . The result is

$$I''_n = eQ \int_0^\infty (q_c(d_b) f_{b,n}(d_b) + \beta g_n(d_b) f_{b,n}(d_b)) d \log d_b. \quad (16)$$

Summing up the currents from Eqs. (15) and (16), the total current for the stage n and a part of the model output is obtained

$$I_n = I'_n + I''_n. \quad (17)$$

One of the main elements of the charge transfer process in a cascade impactor is that the charges of the particles may change after bouncing several times. In the model, this is taken into account by calculating the charge distribution over again after each impactor stage. The change is defined recursively as

$$g_{n-1} = g_n + \int_0^\infty \frac{f_{b,n}(d_b)}{f_{i,n}(d_b)} (q_c(d_b) + \beta g_n(d_b)) d \log d_b. \quad (18)$$

So far, it is shown how the output current I_n is calculated at the stage n and how the particle size distribution f_{n-1} and the charge distribution g_{n-1} continuing to the next stage are determined. Next step is to repeat the procedures for the stage $n-1$.

Not only the model but also the manner it is connected to measurements is a crucial part of this work. If there are measured current distributions with and without the charger, the modeled currents can be fitted into the measured currents by searching optimum values for fitting parameters. The three fitting parameters are the effective density ρ_{eff} , the material coefficient of bouncing α and the contact charge $q_{c,0}$, the latter corresponding particle size $d_{p,0}$ and impaction velocity $v_{i,0}$. According to Eqs. (4) and (7), material coefficient and contact charge are dependent on particle density. Therefore, they are also theoretically dependent on effective density. However, in the fitting process, all these three parameters are equally free and the dependencies do not have any effect on the fitting. The other parameters of charge transfer are kept invariable: $d_{p,0} = 100$ nm, $v_{i,0} = 100$ m/s, $b_c = 3$ and $\beta = 0$. Because the example materials used in this work are insulators, the value of b_c is chosen to be 3, which is supported by the theory and experiments of John et al. (1980). Assuming β to be zero is not as straightforward, but most of the values of β measured by John et al. (1980) and presented earlier in this work are smaller than 0.1. In addition, Fig. 4 shows an example of modeling the effect of β on bounce current, defined by Eq. (11), with a simulated lognormal size distribution. It reveals that growing β can be observed

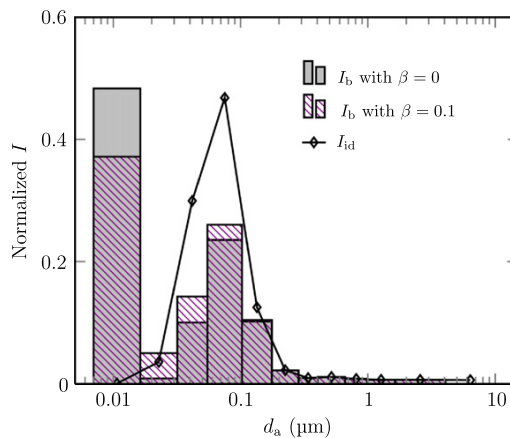


Fig. 4. Modeling the effect of β on bounce current I_b with a simulated lognormal size distribution. Also the ideal current I_{id} without bouncing and charge transfer is shown. Growing β fills the gap between the mode of impacted particles and the filter stage collecting the majority of bounced particles.

in the bounce current distribution. Due to the change in β , the relation of transferred charges in different stages changes, and the change fills the gap between the mode of impacted particles and the filter stage collecting the majority of the bounced particles. Thus, by observing measured bounce current, it is possible to see if β differs significantly from zero. Finally, the success of the fitting method in practice shows the validity of all the parameters.

In the fitting process, the difference between the measured and modeled current distributions is minimized by the method of least squares. Searching of the optimum parameter values is performed with an algorithm called Nelder–Mead simplex algorithm, which is a popular tool for multidimensional unconstrained minimization (Lagarias et al., 1999). The fitting process is divided into two separate parts. In the first part, the values of effective density and material coefficient are defined by fitting the bounce current I_b . The second part consists of fitting the current $I_{ch,off}$ and defining the value of contact charge.

5. Experiment

The experimental section of this work was carried out in a laboratory by measuring bounce and charge transfer behavior of nanoparticles. An ELPI, equipped with a filter stage (Marjamäki et al., 2002) and with an extra stage (Yli-Ojanperä et al., 2010) was used in these experiments. Normally, the substrates of the cascade impactor are coated with grease, which is an efficient means to prevent particle bounce in most cases. However, in this work, particle bounce was desirable. Thus, no grease was spread on the impactor plates and, along with standard steel substrates, also polished steel substrates were used. All the substrates were cleaned in an ultrasonic washing device and dried before assembling them to the impactor. The solution used in the washing device consisted of a 2% (v/v) solution of RBS 25 detergent dissolved in water. In few cases, isopropyl alcohol (IPA) was used instead of the detergent.

A schematic diagram of the experimental setup is seen in Fig. 5. The setup includes nanoparticle generation, an ELPI and a scanning mobility particle sizer (SMPS). The SMPS measures the mobility size distribution of generated particles and it consists of a DMA (TSI model 3081) and a CPC (TSI model 3025). The DMA was run with a sheath flow of 6 lpm and with a sample flow of 0.6 lpm. In the particle generation, an atomizer was used to produce approximately lognormal size distributions for the measurements. After the atomizer, the sample flow was dried either in a silica gel dryer or by diluting it with dry filtered air. Materials used in the watery solution of the atomizer were sodium chloride and levoglucosan. These two materials represent two different forms of solid phase as sodium chloride particles are crystalline and levoglucosan particles have been shown to be in an amorphous phase state (Mikhailov et al., 2009; Saukko et al., 2012). The concentration and the mean particle size of the aerosol led to the instruments could be varied by changing the liquid concentration in the atomizer, the flow rate through the atomizer and the optional dilution after the atomizer.

For each particle distribution, both the currents $I_{ch,on}$ and $I_{ch,off}$ were measured. Although the time resolution of the ELPI is only one second, the currents were averaged over 120 s to correspond the size distribution measured by the SMPS. Each particle size distribution was measured two times because the currents $I_{ch,on}$ and $I_{ch,off}$ could not be measured simultaneously. The currents for a representative analysis were finally measured for six sodium chloride distributions and four levoglucosan distributions. Using polished steel substrates in some cases, the effect of surface could be evaluated. Furthermore, the time dependency of the currents and the effect of substrate loading were observed by monitoring the ELPI currents.

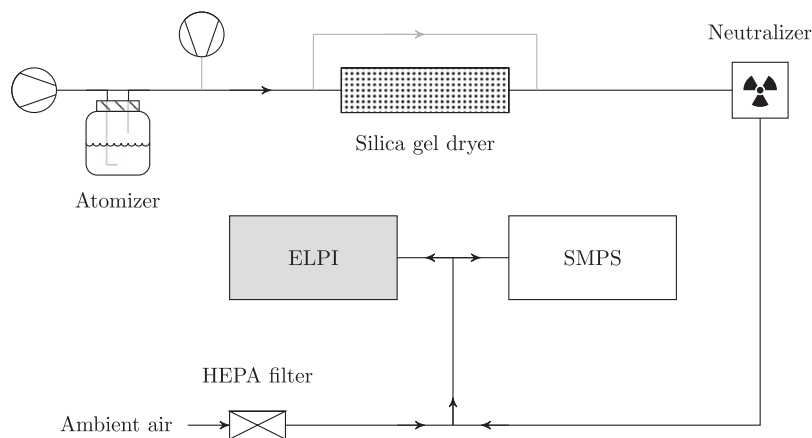


Fig. 5. A schematic diagram of the experimental setup. The dilution by pressurized air after the atomizer was optional as well as the by-passing of the silica gel dryer.

6. Results and discussion

The experimental data was analyzed by the fitting process based on the bounce and charge transfer model. An example of the fitting is seen in Fig. 6. The example shows three different current bar plots, including $I_{\text{ch,on}}$, $I_{\text{ch,off}}$ and normalized I_b , and a mobility size distribution measured with the SMPS. All these are linked to the same sodium chloride distribution. In the current plots, gray bars represent the measured currents and violet bars with a line pattern are the result of the model and the fitting process. Regarding the first two subfigures (Fig. 6(a) and (b)), it is clearly seen that the measured currents $I_{\text{ch,on}}$ and $I_{\text{ch,off}}$ have some irregularities which probably arise from the sensitivity of the charge transfer process. However, those changes seem to be similar in both the currents and they are no more seen in the bounce current (Fig. 6(a)). In fact, this remark is consistent with the theoretical assumption of the model, which states that $\beta \approx 0$ and the charge transfer do not have any effect on bounce current. In addition, there are practically no current in the gap between the mode of impacted particles and the filter stage (compare to the simulated bounce currents in Fig. 4), which supports the assumption of β being close to zero.

The agreement between the measured and modeled currents in Fig. 6(a)–(c) is good. Especially in Fig. 6(c), which shows the result of the first part of the fitting defining the values of ρ_{eff} and α , the agreement is even astonishingly good. Also the ideal current without bouncing and charge transfer is shown in Fig. 6(c). It is calculated from the mobility size distribution using the effective density value, the charging efficiency function, i.e. Eq. (14), and the collection efficiency curves of the ELPI impactor. Here, it could also be possible to use the bounce factor analysis, which can be performed only for the ELPI data. The advantage compared to the former bounce analyses by Virtanen et al. (2010, 2011) would be the concept of bounce current. In this case, where charge transfer is considerable, the usage of the general ELPI current $I_{\text{ch,on}}$ would lead to a negative value of bounce factor. In contrast, the bounce factor analysis together with the bounce current is a good estimation of bounce behavior. However, in this study, the more accurate analysis connected to the theoretical parameters of bouncing and charge transfer is preferred. Comparing the ideal current and the bounce current in Fig. 6(c), it can be seen that bouncing occurs almost in all the particle sizes and most of the bouncing particles finally end up to the filter stage. Practically, this allows one to see the original shape of the distribution in the bounce current and find a good estimate for the effective density in the fitting method.

In the main analysis of the experimental data, the fitting process was performed for six sodium chloride distributions and for four levoglucosan distributions. Parameter values from the fittings are seen in Table 1, which shows the average values of three parameters for each material and standard deviations as approximate error limits. Even though the amount of data is not very large and the deviations are notable especially for levoglucosan, the difference between two different materials can be seen in all parameter values. Nevertheless, the contact charge values may not be comparable with each other because of the uncertainties in the surface conditions of these measurements. This subject will be discussed more below. The most

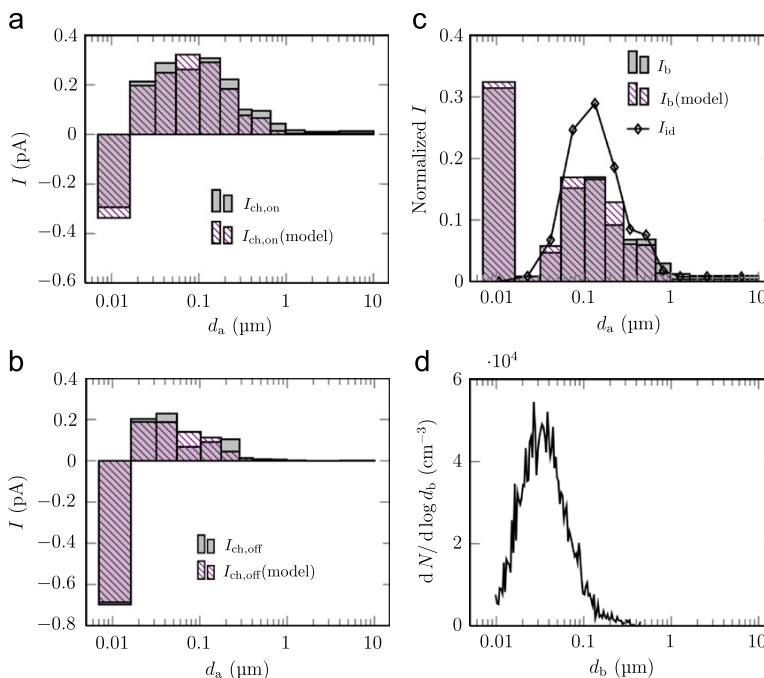


Fig. 6. An example of fitting the bounce and charge transfer model to a measured sodium chloride distribution. The currents measured by the ELPI (a) with the charger $I_{\text{ch,on}}$ and (b) without the charger $I_{\text{ch,off}}$ as well as (c) the normalized bounce current I_b are drawn in gray. Bars with a line pattern represent the modeled currents and the solid line the ideal current I_{id} , which are calculated from (d) the mobility size distribution measured by the SMPS.

Table 1

Parameter values from the fittings. The average values and standard deviations describing the error limits are calculated for six sodium chloride distributions and for four levoglucosan distribution. Bulk densities are shown as a reference to the effective density values.

Particle material	ρ_{bulk} (g/cm ³)	ρ_{eff} (g/cm ³)	α (m ² /s)	$q_{c,0}$
Sodium chloride	2.17 ^a	2.23 ± 0.14	$(5.2 \pm 0.7) \times 10^{-6}$	0.49 ± 0.15
Levoglucosan	1.618 ^b	1.5 ± 0.4	$(7.6 \pm 1.3) \times 10^{-6}$	0.22 ± 0.14

^a CRC Handbook (2007).

^b Rosenørn et al. (2006).

promising results are the effective density values which are comparable to the bulk density values also shown in Table 1. Of course, there are more useful methods for defining the effective density such as the general use of an ELPI and the method introduced by Ristimäki et al. (2002), but these good results strongly support the fitting method and the significance of the other parameter values α and $q_{c,0}$. Surface conditions and particle size may affect these parameters, as discussed more below, but in a single measurement these parameters characterize well the bounce and charge properties of particles.

Looking in detail Table 1, the values of α indicate that sodium chloride particles are more inclined to bounce than levoglucosan particles. The values are of the same magnitude as the previously presented material coefficient values measured in the micrometer size range (Cheng & Yeh, 1979; John, 1995). As presented earlier in Eq. (4), α is dependent on particle density. Taking account this dependency, it is seen that the density partly accounts for the difference between sodium chloride and levoglucosan. According to the values of $q_{c,0}$, sodium chloride would also be more inclined to transfer charge with a steel surface than levoglucosan. However, in this respect, it is reasonable to discuss only about the magnitudes of the results. The contact charge of sodium chloride can be compared to the results of John et al. (1980) by extrapolating the size dependency and impact velocity equations presented earlier. In 100 nm and 100 m/s, the extrapolated value is 0.88. This is of the same magnitude as the result of the fitting method 0.49.

To analyse the possible size dependency of the results given by the fitting method, the parameter values are drawn in Fig. 7 as a function of particle mode GMD. Because of relatively high deviations and small amount of data, it is difficult to analyze the possible size dependency of levoglucosan particles. However, if only the violet circles, representing sodium chloride particles measured with conventional steel substrates, are considered, rather clear size dependency is seen for the parameter α but not for ρ_{eff} and q_c . It means that, for effective density and contact charge, the fitting method works and most of the theoretical assumptions behind the model are relevant at least in this size range. On the other hand, the size dependency of material coefficient probably refers to a disagreement with the theoretical size dependency of the capture limit shown in Eq. (3). The real size dependency of nanoparticles should be studied experimentally in detail in the future to be able to modify the theory and the model. However, the results of the fitting method are still relevant and comparable also for material coefficient, if particle modes are in the same size range.

The parameter values were also viewed as a function of particle concentration but no clear correlation was observed. However, the effect of the substrate roughness, loading and cleaning process are discussed in more detail. In Fig. 7, the triangle markers represent parameter values that are calculated for the measurements with polished steel substrates. Intuitively, a polished steel surface could be seen more efficient and more stable a tool for bouncing and charge transfer measurements compared to a rougher steel surface. In practice, Fig. 7 shows that there is no significant difference in the parameter values between conventional and polished steel substrates except the case of the contact charge of sodium chloride. In that case, higher contact charge values are related to the substrate loading and the time dependency of charge transfer. This will be discussed more below but, altogether, the results measured with both substrates are mostly comparable and there are no advantages in using polished substrates.

Substrate loading and changes in the surface can affect considerably the charge transfer. John et al. (1980) noticed that it took from 20 to 60 min for contact charge to achieve an asymptotic value after starting the measurement with a cleaned substrate. In the experiments of this work, surface exposure times and measured particle concentrations varied. Actually, clearly asymptotic behavior was not observed but changes as a function of time were always seen to some extent in the measured currents. However, the only situation, where it notably affected the final parameter values given by the fitting method, is the case of polished steel substrates and sodium chloride. In Fig. 7(c), the two triangle markers above the others represent this case. These points were measured with fresh cleaned substrates. For some reason, the charge transfer was very intensive at the beginning but it also decreased rather quickly reaching the normal level compared to the other measurements in about 20 min. This example could be regarded as an unsuccessful measurement of contact charge, but interesting is, that it is not unsuccessful in the sense of measuring effective density or material coefficient. As seen in Fig. 7, those parameter values compare well to the other measurements.

Fig. 7 also shows two measurements for levoglucosan, in which the substrates were cleaned with isopropyl alcohol (IPA) instead of RBS. Once again, the difference between these two cleaning procedures is most clearly seen in the contact charge values. According to these measurements, cleaning the steel substrates with RBS seems to result in higher contact charge values and more intense charge transfer than cleaning the substrates with isopropyl alcohol. Other parameter values are not as sensitive to different cleaning procedures. Altogether, obtaining a meaningful contact charge parameter

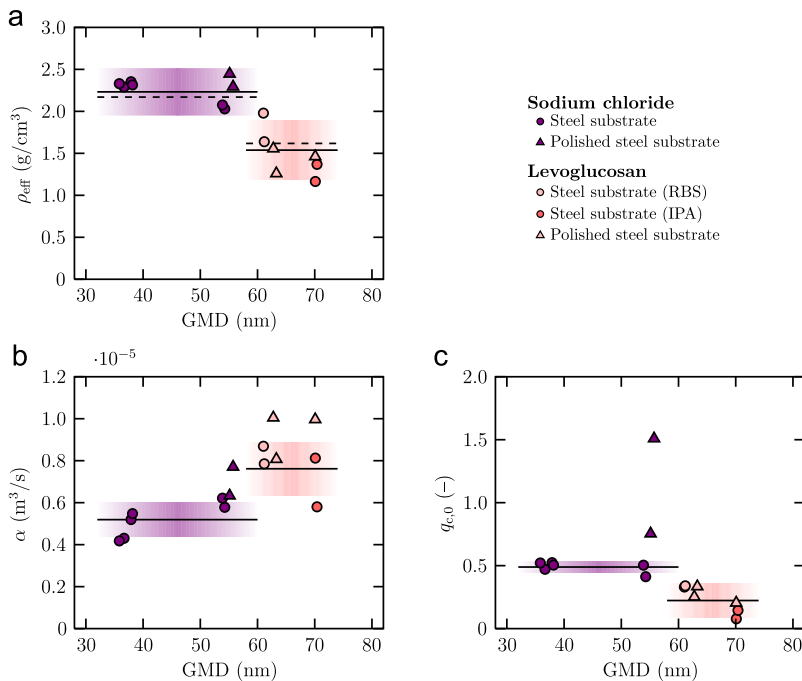


Fig. 7. The parameter values (ρ_{eff} , α and $q_{c,0}$) as a function of particle mode GMD. Representative values are marked with circles and the average values for each material with a solid line. Dashed lines represent the bulk densities and colored bars the standard deviations. For the contact charge parameter, the effect of different cleaning methods (RBS and IPA) and polished substrates can be seen. (For interpretation of the references to color in this figure caption, the reader is referred to the web version of this article.)

experimentally seems to be problematic because of the effect of substrate roughness, substrate loading and cleaning procedures. In a single measurement, the contact charge value provided by the fitting method describes well the charge transfer behavior, but, in order to compare the results of several measurements, the effect of different substrates and surface conditions should be studied in more detail. Even though the contact charge values of sodium chloride in Table 1 were close to the values measured by John et al. (1980) for micrometer-sized sodium chloride particles and a steel substrate, it cannot be said that these values reliably represent the contact charge between a sodium chloride nanoparticle and a steel substrate. To reach the fundamental contact charge values between nanoparticles and different surface materials, extensive measurements for different cleaning procedures and substrate materials are required in the future, for example, using the method introduced in this study.

7. Conclusions

Bouncing of nanoparticles has recently become an important tool in studying the phase state of atmospheric aerosols. Bouncing and its common side effect charge transfer can be considered as fundamental phenomena in aerosol physics. However, these phenomena are not fully understood and there are practically no previous experimental studies or systematic methods presented for bouncing and charge transfer of nanometer-sized particles. This work shows that both bouncing and charge transfer of nanoparticles can be characterized with a new method. The method is based on an ELPI measurement with and without the charger, which enables the separation of the two phenomena. Further analysis relies on a new bouncing and charge transfer model constructed for the ELPI and on a simultaneous measurement with an ELPI and an SMPS. By fitting the modeled ELPI currents to the measured currents, bouncing and charge transfer of nanoparticles can be described by the existing theory of micrometer-sized particles.

The method presented here is a unique tool for defining the theoretical parameters of bouncing and charge transfer from an experimental analysis of nanoparticles. To authors' knowledge, there are no other methods that are capable of this. Although the method is a pioneering one, it is still exceptionally ready for use in different environments and applications. From the point of view of experiments, the straightforward utilization of commercially available measuring devices is a great advantage and no special modifications are required. The method is designed for a polydisperse aerosol distribution which is advantageous in many cases as well. In the fitting process, especially the effective density as a fitting parameter, along with the parameters of bouncing and charge transfer, provides a possibility to evaluate the results given by the fitting method and, in some cases, compare the results with reference data.

This work has been able to emerge the theories of bouncing and charge transfer to the experiments for nanometer-sized particles. There are still some experimental challenges, such as the effect of substrate roughness, substrate loading and cleaning procedures on charge transfer, and theoretical problems, such as the size dependency of bouncing. However, it is important that the tool now exists. In the future, more experiments should be performed for different particle and substrate materials, and the method could be developed further for different applications. To understand the fundamental phenomena of bouncing and charge transfer, totally new approaches may be required, but after this study, the task seems to be more conceivable.

Acknowledgments

This work was supported by a grant from the Nessling Foundation. H. Kuuluvainen acknowledges the support from the Graduate School of Tampere University of Technology.

References

- Arffman, A., Marjamäki, M., & Keskinen, J. (2011). Simulation of low pressure impactor collection efficiency curves. *Journal of Aerosol Science*, 42(5), 329–340.
- Bailey, A.G. (1984). Electrostatic phenomena during powder handling. *Powder Technology*, 37(1), 71–85.
- Bergström, L. (1997). Hamaker constants of inorganic materials. *Advances in Colloid and Interface Science*, 70(1–3), 125–169.
- Chang, M., Seongheon, K., & Sioutas, C. (1999). Experimental studies on particle impaction and bounce: Effects of substrate design and material. *Atmospheric Environment*, 33(15), 2313–2322.
- Cheng, Y.S., & Yeh, H.C. (1979). Particle bounce in cascade impactors. *Environmental Science and Technology*, 13(11), 1392–1396.
- CRC Handbook. (2007). *CRC Handbook of Chemistry and Physics* (88th ed.). CRC Press.
- Dahneke, B. (1971). The capture of aerosol particles by surfaces. *Journal of Colloid and Interface Science*, 37(2), 342–353.
- Froeschke, S., Kohler, S., Weber, A.P., & Kasper, G. (2003). Impact fragmentation of nanoparticle agglomerates. *Journal of Aerosol Science*, 34(3), 275–287.
- Fujitani, Y., Hasegawa, S., Fushimi, A., Kondo, Y., Tanabe, K., Kobayashi, S., & Kobayashi, T. (2006). Collection characteristics of low-pressure impactors with various impaction substrate materials. *Atmospheric Environment*, 40(18), 3221–3229.
- Hinds, W.C. (1999). *Aerosol Technology: Properties, Behavior, and Measurement of Airborne Particles* (2nd ed.). John Wiley & Sons.
- John, W. (1995). Particle–surface interactions: Charge transfer, energy loss, resuspension, and deagglomeration. *Aerosol Science and Technology*, 23(1), 2–24.
- John, W., Reischl, G., & Devor, W. (1980). Charge transfer to metal surfaces from bouncing aerosol particles. *Journal of Aerosol Science*, 11(2), 115–138.
- Kannosto, J., Yli-Pirilä, P., Hao, L., Leskinen, J., Jokiniemi, J., Mäkelä, J. M., Joutsensaari, J., Laaksonen, A., Worsnop, D. R., Keskinen, J., & Virtanen, A. Bounce characteristics of α -pinene derived SOA particles with implications to physical phase. *Boreal Environment Research*, accepted.
- Keskinen, J., Pietarinen, K., & Lehtimäki, M. (1992). Electrical low pressure impactor. *Journal of Aerosol Science*, 23(4), 353–360.
- Kittelson, D.B., Watts, W.F., & Johnson, J.P. (2004). Nanoparticle emissions on Minnesota highways. *Atmospheric Environment*, 38(1), 9–19.
- Kruis, F.E., Fissan, H., & Peled, A. (1998). Synthesis of nanoparticles in the gas phase for electronic, optical and magnetic applications—A review. *Journal of Aerosol Science*, 29(5–6), 511–535.
- Kulmala, M., Vehkamäki, H., Petäjä, T., Maso, M.D., Lauri, A., Kerminen, V.M., Birmili, W., & McMurry, P.H. (2004). Formation and growth rates of ultrafine atmospheric particles: A review of observations. *Journal of Aerosol Science*, 35(2), 143–176.
- Lagarias, J.C., Reeds, J.A., Wright, M.H., & Wright, P.E. (1999). Convergence properties of the Nelder–Mead simplex method in low dimensions. *SIAM Journal on Optimization*, 9(1), 112–147.
- Marjamäki, M., Ntziachristos, L., Virtanen, A., Ristimäki, J., Keskinen, J., Moiso, M., Palonen, M., & Lappi, M. (2002). Electrical filter stage for the ELPI. In: *Society of Automotive Engineers (SAE)*, Technical Paper Series 2002-01-0055.
- Matsusaka, S., Maruyama, H., Matsuyama, T., & Ghadiri, M. (2010). Triboelectric charging of powders: A review. *Chemical Engineering Science*, 65(22), 5781–5807.
- Mikhailov, E., Vlasenko, S., Martin, S.T., Koop, T., & Pöschl, U. (2009). Amorphous and crystalline aerosol particles interacting with water vapor: Conceptual framework and experimental evidence for restructuring, phase transitions and kinetic limitations. *Atmospheric Chemistry and Physics*, 9(24), 9491–9522.
- Mullins, B.J., Agronovski, I.E., & Braddock, R.D. (2003). Particle bounce during filtration of particles on wet and dry filters. *Aerosol Science and Technology*, 37(7), 587–600.
- Reuter-Hack, K., Weber, A.P., Rösler, S., & Kasper, G. (2007). First LDA measurements of nanoparticle velocities in a low-pressure impacting jet. *Aerosol Science and Technology*, 41(3), 277–283.
- Ristimäki, J., Virtanen, A., Marjamäki, M., Rostedt, A., & Keskinen, J. (2002). On-line measurement of size distribution and effective density of submicron aerosol particles. *Journal of Aerosol Science*, 33(11), 1541–1557.
- Rogers, L.N., & Reed, J. (1984). The adhesion of particles undergoing an elastic–plastic impact with a surface. *Journal of Physics D: Applied Physics*, 17(4), 677–689.
- Rosenørn, T., Kiss, G., & Bilde, M. (2006). Cloud droplet activation of saccharides and levoglucosan particles. *Atmospheric Environment*, 40(10), 1794–1802.
- Saukko, E., Kuuluvainen, H., & Virtanen, A. (2012). A method to resolve the phase state of aerosol particles. *Atmospheric Measurement Techniques*, 5(1), 259–265.
- Seipenbusch, M., Toneva, P., Peukert, W., & Weber, A.P. (2007). Impact fragmentation of metal nanoparticle agglomerates. *Particle and Particle Systems Characterization*, 24(3), 193–200.
- Virtanen, A., Joutsensaari, J., Koop, T., Kannosto, J., Yli-Pirilä, P., Leskinen, J., Mäkelä, J.M., Holopainen, J.K., Pöschl, U., Kulmala, M., Worsnop, D.R., & Laaksonen, A. (2010). An amorphous solid state of biogenic secondary organic aerosol particles. *Nature*, 467(7317), 824–827.
- Virtanen, A., Kannosto, J., Kuuluvainen, H., Arffman, A., Joutsensaari, J., Saukko, E., Hao, L., Yli-Pirilä, P., Tiitta, P., Holopainen, J.K., Keskinen, J., Worsnop, D.R., Smith, A., & Laaksonen, A. (2011). Bounce behavior of freshly nucleated biogenic secondary organic aerosol particles. *Atmospheric Chemistry and Physics*, 11(16), 8759–8766.
- Wall, S., John, W., & Wang, H.-C. (1990). Measurements of kinetic energy loss for particles impacting surfaces. *Aerosol Science and Technology*, 12(4), 926–946.
- Watanabe, H., Ghadiri, M., Matsuyama, T., Ding, Y.L., Pitt, K.G., Maruyama, H., Matsusaka, S., & Masuda, H. (2007). Triboelectrification of pharmaceutical powders by particle impact. *International Journal of Pharmaceutics*, 334(1–2), 149–155.
- Weber, A.P., & Wu, T. (2009). Kontaktauflauf von Nanopartikeln bei Impaktion. *Chemie-Ingenieur-Technik*, 81(6), 791–795.
- Yli-Ojanperä, J., Kannosto, J., Marjamäki, M., & Keskinen, J. (2010). Improving the nanoparticle resolution of the ELPI. *Aerosol and Air Quality Research*, 10(4), 360–366.

Paper II

Anssi Arffman, Heino Kuuluvainen, Juha Harra, Ossi Vuorinen, Paxton Juuti, Jaakko Yli-Ojanperä, Jyrki M. Mäkelä, and Jorma Keskinen

“The critical velocity of rebound determined for sub-micron silver particles with a variable nozzle area impactor”

Journal of Aerosol Science, vol. 86, no. 9, pp. 32–43, 2015

doi: 10.1016/j.jaerosci.2015.04.003

© Elsevier B.V.



Contents lists available at ScienceDirect

Journal of Aerosol Science

journal homepage: www.elsevier.com/locate/jaerosci

II

The critical velocity of rebound determined for sub-micron silver particles with a variable nozzle area impactor



Anssi Arffman¹, Heino Kuuluvainen^{*,1}, Juha Harra, Ossi Vuorinen, Paxton Juuti, Jaakko Yli-Ojanperä, Jyrki M. Mäkelä, Jorma Keskinen

Aerosol Physics Laboratory, Department of Physics, Tampere University of Technology, Tampere, Finland

ARTICLE INFO

Article history:

Received 14 January 2015

Received in revised form

20 March 2015

Accepted 7 April 2015

Available online 15 April 2015

Keywords:

Silver nanoparticle

Rebound

Critical velocity

Low-pressure impactor

ABSTRACT

The critical velocity of rebound was determined for spherical silver aerosol particles in the size range of 20–1000 nm. A novel instrument, a variable nozzle area impactor, was especially designed for measuring the particle–surface interaction as a function of the particle impact velocity. The experimental results were combined with a numerical model in order to obtain the impact velocities. The experiments were carried out using a plain aluminum collection substrate in the impactor. Our results show that the critical velocity of rebound decreases from 14 to 0.022 m/s as the particle size increases from 20 to 1000 nm. Furthermore, the critical velocity was found to be proportional to the power of -1.6 of the particle size, instead of the theoretical inverse proportionality. This result is in line with the previous studies for micron-sized particles. In the nanoparticle size range, the obtained values are approximately 3–10 times greater than the recent literature values. This discrepancy can most likely be explained by the different surface materials. All in all, our results give valuable information about the particle–surface interactions in the sub-micron size range.

© 2015 Elsevier Ltd. All rights reserved.

1. Introduction

Particle rebound from a surface is a fundamental phenomenon. Recently, it has been of interest in several fields of aerosol physics, including atmospheric aerosols and aerosol synthesis. For example, Virtanen et al. (2010) found an amorphous solid state of biogenic SOA (secondary organic aerosol) particles by investigating the bounce behavior of the particles. The further development has led to some experimental methods capable of measuring the bounce probability of the SOA particles as a function of the relative humidity in specific low-pressure impactor systems (Bateman et al., 2014; Saukko et al., 2012). Within the field of engineered nanoparticles, the research of the particle–surface interaction has been focused on the fragmentation and binding energy of agglomerates (Froeschke et al., 2003; Ihalainen et al., 2014; Seipenbusch et al., 2007, 2010). However, the lack of knowledge of the fundamental bounce properties of ultrafine particles limits the reliability of these methods.

When a particle impacts on a firm surface, it may either stick to it or be reflected. The process is mainly affected by three factors: the adhesion, the energy loss mechanisms in the particle and the initial velocity of the particle. With low initial

* Corresponding author.

E-mail address: heino.kuuluvainen@tut.fi (H. Kuuluvainen).¹ A. Arffman and H. Kuuluvainen contributed equally to this work.

velocities, the energy losses dominate and the particle is captured by the surface. When the initial velocity increases up to a critical velocity, the kinetic energy, even when reduced by the energy losses, is sufficient to overcome the adhesion energy and the particle rebounds. According to theoretical knowledge, the critical velocity is inversely proportional to the particle size (Dahneke, 1971; Wang & Kasper, 1991; Weir & McGavin, 2008). Experimentally, the values of the critical velocity have been determined for different materials of micron-sized particles and substrates (Wall et al., 1990), and for silver and sodium chloride nanoparticles on a mica substrate in the size range of 10–80 nm (Rennecke & Weber, 2013a). Both the datasets show similar particle size dependency compared to the theories, but the critical velocity values have a difference of several orders of magnitude if extrapolated into the same size range.

The experimental challenges in measuring the particle rebound of nanoparticles are often related to low-pressure conditions required for the impaction and to the detection of the particles in these conditions. The experimental method used by Rennecke & Weber (2013a) was based on scanning the impact velocity by means of the impaction pressure. By continuously measuring the electrical current downstream and the particle concentration upstream, the penetration of the impactor could be defined as a function of the impaction pressure. The advantage of the electrical detection of particles in low-pressure conditions is its accuracy and a good time resolution. Optical detection of particles has also been used in the bounce and fragmentation studies of nanoparticles (Ihalainen et al., 2014; Saukko et al., 2012). Its advantage is that the possible charge transfer is not affecting the detection. However, the optical detection cannot practically be used continuously in low-pressure conditions.

Measurement of the impact velocity of a single particle can be performed for micron-sized particles with a laser Doppler velocimetry (Wall et al., 1990). Because of limitations in the optical detection, the same method cannot generally be exploited for nanoparticles. Reuter-Hack et al. (2007) have applied the laser Doppler velocimetry method for agglomerates with mobility diameters below 500 nm, but for spherical particles that would not be possible. The lack of experimental methods has led to the utilization of numerical methods and computational fluid dynamics (CFD) simulations in defining the impact velocity for nanoparticles (Ihalainen et al., 2014; Kuuluvainen et al., 2013; Rennecke & Weber, 2013a; Virtanen et al., 2011). These studies are mainly based on the previous work of modeling the impactor flow field and collection efficiency curves (Arffman et al., 2011; Rennecke & Weber, 2013b). According to the study by Arffman et al. (2012), the impactor geometry significantly affects the size resolution of an impactor. The best results were obtained with a slit type low-pressure impactor having a minimized nozzle throat length. The advantage of this type of an impactor is a very small deviation in the impact velocity of a certain particle size. This is also a great advantage in defining the critical velocity for nanoparticles.

This study presents a new method for measuring the critical velocity of nanoparticles using a variable nozzle area impactor, and reports the results for spherical silver particles in the size range of 20–1000 nm. The method is based on an impactor design, where the deviation of the impact velocities in a single measurement for a certain particle size is minimized, and the pressure conditions controlled. The impactor consists of a narrow slit with a short nozzle throat length, and the nozzle area can be varied by changing the slit length. By decreasing the slit length, the impact velocity of a particle increases. Furthermore, the impact velocities are calculated for different particle sizes and different slit lengths with numerical methods.

2. Theoretical background

The theory of aerosol particle rebound from a firm surface was first introduced by Dahneke (1971). The theory includes the effect of the adhesion, the energy loss mechanisms in a particle and the particle initial velocity. Assuming a spherical particle and an infinite firm surface, the adhesion energy between the particle and the surface can be written as

$$E_{\text{adh}} = \frac{A_H d_p}{12z_0}, \quad (1)$$

where d_p is the particle diameter, A_H is the Hamaker constant and z_0 is the separation distance, usually assumed to be 0.4 nm. The Hamaker constant arises from the van der Waals interaction of molecules and is dependent on both particle and surface materials.

The amount of energy loss in the collision is mainly dependent on the mode of deformation in the particle. Fully elastic deformation completely restores the kinetic energy of the particle, and the velocity after the rebound equals the initial velocity. Practically, this sort of collisions only takes place among molecules and atoms. Considering the collisions of aerosol particles and firm surfaces, plastic deformation is always present to some extent. Plastic and elastic behavior of aerosol particles during rebound was extensively studied first by Rogers & Reed (1984). Thereafter, Wang & Kasper (1991) and Weir & McGavin (2008) developed the theoretical approach for the elastic and plastic behavior, respectively.

Depending on the energy losses and adhesion energy, the particle may either rebound or stick to the surface. For the initial velocity, there is a certain capture limit v_{crit} , i.e. the critical velocity of rebound. The relation between the initial velocity of the particle, perpendicular to the surface, and the rebound velocity of the particle is called the coefficient of restitution C_R . Combining Eq. (1) and the definition of the coefficient of restitution, the critical velocity of rebound can be written as

$$v_{\text{crit}} = \alpha d_p^2, \quad (2)$$

where the material coefficient

$$\alpha = \left(\frac{A_H (1 - C_R^2)}{\pi z_0 \rho_p C_R^2} \right)^{1/2}, \quad (3)$$

is dependent on the coefficient of restitution, the Hamaker constant and the particle density ρ_p . According to the theory of Dahneke (1971), the critical velocity is inversely proportional to the particle diameter, so the exponent β is set to be -1 . The same proportionality is also found in the more recent models based on both the elastic (Wang & Kasper, 1991) and plastic (Weir & McGavin, 2008) deformation of particles. The difference between the elastic and plastic models is that the material coefficient α obtains significantly higher values in the latter case.

Majority of the previous experimental studies regarding the critical velocity have found a dependence on the particle size similar to Eq. (2). However, in contrast to the theoretical models, the exponent values (β) may significantly differ from -1 . As reviewed by Wall et al. (1990), the exponents were usually between -1.2 and -1.8 including the results of four different studies for micron-sized particles (Cheng & Yeh, 1979; D'Ottavio et al., 1982; Wall et al., 1990; Wang & John, 1988). Only the results of Esmen et al. (1978) showed a smaller exponent value (-0.39) and the highest values were measured for harder materials such as copper and glass (Rogers & Reed, 1984). Also the results of Rennecke & Weber (2013a) for silver nanoparticles obey Eq. (3) and are proportional to the power of -3.0 of the particle size, resulting a relatively steep slope. With respect to the theoretical knowledge, the steeper slopes obtained from the measurements are explained with a transition from elastic to plastic deformation. The transition would require some of the factors in Eq. (3) to be particle size dependent. That might be the Hamaker constant or the coefficient of restitution (Tsai et al., 1990).

3. Experimental method

3.1. Variable nozzle area impactor

An illustration representing the key features of the variable nozzle area impactor is shown in Fig. 1. The impactor consists of a nozzle plate, an adjustable cover and an impaction substrate. The nozzle plate contains a rectangular slit with a width of 0.3 mm and a maximum length of 30 mm. The adjustable cover can be slid manually on top of the nozzle in order to decrease the slit length down to 3 mm, and, thus, vary the nozzle area. The impactor stage was made vacuum tight by using O-ring sealings up- and downstream. The opening where the adjustable cover is connected to the impactor was machined as tight as possible, and further sealed with mould silicon. The nozzle throat length in the impactor (also the thickness of the nozzle plate) is 0.1 mm and the jet-to-plate distance is 0.5 mm. The impaction substrate material used in this study was machined aluminum. Measurements were carried out using both plain and greased (Apiezon vacuum grease) substrates. The function of the grease was to prevent particle bounce, and, thus, serve as a reference measurement.

3.2. Setup for 20–200 nm particles

A schematic presentation of the experimental setup is shown in Fig. 2. Spherical and monodisperse silver nanoparticles, in the size range of 20–200 nm, were generated via evaporation–condensation method followed by sintering and size

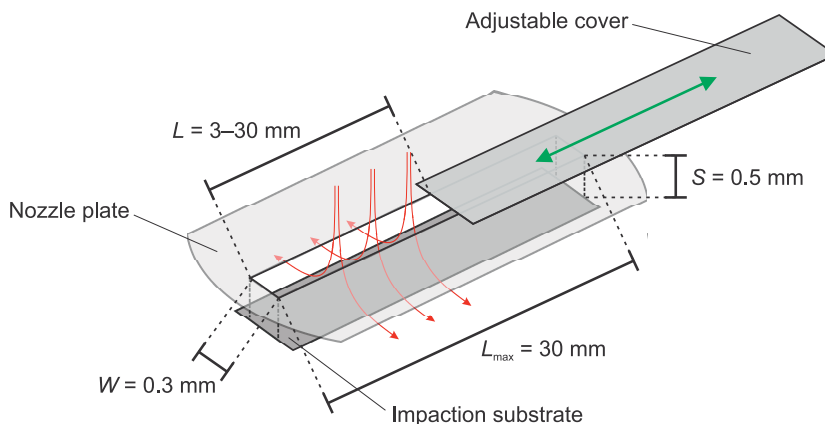


Fig. 1. An illustration of the variable nozzle area impactor. W is the slit width, S is the jet-to-plate distance, L_{\max} is the maximum slit length and L is the slit length. By changing the slit length with the adjustable cover (green arrow), the area of the nozzle ($L \times W$) can be varied. The red arrows represent the flow lines through the nozzle. Note that the figure is out of scale. (For interpretation of the references to color in this figure caption, the reader is referred to the web version of this paper.)

selection (Harra et al., 2012; Scheibel & Porstendörfer, 1983). Silver was evaporated from a small amount of bulk material situated at the center of a tube furnace at temperatures of 1200–1500 °C, depending on the desired particle size. The metal vapor was first carried out of the furnace (3 lpm) and then diluted with nitrogen gas (3 lpm). The silver particles, formed by condensation after cooling, were passed through a coagulation chamber before the sintering step. In order to sinter relatively large particles (~100 nm), two successive furnaces were employed. Depending on the particle size, the flow rate through the furnaces was 0.3–1 lpm. The function of the latter furnace (400 °C) was to smooth the particle surfaces from bumps caused by the partial evaporation and subsequent formation of smaller particles near the bulk melting point (Schmidt-Ott, 1988; Zihlmann et al., 2014) in the first sintering furnace (600–800 °C). After sintering, a monodisperse particle mobility size distribution was realized with a Vienna-type differential mobility analyzer (DMA). Because of the nitrogen gas used in the sheath flow and as a carrier gas in the previous steps, the final sample was extremely dry (RH < 1%).

After the DMA, a bridge dilution system followed by a simple corona charger were used to control the particle number concentration entering the impactor. For the corona charger, the particle charging efficiency has been previously determined by Arffman et al. (2014). The charger was used for particle sizes larger than 40 nm, and the dilution was adjusted so that the total measured current was approximately 20 fA. This ensured that the impactor plate would not overly load from the collected particles and, thus, interfere with the particle rebound from the surface. The maximum particle area fraction on the impactor plate during the measurements was estimated to be approximately 5%. A vacuum pump was used to attain the required low-pressure conditions (106–256 mbar) in the variable nozzle area impactor. Pressures were measured before and after the impactor. Furthermore, a critical orifice inlet assured a constant volumetric flow rate (1.18 lpm). The particles were measured using electrical detection. The impactor substrate and a filter downstream were connected to electrometers. Particle samples were collected on a carbon film using a sampler based on electrical field deposition and analyzed with a transmission electron microscope (TEM, Jeol JEM-2010).

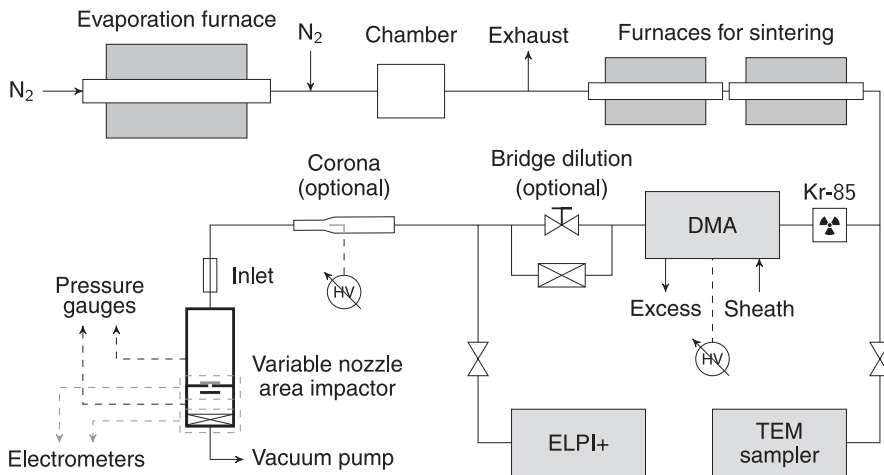


Fig. 2. A schematic of the generation and measurement setup of 20–200 nm silver particles.

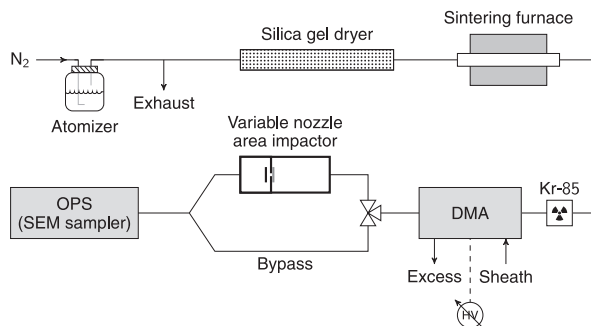


Fig. 3. A schematic of the generation and measurement setup of 400–1000 nm silver particles. For collecting particle samples, the OPS was replaced by the SEM sampler.

3.3. Setup for 400–1000 nm particles

Figure 3 shows the generation and measurement setup for silver particles in the size range of 400–1000 nm. Commercial silver powder (Inframat Advanced Materials, purity 99.95%, average size 0.7–1.5 μm , near-spherical) was dispersed in water and sprayed with an atomizer aerosol generator (Topas ATM 220). Due to a relatively small size of the generated droplets (Harra et al., 2013), we were unable to utilize the largest ($> 1 \mu\text{m}$) particles in the powder. In order to prevent sedimentation, the dispersion was ultrasonicated and stirred with a magnetic mixer before and during the spraying process, respectively. When leaving the atomizer, the aerosol was dried with a silica gel dryer ($\text{RH} < 10\%$) and sintered in a furnace (600°C). Particle size selection was carried out with a Vienna-type DMA which was followed by the variable nozzle area impactor. Here, the impactor pressure and the flow rate were 960 mbar and 1.0 lpm, respectively. Because the measurements of the nearly micron-sized particles were conducted in atmospheric pressures, and the particle concentration was low, in the order of 10 cm^{-3} , an optical particle sizer (OPS, TSI 3330) was used as a particle number counter instead of electrical detection. This also meant that the critical orifice inlet and the filter before and after the impactor, respectively, were not used. Reference particle concentration was measured by bypassing the impactor. Particle samples were collected on a holey carbon film using a flow-through sampler and analyzed by a scanning electron microscope (SEM, Zeiss ULTRA PLUS).

4. Numerical simulations

CFD simulations were used to determine the impaction velocities. The description of the employed methods can be found in a previous study (Arffman et al., 2011), and only a brief description of the methods is given here. First, we simulated the flow fields in the impactor with Ansys Fluent, Release 14.1 software. Simulations were carried out in 2D, and the boundary conditions were the mass flow rate and the static pressure at the outlet. Flows were assumed to be laminar as the Reynolds' numbers were in the order of 500 at the maximum. The grid was made very dense near the collection plate and the wall distances were in the range of 0.5–1 μm above the collection plate. Changing the nozzle area (i.e. the slit length) was taken into account in the simulations by changing the mass flow rate per depth of the slit length. Particle tracking simulations were carried out using Ansys Fluent complemented with a user defined function to calculate the particle drag in the slip regime. The particles were released a few centimeters upstream of the nozzle and tracked until they impacted to the collection plate or reached the flow outlet. Figure 4(a) shows the simulated normal component of the impaction velocities for the particle size of 500 nm with different slit lengths. The normalized distance from the center of the nozzle is on the horizontal axis, and the impaction velocity is on the vertical axis. Figure 4(a) shows that the impaction conditions and the impaction velocities can be well controlled in the slit type impactor.

From the particle track data, also the collection efficiencies can be determined. Figure 4(b) shows this for the operation pressures of the study. The markers represent the simulated cutpoints and the solid lines are linear fits. By measuring the cutpoint as a function of the slit length for monodisperse particles, it is possible to determine the effective density of the particles. This is accomplished by comparing the measured cutpoint to the simulated aerodynamic cutpoint. This can be defined from Fig. 4(b), as the cutpoint is now defined as a function of the slit length. Finally, the following equation can be used to calculate the effective density (Kelly & McMurry, 1992):

$$\rho_{\text{eff}} = \frac{C_a d_a^2}{C_m d_m^2} \rho_0, \quad (4)$$

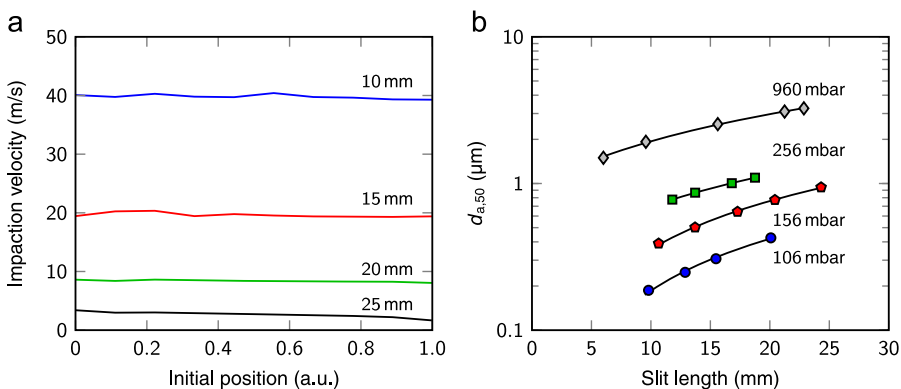


Fig. 4. (a) The normal component of the impaction velocity of 500 nm (aerodynamic diameter) particles as a function of the initial position (normalized distance from the center of the nozzle) of the particles for different slit lengths. The pressure is 106 mbar and the flow rate is 1.18 lpm. (b) The simulated cutpoint diameters as a function of the slit length for different operation pressures. The flow rate is 1.18 lpm for pressures 106–256 mbar and 1.0 lpm for 960 mbar.

where d_a and d_m are the aerodynamic and the mobility diameters, respectively, C_a and C_m are the corresponding slip correction factors and ρ_0 is the unit density.

In this study, the simulated and measured cutpoints are matched by using the effective density as a fitting parameter. The parameter is only an estimate of the effective density, because it includes non-idealities such as the width of the DMA output and uncertainties in the measured flow rates and pressures. However, if the effective density is known a priori (e.g. bulk density) or measured with a reference method, it also provides a way to validate the model. Figure 5(a) schematically shows the fitting procedure of the simulated and measured collection efficiencies for a certain particle size. Also two different methods for defining the essential parameters are illustrated. The slit length where the bounce is initiated is referred as the critical slit value and abbreviated with L_{crit} . The slit length corresponding to a collection efficiency of 50% is referred as L_{50} . In the fitting procedure, the L_{50} values of the simulated and measured collection efficiencies are superimposed by changing the effective density of the particles. As the schematic example in Fig. 5(a) shows, the simulated collection efficiency curves are steeper than the measured ones as a consequence of the non-idealities in the measurement.

There are two different methods for defining the critical slit length principally shown in Fig. 5(a). In the first method (1), the critical slit length $L_{crit,1}$ is obtained straightforwardly from the measured curve corresponding to the onset of rebound. The problem with this method is that it may result in too low impact velocities or even non-impacting particles with the collection efficiencies below 50% arising from the steepness of the simulated curve. The solution is the second method (2) in which we take the critical collection efficiency $\eta_{crit,2}$ corresponding to the onset of the rebound and obtain the critical slit length $L'_{crit,2}$ from the simulated curve. However, this method is sensitive only in a region where the collection efficiency is linearly dependent on the impact velocity. Similar observation on the dependence of normalized impact velocity on collection efficiency in the low pressure impactor was presented also by Rennecke & Weber (2013a). Figure 5(b) illustrates this dependency for a simulated dataset. In other words, the critical collection efficiency is no more unambiguous for high impact velocities. Based on the pros and cons of these two methods, we use the first method (1) when the onset of rebound is seen with the collection efficiencies above 50% and the second method for the collection efficiencies below 50%. The fitting procedure assures that two methods agree at L_{50} .

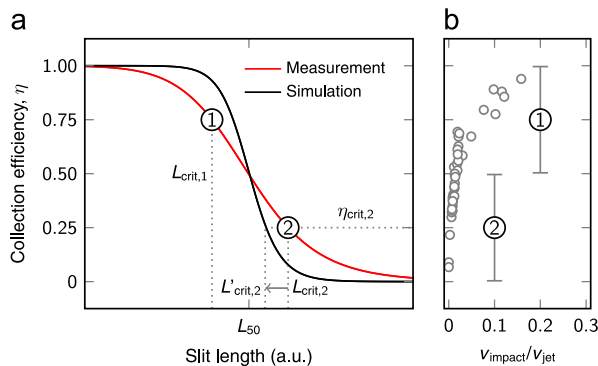


Fig. 5. (a) An example of a measured and simulated collection efficiency curve as a function of the slit length. Two different methods for defining the critical slit length are presented. (b) Normalized impact velocity as a function of the collection efficiency and the operation ranges of the methods.

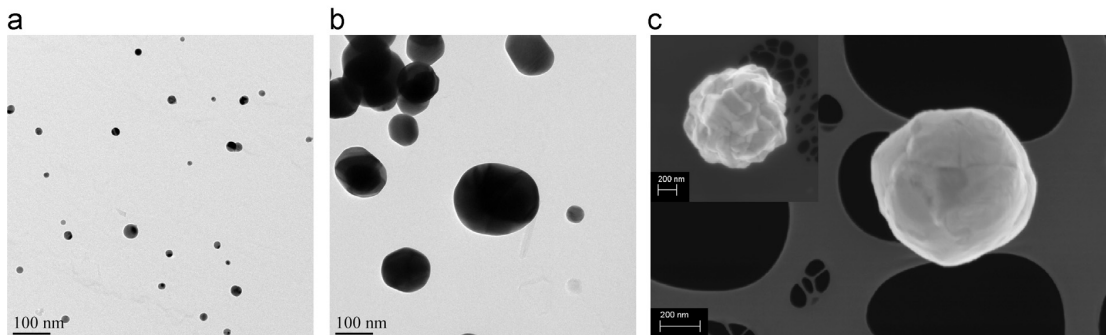


Fig. 6. (a–b) TEM micrographs of the silver nanoparticles generated with the evaporation–condensation method. The temperature of the evaporation furnace ($^{\circ}\text{C}$), the temperature of the first sintering furnace ($^{\circ}\text{C}$) and the flow rate in the sintering furnaces (lpm) were (a) 1200, 600 and 1.0 and (b) 1500, 800 and 0.3, respectively. Both micrographs have the same size bar of 100 nm. (c) An SEM micrograph of a micron-sized silver powder particle sintered at 600 $^{\circ}\text{C}$. The inset shows an unsintered particle. The size bars are 200 nm.

5. Results and discussion

5.1. Morphology and density

In order to be certain that the generated silver particles were spherical, both the morphology and density of the particles were characterized. Figure 6(a) and (b) shows TEM micrographs of the extreme cases, i.e., smallest (~ 20 nm) and largest (> 100 nm) silver particles generated using the evaporation–condensation method. It should be noted that the TEM samples were collected before the size selection. However, even the largest particles (~ 200 nm) are quite spherical with smooth surfaces. An SEM micrograph in Fig. 6(c) shows that an unsintered micron-sized powder particle is near spherical, although somewhat angular shaped. After sintering, the particle surface becomes smoother.

The effective density of the particles was measured and calculated by a method described by Ristimäki et al. (2002), and more recently by Kuuluvainen et al. (2015). In this study, the particles classified by the DMA were measured with an electrical low pressure impactor (Dekati ELPI+) (Järvinen et al., 2014; Keskinen et al., 1992). The first instrument classifies the particles according to their mobility diameter while the latter measures the aerodynamic diameter of the particles. These two particle sizes can be used to calculate the effective density of the particles with Eq. (4).

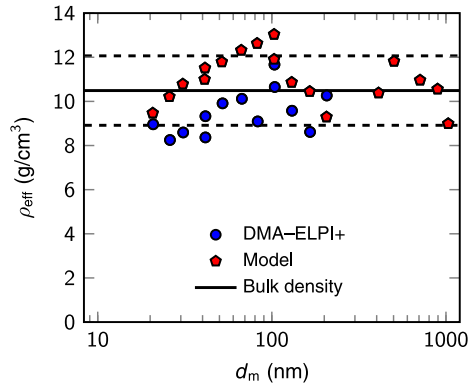


Fig. 7. The effective density of the silver particles as a function of the particle mobility size. Both measured values (DMA–ELPI+) and values obtained from the model are shown. The black line corresponds to the bulk density of silver and the dashed lines give an idea of the estimated experimental error of the method ($\pm 15\%$).

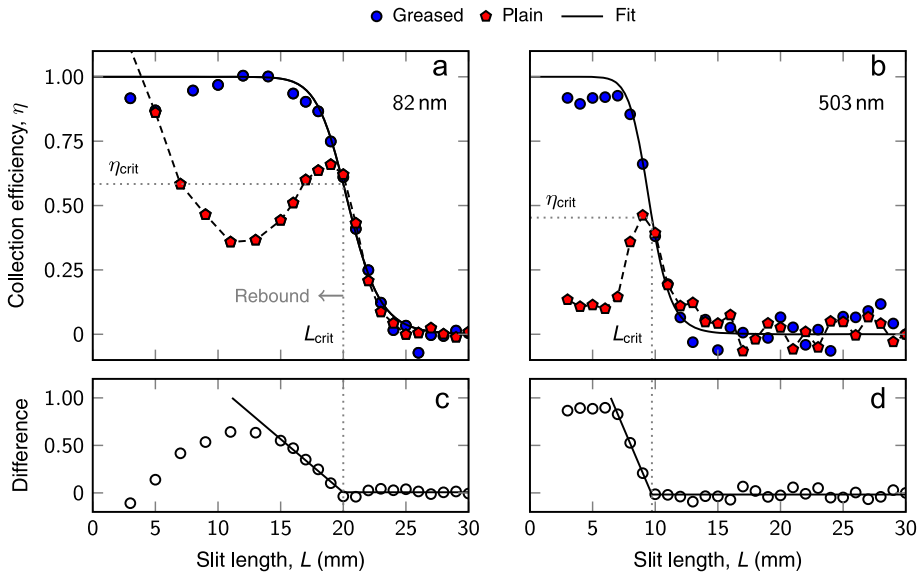


Fig. 8. The collection efficiency of (a) 82 nm (pressure 156 mbar, flow rate 1.18 lpm) and (b) 503 nm (960 mbar, 1.0 lpm) silver particles as a function of the slit length for a greased and a plane impactation surface. An electrical and an optical detection was used for the 82 nm and the 503 nm particles, respectively. (c–d) The onset of rebound is determined from the difference between the fitted collection efficiency curve and the results obtained for the plain surface.

The obtained results (Fig. 7), ranging approximately from 8 to 11 g/cm³, are close to the bulk value of silver (10.49 g/cm³), indicating that the particle material is silver and the shape is spherical. The experimental error using a similar method was reported to be approximately 15% (Ristimäki et al., 2002). Additional discrepancies from the bulk value at smaller particle sizes are likely caused by impurities (de la Mora et al., 2003), whereas, lower effective density of larger particles can most likely be attributed to minor deviations from spherical shape (Brockmann & Rader, 1990). The modeled densities are calculated as described in Section 4. The modeled effective densities are close to the bulk value and measured densities which verifies the validity of the used simulation methods.

5.2. Collection characteristics

Figure 8 shows two examples of the particle collection efficiency curves measured by using a plain and a greased surface in the variable nozzle area impactor. The measurement procedure started in every case with the slit fully open at 30 mm, and the slit length was gradually shortened at intervals of 1 mm down to 3 mm. At longer slit lengths, corresponding to lower particle velocities, no particle impaction on the surface occurs. When the slit length decreases, the particle velocity increases, and, thus, the particles start to impact. When using a greased surface, the collection efficiency reaches ~100% at a sufficiently low slit length.

In the case of the plain surface, the collection efficiency follows the curve obtained with the greased surface, until, at shorter slit lengths it begins to decrease due to the particle rebound from the surface. The slit length corresponding to the point where the efficiency curves diverge is the critical slit length L_{crit} , that is used to calculate the critical velocity of rebound. To define the critical slit lengths from the experimental data, the difference between the fitted collection efficiency curve and the results obtained for the plain surface is used as shown in Fig. 8(c) and (d). The onset of rebound is determined from the intersection of two linear fits.

Interestingly, when using electrical detection, the “collection efficiency” in the case of the plain surface begins to increase again at the shortest slit lengths (high velocities), at some cases reaching even values much higher than 1. This can be inferred as charge transfer between the particles and the surface. There seems to be a certain velocity limit after which the charge transfer phenomenon rapidly increases and starts to dominate the electrical detection at higher velocities. This may refer to the onset of plastic deformation strongly affecting the material properties of the particle or the contact area between the surface and the particle. From Fig. 8(a), we can estimate that this onset for 82 nm particles is at a slit length of approximately 15 mm, which corresponds to an impact velocity of approximately 7.8 m/s. In order to better understand this phenomenon, further research is required.

Figure 9 shows the critical slit values and corresponding critical collection efficiencies as a function of the mobility particle size. As already discussed in Section 4, depending on the critical collection efficiency value either critical collection efficiency or the critical slit value is used to simulate the critical velocities. Error bars in the critical collection efficiency values are calculated by assuming uncertainty of 1 mm in the measured critical slit length.

5.3. Critical velocity of rebound

Figure 10 shows the determined critical velocities of rebound for silver particles as a function of the particle diameter. Colors indicate different operation pressures used in the measurements. Also, the critical velocities for large unsintered particles are shown (see inset in Fig. 6(c)). The different operation pressures were mainly used in order to adjust the cutpoint and operate in different particle size ranges. To be sure that the operation pressure does not affect the results, several particle sizes were measured with different operation pressures. The flow rates were 1.18 and 1.0 lpm for the operation pressures of 106–256 and 960 mbar, respectively. The error bars in Fig. 10 describe the sensitivity of the method

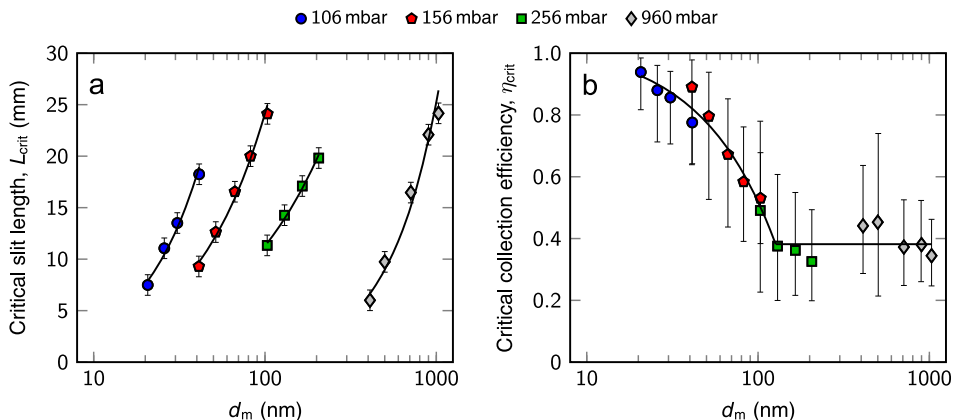


Fig. 9. (a) The critical slit length and (b) the critical collection efficiency as a function of the particle mobility size. The error bars represent an uncertainty of 1 mm in the determined slit length. Solid lines are guides for an eye.

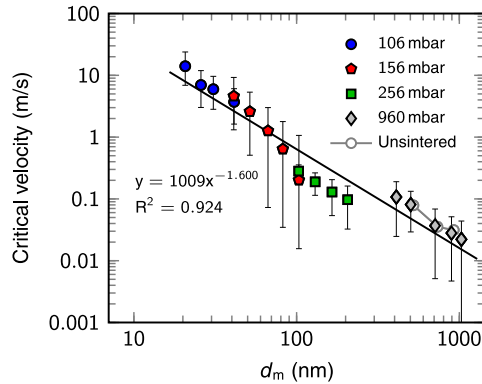


Fig. 10. The critical velocity as a function of the particle mobility diameter. The error bars correlate to an uncertainty of ± 1 mm in determining the critical slit length. Note that the asymmetric error bars are not an effect of the log scale. A power fit (solid line) to the results gives an exponent of -1.6 . (For interpretation of the references to color in the text, the reader is referred to the web version of this paper.)

Table 1

The results and important parameters corresponding to the experiments and the determination of the critical velocity. The effective density ρ_{eff} is a fitting parameter obtained from the model.

d_m (nm)	p (mbar)	L_{50} (mm)	L_{crit} (mm)	ρ_{eff} (g/cm ³)	v_{crit} (m/s)
21	106	9.8	7.5	9.4	14.03
26	106	12.9	11.1	10.2	6.97
31	106	15.5	13.5	10.8	5.96
41	106	20.1	18.2	11.5	3.71
41	156	10.6	9.3	11.0	4.60
52	156	13.7	12.6	11.8	2.59
67	156	17.3	16.5	12.3	1.26
82	156	20.4	20.0	12.6	0.641
103	156	24.3	24.1	13.1	0.202
103	256	11.8	11.3	11.9	0.281
130	256	13.7	14.3	10.9	0.189
165	256	16.8	17.1	10.4	0.129
206	256	18.8	19.8	9.3	0.097
410	960	6.0	7.1	10.4	0.107
503	960	9.6	9.7	11.8	0.081
710	960	15.6	16.5	11.0	0.037
895	960	21.2	22.1	10.6	0.028
1030	960	22.9	24.2	9.0	0.022
522*	960	9.7	10.0	11.2	0.079
735*	960	15.9	16.8	10.3	0.035
924*	960	22.2	23.0	10.5	0.031

* Unsintered.

with respect to the critical slit length. The sensitivity analysis limits are calculated by adding and subtracting 1 mm from the defined critical slit values. Table 1 shows the critical velocity values for each experiment and all the important parameters. As explained in Section 2, according to the current theoretical knowledge, the critical velocity of rebound is inversely proportional to the particle size with an exponent of -1 . However, a fit to the entire experimental data of this work provides an exponent value of -1.6 ($R^2 = 0.924$). The results for unsintered particles show that the fine structure of the particle surface has practically no effect on the critical velocity.

Figure 11 shows the results of this work in relation to the results of other studies. As seen in the variation of the results for micron-sized particles, particle and surface materials significantly affect the critical velocity of rebound. The results of this work are unfortunately not strictly comparable to these, because there are no previous results available for micron-sized spherical silver particles. However, the dependency on the particle size seems to be very similar with several other studies, and the exponent values in Eq. (3) are close to each other. The results of this work differ most from the results by Rogers & Reed (1984) for copper particles on a glass substrate. The amount of data points and the observed particle size range in their study are rather small, which most likely results in a significant uncertainty in the obtained exponent value of -4.8 . However, even if copper can be regarded as similar material compared to silver, there is a difference of several orders of

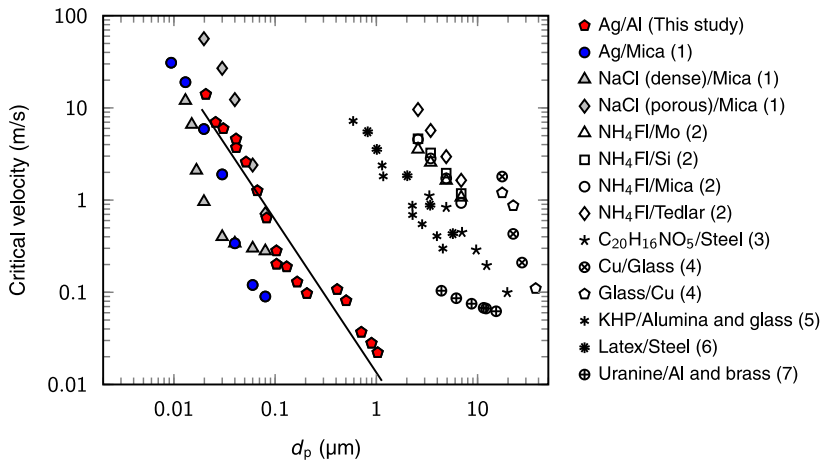


Fig. 11. The results of this work in relation to the previous studies by (1) Rennecke & Weber (2013a), (2) Wall et al. (1990), (3) Wang & John (1988), (4) Rogers & Reed (1984), (5) D'Ottavio et al. (1982), (6) Cheng & Yeh (1979) and (7) Esmen et al. (1978). The legend shows the material of the particle/surface. For spherical particles, the mobility diameter equals the physical particle size.

magnitude in the critical velocity. This implies that the critical velocity of rebound can be highly dependent on both the particle and surface materials.

The results of Rennecke & Weber (2013a), shown in Fig. 11, are determined for spherical silver nanoparticles. Their results differ by a factor of 3–10 from the results of this work. The dependency on the particle size is steeper compared to the results of this work as the exponent value is -3.0 . A power fit to their data set is fairly good ($R^2 = 0.978$), but the size range is restricted and the uncertainty of single data points has not been estimated, except a lower resolution limit. The data points above 40 nm were even below the resolution limit, serving only as an upper limit for the critical velocity. However, compared to the results of micron-sized particles, the results of this work and the results of Rennecke & Weber (2013a) are actually rather close to each other. The discrepancies could be explained by the difference in the surface material used in the experiments. The surface material in this study was aluminum while Rennecke & Weber (2013a) used mica. Unfortunately, there are no literature values of Hamaker constants available for these material pairs. Also the coefficient of restitution is unknown.

One aspect that was theoretically speculated by Rennecke & Weber (2013a) was that they see a transition from the elastic to plastic deformation in their results, and therefore the dependency of critical velocity of rebound on particle size is very steep in their results. They explained that their results cover this transition region, and that the slope of the critical velocity is changing after approximately 40 nm with increasing particle size. Within the accuracy of the method, the results of this study refer to a completely different conclusion: the critical velocity will decay exponentially at least up to one micron. On the other hand, even if the methods exploited in these two studies are close to each other, there are differences in the impactor design, experimental procedures, data interpretation and simulation of the impaction velocities. It might be difficult to recognize all the possible factors affecting the accuracy of the determined critical velocities. We believe that the variable nozzle area impactor with its advantages, connected to the simulation of the impaction velocities and the precise analysis of the particle effective density, provides an accurate method for determining the critical velocity of rebound.

6. Conclusions

The critical velocity of rebound was determined for spherical silver particles covering for the first time the size range from nanoparticles to micron-sized particles. The results show that the critical velocity of rebound decreases from 14 m/s to 0.022 m/s as the particle size increases. Furthermore, a clear exponential decay was observed and the proportionality to the power of -1.6 of the particle size maintained throughout the wide size range. No transitions were seen, even if the present theories, including different approaches to the plastic and elastic deformation of particles, would predict this exponent to be -1 . The obtained exponent value is also very close to the average value of the previous experimental studies. The reliability of the exponent value obtained in this work is also supported by the wide particle size range and a large number of data points. It seems that there might be a yet theoretically unknown physical factor affecting the size dependency of the critical velocity, or the transition from elastic to plastic deformation is evenly covering almost the whole size range of aerosol particles. One possible reason for this would be a size dependency in the Hamaker constant or in the coefficient of restitution.

Comparing the results of this work to the previous studies, it is evident that both the particle and surface material properties can highly affect the critical velocity of rebound. The critical velocities for the micron-sized particles, if extrapolated into the submicron size range, would be one to two orders of magnitude higher than the values measured here

for silver particles. Most of the particle materials measured earlier in the supermicron size range would even require supersonic velocities to bounce in the nanoparticle range. The best agreement with the previous studies was obtained for nanoparticles (Rennecke & Weber, 2013a). However, there were still discrepancies of a magnitude at the maximum. The reason for these discrepancies may lie in the different surface material used in the experiments. Because the methods determining the critical velocities are not so straightforward, it may be difficult to assess the accuracy of the results.

The results of this work fill the gap between the previous experimental studies of the critical velocity for micron-sized particles (Wall et al. 1990) and the more recent results for silver nanoparticles (Rennecke & Weber, 2013a). This is an important step towards understanding the fundamental phenomenon of particle bounce from the molecular to macroscopic size range. As shown in the previous studies for micron-sized particles, the critical velocity can strongly be dependent on the particle and surface materials. This is most likely true also in the case of smaller particles and extended size ranges. Thus, further research is required with different particle materials and different surfaces. The methods introduced in this work, including the variable nozzle area impactor and the determination of the impact velocities with numerical simulations, will be useful in future studies.

Acknowledgements

H. Kuuluvainen and J. Harra acknowledge the TUT's graduate school for financial support. The authors thank Dr. Mari Honkanen and Dr. Essi Sarlin at the Department of Materials Science (TUT) for the electron microscopy images.

References

- Arffman, A., Marjamäki, M., & Keskinen, J. (2011). Simulation of low pressure impactor collection efficiency curves. *Journal of Aerosol Science*, 42(5), 329–340.
- Arffman, A., Yli-Ojanperä, J., Kalliokoski, J., Harra, J., Pirjola, L., Karjalainen, P., Rönkkö, T., & Keskinen, J. (2014). High-resolution low-pressure cascade impactor. *Journal of Aerosol Science*, 78, 97–109.
- Arffman, A., Yli-Ojanperä, J., & Keskinen, J. (2012). The influence of nozzle throat length on the resolution of a low pressure impactor—An experimental and numerical study. *Journal of Aerosol Science*, 53, 76–84.
- Bateman, A., Belassein, H., & Martin, S. (2014). Impactor apparatus for the study of particle rebound: Relative humidity and capillary forces. *Aerosol Science and Technology*, 48(1), 42–52.
- Brockmann, J.E., & Rader, D.J. (1990). A response to nonspherical particles and experimental determination of dynamic shape factor. *Aerosol Science and Technology*, 13(2), 162–172.
- Cheng, Y.-S., & Yeh, H.-C. (1979). Particle bounce in cascade impactors. *Environmental Science and Technology*, 13(11), 1392–1396.
- Dahneke, B. (1971). The capture of aerosol particles by surfaces. *Journal of Colloid and Interface Science*, 37(2), 342–353.
- de la Mora, J.F., de Juan, L., Liedtke, K., & Schmidt-Ott, A. (2003). Mass and size determination of nanometer particles by means of mobility analysis and focused impaction. *Journal of Aerosol Science*, 34(1), 79–98.
- D'Ottavio, T., Goren, S.L., & Samuvel, D. (1982). Aerosol capture in granular beds in the impaction dominated regime. *Aerosol Science and Technology*, 2(2), 91–108.
- Esmen, N.A., Ziegler, P., & Whitfield, R. (1978). The adhesion of particles upon impaction. *Journal of Aerosol Science*, 9(6), 547–556.
- Froeschke, S., Kohler, S., Weber, A.P., & Kasper, G. (2003). Impact fragmentation of nanoparticle agglomerates. *Journal of Aerosol Science*, 34(3), 275–287.
- Harra, J., Mäkitalo, J., Siikonen, R., Virkki, M., Genty, G., Kobayashi, T., Kauranen, M., & Mäkelä, J.M. (2012). Size-controlled aerosol synthesis of silver nanoparticles for plasmonic materials. *Journal of Nanoparticle Research*, 14(6), 870.
- Harra, J., Nikkanen, J.-P., Aromaa, M., Suhonen, H., Honkanen, M., Salminen, T., Heinonen, S., Levänen, E., & Mäkelä, J.M. (2013). Gas phase synthesis of encapsulated iron oxide-titanium dioxide composite nanoparticles by spray pyrolysis. *Powder Technology*, 243, 46–52.
- Ihalainen, M., Lind, T., Arffman, A., Torvela, T., & Jokiniemi, J. (2014). Break-up and bounce of TiO₂ agglomerates by impaction. *Aerosol Science and Technology*, 48(1), 31–41.
- Järvinen, A., Aitoma, M., Rostedt, A., Keskinen, J., & Yli-Ojanperä, J. (2014). Calibration of the new electrical low pressure impactor (ELPI+). *Journal of Aerosol Science*, 69, 150–159.
- Kelly, W.P., & McMurry, P.H. (1992). Measurement of particle density by inertial classification of differential mobility analyzer-generated monodisperse aerosols. *Aerosol Science and Technology*, 17(3), 199–212.
- Keskinen, J., Pietarinen, K., & Lehtimäki, M. (1992). Electrical low pressure impactor. *Journal of Aerosol Science*, 23(4), 353–360.
- Kuuluvainen, H., Arffman, A., Saukko, E., Virtanen, A., & Keskinen, J. (2013). A new method for characterizing the bounce and charge transfer properties of nanoparticles. *Journal of Aerosol Science*, 55, 104–115.
- Kuuluvainen, H., Karjalainen, P., Bajamundi, C.J.E., Maunula, J., Vainikka, P., Roppo, J., Keskinen, J., & Rönkkö, T. (2015). Physical properties of aerosol particles measured from a bubbling fluidized bed boiler. *Fuel*, 139, 144–153.
- Rennecke, S., & Weber, A. (2013a). The critical velocity for nanoparticle rebound measured in a low pressure impactor. *Journal of Aerosol Science*, 58, 135–147.
- Rennecke, S., & Weber, A. (2013b). A novel model for the determination of nanoparticle impact velocity in low pressure impactors. *Journal of Aerosol Science*, 55, 89–103.
- Reuter-Hack, K., Weber, A.P., Rösler, S., & Kasper, G. (2007). First LDA measurements of nanoparticle velocities in a low-pressure impacting jet. *Aerosol Science and Technology*, 41(3), 277–283.
- Ristimäki, J., Virtanen, A., Marjamäki, M., Rostedt, A., & Keskinen, J. (2002). On-line measurement of size distribution and effective density of submicron aerosol particles. *Journal of Aerosol Science*, 33(11), 1541–1557.
- Rogers, L.N., & Reed, J. (1984). The adhesion of particles undergoing an elastic-plastic impact with a surface. *Journal of Physics D: Applied Physics*, 17(4), 677–689.
- Saukko, E., Kuuluvainen, H., & Virtanen, A. (2012). A method to resolve the phase state of aerosol particles. *Atmospheric Measurement Techniques*, 5(1), 259–265.
- Scheibel, H.G., & Porstendörfer, J. (1983). Generation of monodisperse Ag- and NaCl-aerosols with particle diameters between 2 and 300 nm. *Journal of Aerosol Science*, 14(2), 113–126.
- Schmidt-Ott, A. (1988). New approaches to *in situ* characterization of ultrafine agglomerates. *Journal of Aerosol Science*, 19(5), 553–563.
- Seipenbusch, M., Rothenbacher, S., Kirchoff, M., Schmid, H.-J., Kasper, G., & Weber, A. (2010). Interparticle forces in silica nanoparticle agglomerates. *Journal of Nanoparticle Research*, 12(6), 2037–2044.
- Seipenbusch, M., Toneva, P., Peukert, W., & Weber, A.P. (2007). Impact fragmentation of metal nanoparticle agglomerates. *Particle and Particle Systems Characterization*, 24(3), 193–200.

- Tsai, C.-J., Pui, D.Y., & Liu, B.Y. (1990). Capture and rebound of small particles upon impact with solid surfaces. *Aerosol Science and Technology*, 12(3), 496–507.
- Virtanen, A., Joutsensaari, J., Koop, T., Kannosto, J., Yli-Pirilä, P., Leskinen, J., Mäkelä, J.M., Holopainen, J.K., Pöschl, U., Kulmala, M., Worsnop, D.R., & Laaksonen, A. (2010). An amorphous solid state of biogenic secondary organic aerosol particles. *Nature*, 467(7317), 824–827.
- Virtanen, A., Kannosto, J., Kuuluvainen, H., Arffman, A., Joutsensaari, J., Saukko, E., Hao, L., Yli-Pirilä, P., Tiihonen, P., Holopainen, J.K., Keskinen, J., Worsnop, D.R., Smith, J.N., & Laaksonen, A. (2011). Bounce behavior of freshly nucleated biogenic secondary organic aerosol particles. *Atmospheric Chemistry and Physics*, 11(16), 8759–8766.
- Wall, S., John, W., Wang, H.-C., & Goren, S.L. (1990). Measurements of kinetic energy loss for particles impacting surfaces. *Aerosol Science and Technology*, 12(4), 926–946.
- Wang, H.-C., & John, W. (1988). Dynamic adhesion of particles impacting a cylinder. In K.L. Mittal (Ed.), *Particles on Surfaces 1: Detection, Adhesion, and Removal*. Plenum Press: New York, pp. 211–224.
- Wang, H.-C., & Kasper, G. (1991). Filtration efficiency of nanometer-size aerosol particles. *Journal of Aerosol Science*, 22(1), 31–41.
- Weir, G., & McGavin, P. (2008). The coefficient of restitution for the idealized impact of a spherical, nano-scale particle on a rigid plane. *Proceedings of the Royal Society A: Mathematical, Physical and Engineering Sciences*, 464(2093), 1295–1307.
- Zihlmann, S., Lüönd, F., & Spiegel, J.K. (2014). Seeded growth of monodisperse and spherical silver nanoparticles. *Journal of Aerosol Science*, 75, 81–93.

Paper III

Heino Kuuluvainen, Anssi Arffman, Anssi Järvinen, Juha Harra, and Jorma Keskinen,

“The effect of materials and obliquity of the impact on the critical velocity of rebound”



Aerosol Science and Technology, Published online 14 Nov 2016

doi: 10.1080/02786826.2016.1260088

© Taylor & Francis Group



The effect of materials and obliquity of the impact on the critical velocity of rebound

Heino Kuuluvainen , Anssi Arffman, Anssi Järvinen, Juha Harra , and Jorma Keskinen

Department of Physics, Tampere University of Technology, Tampere, Finland

ABSTRACT

The critical velocity of rebound was determined for spherical ammonium fluorescein particles in the size range of 0.44–7.3 μm . The method was based on measurements with a variable nozzle area impactor (VNAI) and numerical simulations. A comparison to previous results with spherical silver particles obtained with the same method showed that the critical velocity was approximately two orders of magnitude higher for ammonium fluorescein than for silver at the same size range. Among the hard test materials, including steel, aluminium, molybdenum, and Tedlar, the surface material had no significant effect on the critical velocity of rebound within the accuracy of the method. On the contrary, the critical velocity was observed to be highly dependent on the obliquity of the impact at the onset of rebound. While the ratio of the maximum tangential and normal velocities was defined as a measure for the obliquity, the critical velocity was found to be more than a magnitude smaller for very oblique impacts with the velocity ratio above 9 than for close-to-normal impacts with the velocity ratio below 1.5. The results of this study can be considered as a link between the recently published critical velocity results for nanoparticles and the older results for micron-sized particles.

ARTICLE HISTORY

Received 11 August 2016
Accepted 4 November 2016

EDITOR



Yannis Drossinos

1. Introduction

Particle rebound from a surface is of interest in many fields of aerosol science. It has been known for a long time as an unwanted phenomenon causing artifacts in inertial impactors (Dzubay et al. 1976; Chang et al. 1999) and triboelectric charging of particles in medical inhalators (Matsusaka et al. 2010). Also in aerosol mass spectrometers, the particle rebound has more recently been recognized as a significant source of error and uncertainty (Kang et al. 2015). On the other hand, the research of the particle rebound has provided valuable information on some particle properties. The amorphous solid state of secondary organic aerosol particles (SOA) was discovered by investigating the bounce behavior of the particles in a cascade impactor (Virtanen et al. 2010). The research has been further developed toward monitoring the particle rebound as a function of the relative humidity in specific low pressure impactor systems (Saukko et al. 2012; Bateman et al. 2014; Pajunoja et al. 2015). In the field of engineered nanoparticles, the particle rebound and fragmentation has been exploited to study the binding energies of agglomerates (Froeschke et al. 2003; Seipenbusch et al. 2007; Ihalainen et al.

2014). Recently, the triboelectric charging during resuspension and rebound was proposed to have a significant effect on the dynamics, sampling, and filtration of indoor aerosols such as fungal spores (Kuuluvainen et al. 2016).

The critical velocity of rebound is a fundamental parameter in the interaction of a particle and a surface. It is the smallest incident velocity with which the particle rebounds from the surface. A theory predicting the critical velocities for aerosol particles was formed by Dahneke (1971) and later specified by Wall et al. (1990). The basic idea in the theory is that the sum of the initial kinetic energy and the potential energy of the adhesion force field, reduced by the energy losses during the collision, has to be larger than the adhesion energy for a particle to rebound. According to the theory, the critical velocity is inversely proportional to the particle size and it depends on the material properties of both the particle and the surface. The effect of adhesion in the particle–surface interaction can be described quantitatively with the Hamaker constant and the energy losses with a coefficient of restitution, i.e., the relation of the rebound and incident velocities. The critical velocity of rebound is in principle linked to a normal impact or to the normal component of

CONTACT Heino Kuuluvainen  heino.kuuluvainen@tut.fi  Department of Physics, Tampere University of Technology, Korkeakoulunkatu 3, 33720 Tampere, Finland.

Color versions of one or more of the figures in the article can be found online at www.tandfonline.com/uast.

© 2016 American Association for Aerosol Research

the incident velocity. However, it has been found that in oblique impacts the capture limit for the normal velocity may be lower than in normal impacts. The experiments with large microspheres have shown that the coefficient of restitution may increase with a decreasing contact angle on rough surfaces, even up to unrealistically high values above unity with contact angles smaller than 10° (Brach et al. 2000). Wang and John (1988) concluded that the critical velocity of micron-sized particles determined with an impactor was lower than the critical velocity based on the direct measurement of the velocities and the coefficient of restitution, because of the tangential velocity in the impactor. However, they did not present any quantitative analysis on the effect of the obliquity on the critical velocity. Also a recent modeling work by Chen et al. (2015) predicted a rapidly decreasing critical velocity with an increasing contact angle.

Experimental results for the critical velocity of rebound in the size range above $1\ \mu\text{m}$ were reviewed by Wall et al. (1990). They found differences of more than a magnitude between the critical velocities for different particle and surface materials. However, the variety of different experimental methods and the lack of uncertainty estimation may prevent to reveal the actual role of material properties and their effect on the critical velocity. The critical velocity of rebound has also recently been determined in the sub-micron size range. Rennecke and Weber (2013) obtained critical velocity values for silver and sodium chloride nanoparticles using a combination of experimental and numerical methods for inertial impactors. A similar method with a new type of an impactor, the variable nozzle area impactor (VNAI), was exploited to determine the critical velocity of rebound for spherical silver particles in a wide size range from 20 nm to $1\ \mu\text{m}$ (Arffman et al. 2015). Both of these studies in the sub-micron size range predicted an exponential decay of the critical velocity as a function of the increasing particle size, similar to the results reviewed by Wall et al. (1990). However, if these critical velocity values are extrapolated to the same particle size range, a difference of several orders of magnitude would be seen. Despite the relatively large amount of data, it is still unclear what is the role of different particle and surface materials on the critical velocity. Furthermore, it is not known if the different methods used in the experiments and data analysis agree with the same materials and in the same size range. The experimental data of the critical velocity of rebound have also recently motivated researchers to develop and improve theoretical models (Stace 2015; Xie et al. 2016).

In this study, we present new results for the critical velocity of rebound for ammonium fluorescein particles, obtained using the recently introduced VNAI and numerical simulations. The main idea of this study is to

compare the critical velocity for different particle and surface materials determined with the same method, and, on the other hand, discuss about the differences between the various experimental methods. The goal of this study is to form a link between the recently published critical velocity results for nanoparticles and the older results for micron-sized particles. In addition, we investigate the effect of tangential velocity component on the critical velocity in the impactor.

2. Methods

2.1. Particle generation and size classification

Solid spherical ammonium fluorescein ($\text{C}_{20}\text{H}_{16}\text{NO}_5$) particles in the size range of 2–8 μm were generated using a vibrating orifice aerosol generator (VOAG) introduced by Berglund and Liu (1973). In the VOAG, a liquid solution is fed into a vibrating orifice generating highly monodisperse droplets. Then the liquid droplets are dispersed and dried in order to generate a monodisperse aerosol of desired nonvolatile material and particle size. The diameter of the liquid droplet can be calculated through an equation depending on the volumetric liquid feed flow and the frequency of the disturbance in the vibrating orifice (Berglund and Liu 1973). The final particle diameter is a function of the droplet diameter and the volumetric concentration of a nonvolatile solute in a volatile solvent. In this study, solutions of ammonium fluorescein were prepared by dissolving fluorescein powder ($\text{C}_{20}\text{H}_{12}\text{O}_5$, Alfa Aesar, purity 90 + %) in aqueous ammonia (NH_4OH) as described by Vanderpool and Rubow (1988). The final concentration of ammonium fluorescein varied from 0.08 to 2.2 g/m^3 and the frequency of the disturbance was 33 or 60 Hz. The feed flow induced by a syringe pump was kept constant (10 ml/h) and the diameter of the orifice was 20 μm . The relative humidity (RH) of the dispersion and dilution air was adjusted to 30% in order to prevent too fast drying of the droplets as described by Wall et al. (1990). A schematic of the experimental setup using the VOAG is seen in Figure 1a. The generated particles were neutralized with a radioactive source (Am-241) after the VOAG. The stability of the generator was monitored along with the particle detection as described later.

Particles in the size range below $1\ \mu\text{m}$ were generated using an atomizer aerosol generator (Topas ATM 220) and an ammonium fluorescein solution with a concentration of 8.8 g/m^3 . After the atomizer, the aerosol was dried with a humidity-controlled dilution air flow (RH 30–32%). The particles were size-classified with a Vienna type differential mobility analyzer (DMA). A schematic of the measurement setup is seen in Figure 1b. Because of

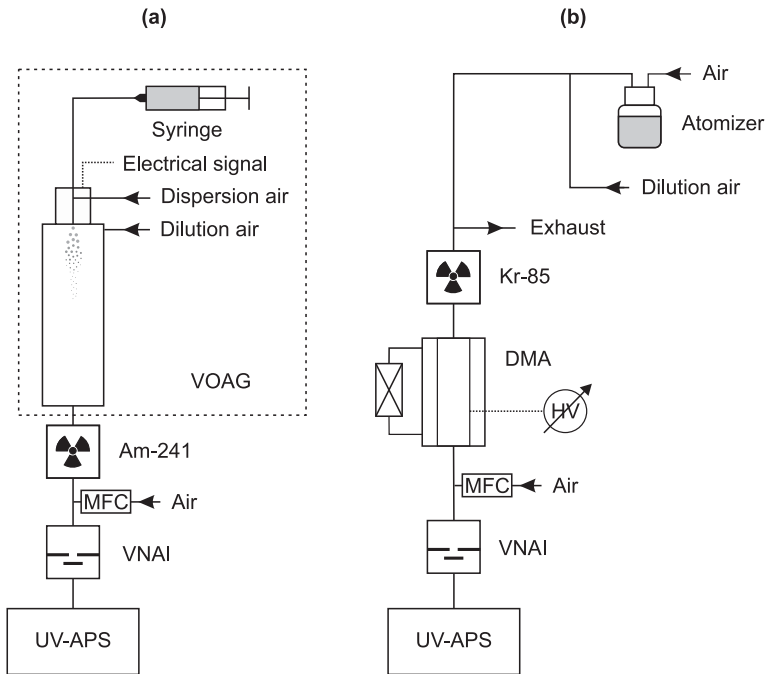


Figure 1. Schematics of the measurement setups (a) for the particles generated with a vibrating orifice aerosol generator (VOAG) covering the particle size range of 2–8 μm , and (b) for the particles generated with an atomizer and classified with a differential mobility analyzer (DMA) covering the size range below 1 μm . MFC is an abbreviation for a mass flow controller, VNAI for a variable nozzle area impactor, and UV-APS for an ultraviolet aerodynamic particle sizer.

multiply charged particles, the output of the DMA was not ideally monodisperse and the multiply charged particles were distinguished with the detection method. A radioactive source (Kr-85) was used before the DMA to create a net neutral equilibrium charge distribution for the aerosol.

2.2. Critical velocity experiment

The measurements were carried out using a variable nozzle area impactor (VNAI). This recently introduced instrument (Arffman et al. 2015) is designed to study the critical velocity of rebound and other surface interaction phenomena as a function of the particle impact velocity. It consists of a narrow slit, and the nozzle area can be varied by manually changing the slit length (3–30 mm). A detailed description of the VNAI can be found from the work of Arffman et al. (2015). In this study, some of the dimensions and parameters of the impactor varied between different experiments. The volumetric flow through the impactor varied from 0.7 to 10 lpm, the impactor nozzle width from 0.1 to 2.0 mm, and the jet-to-plate distance from 0.5 to 2.0 mm, depending on the operated particle size range. The impactor flow was adjusted with the help of a mass flow controller (MFC) before the

VNAI (Figure 1). Four different substrate materials, including steel, aluminium, molybdenum, and Tedlar[®] (polyvinyl fluoride), and a substrate greased with Apiezon-L vacuum grease were used in the impactor. The metal substrates were equally manufactured and finally polished. The Tedlar substrate was compiled from a steel substrate that was covered with a layer of commercial adhesive tape with a Tedlar backing (3M, Weather Resistant Film Tape 838). Before the experiments, the non-greased substrates were flushed with isopropanol, distilled water, and clean pressurized air, respectively.

The collection efficiency of the VNAI was determined as a function of the slit length by measuring the particle concentration after the impactor and dividing it by a reference. As a primary reference, the concentration was measured after the impactor with the slit fully open. The secondary reference was the concentration measured by bypassing the impactor, but this was only used to ensure that the collection efficiency of the impactor was insignificant with the slit fully open. Different detection methods were used to measure the particle concentration, depending on the operated particle size range. For the particles generated with the VOAG, the concentration was measured with an ultraviolet aerodynamic particle sizer (UV-

Table 1. Experimental parameters for each particle size. VOAG refers to a vibrating orifice aerosol generator. Either (1) the concentration of a single size distribution channel or (2) the total concentration of an ultraviolet aerodynamic particle sizer (UV-APS) was used in the detection. The impactor nozzle width, jet-to-plate distance and flow are the parameters of a variable nozzle area impactor (VNAI).

d_p (μm)	Generation method	Detection method	Impactor nozzle width (mm)	Impactor jet-to- plate (mm)	Impactor flow (lpm)
0.44	Atomizer	UV-APS ¹	0.1	0.5	4.8
0.87	Atomizer	UV-APS ¹	0.1	0.5	0.7
2	VOAG	UV-APS ²	0.5	0.5	2.0
2.5	VOAG	UV-APS ²	2.0	2.0	10.0
3.4	VOAG	UV-APS ²	0.5	2.0	1.0
4.3	VOAG	UV-APS ²	0.5/2.0	2.0	1.0/4.0
5.2	VOAG	UV-APS ²	2.0	2.0	4.0
7.3	VOAG	UV-APS ²	2.0	2.0	4.0

APS, Model 3314, TSI Inc., Shoreview, MN, USA) using the total concentration given by the instrument. In the size range of 0.47–1.0 μm , the concentration was also measured with the UV-APS, but only a single channel from the size distribution, corresponding to the singly charged particle size penetrated through the DMA, was taken into account. In both cases, the UV-APS was used without the ultraviolet laser and fluorescence measurement, operating as an aerodynamic particle sizer.

An overview of the conducted experiments can be seen in Table 1. Altogether, nine different particle sizes were measured, two different particle generation methods were used and the concentration was measured using two different detection methods. The particle sizes for the VOAG generated particles were calculated and the particle sizes classified with the DMA were determined from the voltage and sheath flow. Table 1 also includes the impactor nozzle width and impactor flow that are crucial input parameters for the numerical simulation and the determination of the impact velocities. Each particle size was measured with a greased impactor substrate and with four different non-greased substrates. An experiment for one particle size with a single substrate included the measurement of the collection efficiency of the VNAI as a function of the slit length. The concentration was measured from 30 to 60 s for a single slit length in order to minimize the effect of random noise to the results. The reference concentration measured with the slit fully open was taken between every fourth or fifth slit lengths. The substrate loading caused by the collected particles was calculated to be less than 5%.

2.3. Numerical simulation

The impact velocities were determined by using computational fluid dynamics (CFD) simulation. A detailed description and the principles of the method can be found

in previous studies (Arffman et al. 2011, 2015). Briefly, the simulations were conducted in two steps. The flow field was first simulated (2D) with ANSYS Fluent software by using the mass flow rate through the impactor and the static pressure at the outlet as boundary conditions. As the Reynolds' numbers were in the order of 500, the flow field could be assumed to be laminar. The changes of the slit length and the nozzle area were taken into account in the simulation by changing the mass flow rate per depth of the slit length. In the second step, the particle trajectories were solved using a Lagrangian particle tracking method. By solving the trajectories, we were able to determine the collection efficiencies and impact velocities of the particles. The computation grid independence of the results was confirmed by adapting the grid until the results remained unaffected by further refinements. The grid had to be more dense near the collection substrate, where the resolution of the grid was below 1 μm .

Experimental and simulated collection efficiency curves were fitted by superimposing the cutpoints of the two curves. The outcome from the fit was the effective density parameter obtained for each measurement with greased substrates. The effective density parameter was not only an estimate for the particle density, but it could be used to validate the simulation method as described by Arffman et al. (2015). Several non-idealities, such as the uncertainties in the measured flow rates and pressures, could slightly affect the value of the effective density parameter. However, as the density of the particle material was known a priori, a comparison of the effective density values to the material density could be used as a validation for the simulation.

Two parameters obtained from the measurement, corresponding to the onset of rebound, were used for the simulation to determine the critical velocity of rebound. They were the critical slit length and the critical collection efficiency, for which the experimental determination is presented later. Because the simulated collection efficiency curves were sharper compared to measured ones, the impact velocities had to be determined using a parameterization when the collection efficiency was below 50%. At this region, the critical collection efficiency was used to determine the corresponding slit length on the simulated collection efficiency curve. Above 50%, the critical slit length obtained from the measured curve was directly used for the simulation. This procedure and the parameterization was described in detail by Arffman et al. (2015).

3. Results and discussion

3.1. Morphology, density, and collection efficiency

In order to have a fundamental approach on the critical velocity of rebound for ammonium fluorescein particles

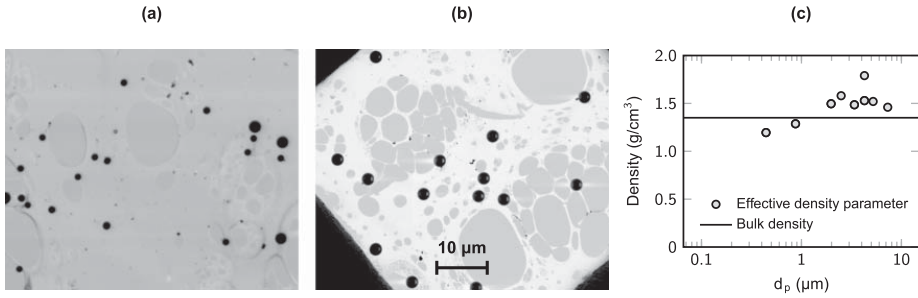


Figure 2. (a–b) Scanning electron microscope (SEM) micrographs of the ammonium fluorescein particles and (c) the effective density parameter obtained from the fitting process as a function of the particle size. (a) 0.47 μm particles were generated with an atomizer and size-classified with a differential mobility analyzer (DMA). Also doubly charged larger particles penetrated through the DMA can be seen. Monodisperse (b) 2.5 μm particles were generated with a vibrating orifice aerosol generator (VOAG). (c) The solid line represents the bulk density of ammonium fluorescein.

corresponding to previous studies (Wang and John 1988; Wall et al. 1990), we wanted to measure dense and spherical particles. Figures 2a and b show two examples of the scanning electron microscope (SEM) micrographs of the generated ammonium fluorescein particles. A clear spherical morphology can be seen in both of these micrographs, despite of the variation of the generation method and the particle size. The 2.5 μm particles generated with the VOAG (Figure 2b) seemed to have a slightly apple-like morphology with a pit on top of the particles. However, the projection of the particles was spherical with very smooth surface and dense structure. Among the 0.47 μm particles generated with the atomizer and size-classified with a DMA (Figure 2a), also larger doubly charged particles, penetrated through the DMA but not detected for the collection efficiency, can be seen. The morphology seemed to be very spherical in a wide particle size range with this generation method.

The effective density values obtained from the fitting process of the model and the experiment are seen in Figure 2c. The values were close to the bulk density of ammonium fluorescein that is 1.35 g/cm^3 according to Stöber and Flachsbarth (1973). This verified the validity of the used simulation methods because the use of the effective densities close to the bulk density provided simulated collection efficiencies corresponding to the measured collection efficiencies. Therefore, also the impact velocities provided by the simulation could be assumed to be realistic. A similar validation for the same method was carried out by Arffman et al. (2015) with spherical silver particles.

Figure 3 shows two examples of the collection efficiency of the VNAI as a function of the slit length. Both of these examples were measured using a greased substrate and a non-greased steel substrate in the impactor. In every case, the collection efficiency was approximately

zero at the slit lengths close to the maximum. When the slit length was shortened, the collection efficiency started to increase, reaching approximately one with the greased substrate. With the non-greased substrate, the collection efficiency differed from the curve measured with the greased substrate at some point, indicating the onset of rebound. The slit length and the collection efficiency corresponding to the onset of rebound were the critical slit length L_{crit} and the critical collection efficiency η_{crit} , respectively. The reincrease of the collection efficiency seen in Figure 3a with slit lengths below 20 mm most probably referred to the onset of plastic deformation with higher impact velocities. Similar behavior was also observed by Arffman et al. (2015) for silver particles.

3.2. Critical velocity of rebound and obliquity of impacts

In an impactor, particles can impact with different normal and tangential velocities as shown in the schematic in Figure 4a. At the onset of rebound, some of the impacted particles have a normal velocity that exceeds the critical velocity and they rebound. According to previous studies, the presence of the tangential velocity component may lower the critical normal velocity required for the rebound (Wang and John 1988; Brach et al. 2000). This may lead to a situation where the rebound begins at a certain location on the impactor substrate from the particles having a lower normal velocity and higher tangential velocity compared to the particles impacting with the maximum normal velocity. It is not possible to distinguish the location of the onset of rebound and the exact velocity components involved. The maximum normal velocity forms an upper limit for the critical velocity of rebound and the lower limit is the normal velocity component from the particles with the

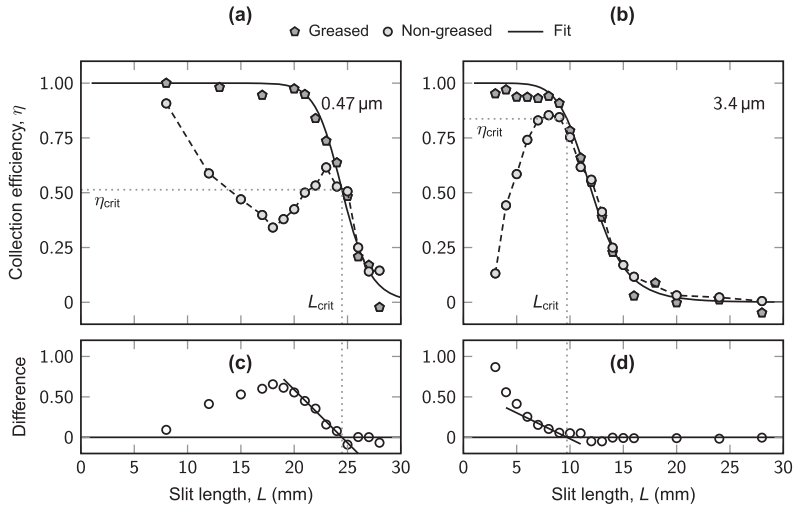


Figure 3. (a–b) Two examples of the collection efficiency of a variable nozzle area impactor (VNAI) as a function of the slit length. In these examples, the non-greased substrate was steel. The onset of rebound was determined from (c–d) the difference of the non-greased collection efficiency and the fitted curve. The critical slit length L_{crit} and the critical collection efficiency η_{crit} correspond to the onset of rebound.

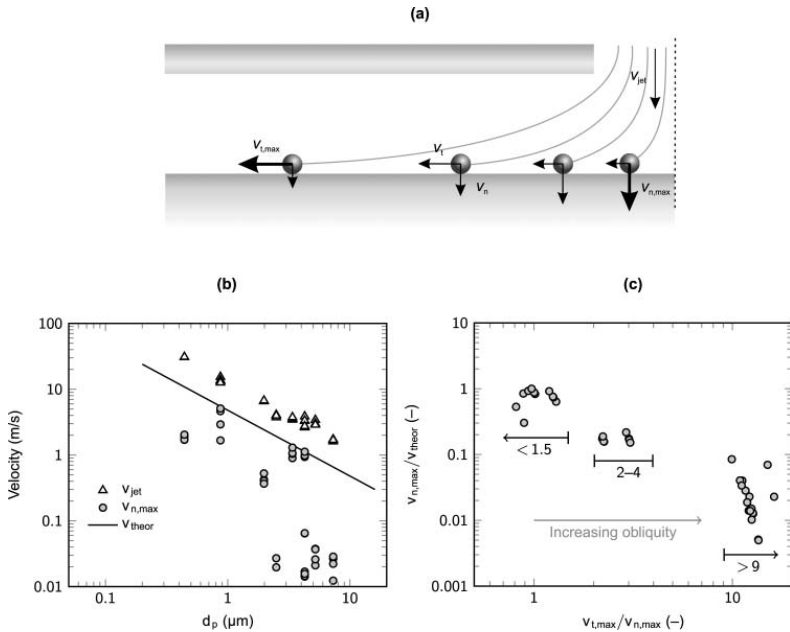


Figure 4. (a) A schematic of the particles impacting with different normal and tangential velocities. Bold arrows represent the maximum values of these components. (b) The velocities corresponding to the onset of rebound as a function of the particle size for ammonium fluorescein particles. The maximum value of the normal velocity component $v_{n,max}$ and the jet velocity v_{jet} were determined using simulations. Also the theoretical size dependency of the critical velocity of rebound v_{theor} is shown. (c) The maximum normal velocity normalized with the theoretical critical velocity as a function of the ratio of the maximum tangential $v_{t,max}$ and normal velocities. The ratio of the maximum tangential and normal velocities corresponds to the obliquity of the impact. Three different groups of data can be seen.

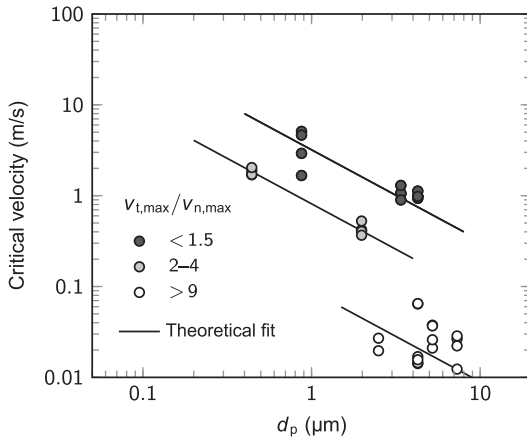


Figure 5. The critical velocity of rebound as a function of the particle size for ammonium fluorescein particles with respect to the obliquity of the impact. Three different groups having different ratios of the maximum tangential and normal velocities are distinguished. Also the theoretical fits are shown, separately for different groups.

maximum tangential velocity. For the experiments of this work, the lower limit was calculated to be close to the upper limit. Even in the worst case, it was approximately 40% of the upper limit. We could have chosen any estimate between these limits to represent the critical velocity, but to be comparable also with the previous studies (Wang and John 1988; Rennecke and Weber 2013; Arffman et al. 2015), we used the maximum normal velocity $v_{n,max}$. Furthermore, the maximum tangential velocity $v_{t,max}$ was used to describe the obliquity of the impact. These values, as well as the jet velocity v_{jet} , were obtained from the simulation.

Figure 4b shows the maximum normal velocity and the jet velocity corresponding to the onset of rebound as a function of the particle size. It should be noted that the jet velocity was only one factor describing the impactor flow field at the onset of rebound. Also the flow through the impactor and the nozzle width had been changed between different measurements. A lot of deviation can be seen in the maximum normal velocities compared to the theoretical particle size dependency shown in Figure 4b. The theoretical critical velocity v_{theor} shown in Figure 4b is inversely proportional to the particle size and it was fitted to form an upper limit for the experimental values. The explanation for the deviation of the experimental values was found in the variation of the impactor flow field and the tangential velocity component between different measurements. The ratio of the maximum tangential and normal velocities was defined as a measure of obliquity for the impact. Furthermore,

we normalized the maximum normal velocity at the onset of rebound with v_{theor} in order to have a size-independent but arbitrary quantity for the critical velocity. This normalized maximum normal velocity is presented as a function of the ratio of the maximum tangential and normal velocities in Figure 4c. The results showed that the increase of obliquity and the tangential velocity component remarkably decreased the normal velocity required for the rebound. Figure 4c also shows that the data could be divided into three different groups. The first group was formed for the data of close-to-normal impacts with the velocity ratio below 1.5 and the second group for higher obliquity and the velocity ratios between 2 and 4. In the third group, the impacts were extremely oblique with the velocity ratio above 9.

Consequently, the results of the critical velocity corresponding the maximum normal velocity are shown in Figure 5 divided into the three groups. The obliquity seemed to affect significantly the critical velocity of rebound. Based on the fits with the same theoretical size dependency, the data for velocity ratios of 2–4 differed from the data of the close-to-normal impacts (ratio < 1.5) by a factor of 4. The critical velocity values for the most oblique impacts with a velocity ratio above 9 were more than a magnitude lower than the critical velocities for the close-to-normal impacts. The latter data had a significant deviation and uncertainty in the particle size dependency because of the decreasing accuracy of the simulation with extremely low velocities. These results are in line with the previous observations (Wang and John 1988; Brach et al. 2000; Chen et al. 2015). Based on our results, it is possible to estimate quantitatively the effect of obliquity on the critical velocity in impactors.

3.3. Effect of different particle and surface materials

Based on the observation of the critical velocity of rebound and the obliquity of impacts, we use the data of the close-to-normal impacts for a detailed analysis and comparison to previous studies. Figure 6 shows this critical velocity as a function of the particle size with respect to the previous results for silver particles (Arffman et al. 2015) and for ammonium fluorescein particles (Wang and John 1988; Wall et al. 1990). We concentrate on three issues, which are the effect of the particle material, the effect of the surface material, and different methods in determining the critical velocity of rebound.

To be sure that the results of Arffman et al. (2015) were comparable to the results of this work, the old results were resimulated and the impacts were found to be close-to-normal with a velocity ratio below 2. The effect of the particle material on the critical velocity seemed to be significant. Arffman et al. (2015) used

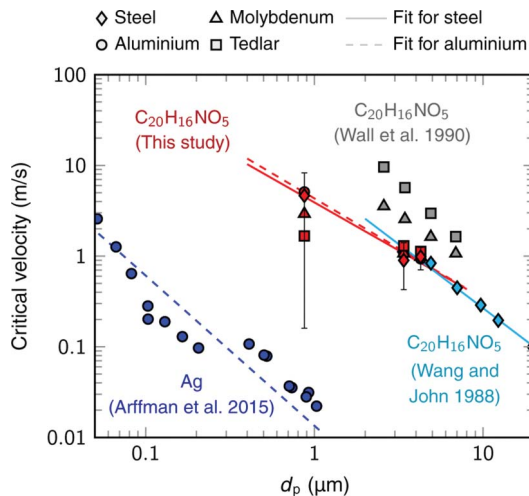


Figure 6. The critical velocity of rebound as a function of the particle size. The results of this study for ammonium fluorescein ($\text{C}_{20}\text{H}_{16}\text{NO}_5$) are shown with respect to the previous results for silver particles (Arffman et al. 2015) and for ammonium fluorescein particles (Wang and John 1988; Wall et al. 1990). The marker shape represents the surface material. Power fits for steel (solid lines) and aluminium (dashed lines) are shown. The error bars, shown as an example for steel, represent the sensitivity of the method.

an aluminium surface for silver particles, but the difference to the results of this study for ammonium fluorescein particles with the same surface material and the same method was substantial (Figure 6). At the particle size of one micron, the difference in the critical velocity was approximately two orders of magnitude. There was also a difference in the particle size dependence of these two particle materials. A power fit for the silver data resulted in an exponent value of -1.6 and for the ammonium fluorescein data an exponent value of -1.1 . However, the value for ammonium fluorescein may not be as reliable as for silver because of a smaller amount of data, more restricted size range and uncertainty related to some of the data points. The error bars for our results describing the sensitivity of the method were estimated by assuming an uncertainty of ± 1 mm in the measured critical slit length (Figure 6). The particle sizes of 3.4 and 4.3 μm were the most reliable data points in this respect. It should be noted that the error bars only formed an estimation for the accuracy of the method, and also a different estimation could have been used, for example, by assuming a smaller uncertainty in the measured critical slit length. However, with the current error limits, we were able to estimate the relative reliability of different data points and the overall accuracy of the method.

A good agreement was achieved between the results of this study for ammonium fluorescein particles on a steel surface and the results of Wang and John (1988) with the same materials (Figure 6). The agreement was especially good with the most reliable data points of our results. Wang and John (1988) also used an impactor and computational methods to determine the critical velocity. Comparing the results of this study for molybdenum and Tedlar surfaces to the results of Wall et al. (1990) with the same materials showed relatively small but clear differences (Figure 6). Wall et al. (1990) used laser Doppler velocimetry to measure the impact and rebound velocity in accurately normal collisions. In an impactor, particles always have some tangential velocity when they impact, which may result in lower critical velocities compared to the laser Doppler velocimetry measurements. This explanation was already raised by Wang and John (1988) and it is in line with our results for increasing obliquity.

The surface material seemed to have no observable effect on the critical velocity of rebound (Figure 6). It is possible that the effect of the surface material was hidden in the uncertainty of the method and could be seen with a more accurate method. However, no difference was seen between the test materials even for the most reliable data points of our results. Also the power fits shown in Figure 6 for steel and aluminium were almost the same with the exponent value of -1.1 . All of the surface materials used in this work were hard and plane on a macroscopic scale, including three metals and one plastic material. Most likely, the results would have been different with softer or porous materials. Even if the effect of obliquity on the critical velocity is linked to the microscopic surface roughness, we did not see any clear differences between the polished metal surfaces and the Tedlar surface. Wall et al. (1990) reported that the adhesion surface energy was an important factor affecting the critical velocity of rebound. However, the effect of the surface energy was small compared to the effect of the particle material and the obliquity of the impact found in this study, as well as, compared to the accuracy of our method. To investigate the effect of the surface material properties on the critical velocity of rebound, measurements for soft and porous materials should be conducted in future and the accuracy of the method should be improved.

4. Summary and conclusions

In this study, the critical velocity of rebound was determined for ammonium fluorescein particles in a size range of 0.44 – 7.3 μm by using a variable nozzle area impactor (VNAI) and numerical simulations. The variation of impactor parameters, primarily used for covering different particle sizes, caused a divergence of the critical

velocities. It was found that the obliquity of the impact and the tangential velocity component remarkably lowered the normal velocity required for the rebound, i.e., the critical velocity. The obliquity was characterized quantitatively by the ratio of maximum tangential and normal velocities at the onset of rebound. For velocity ratios of 2–4, the critical velocities were four times lower than the critical velocities for close-to-normal impacts having a velocity ratio smaller than 1.5. The most oblique impacts with a velocity ratio above 9 resulted in critical velocities more than a magnitude smaller compared to the close-to-normal impacts. The strong dependence of the critical velocity on the obliquity of the impact may have an influence on the impactor design and instrument development. Depending on the application, if particle rebound must be avoided or is desired, the impactor should be designed to have high or low tangential velocities, respectively. The effect of obliquity on the critical velocity can be estimated qualitatively in impactors based on the results of this study.

The surface material was found to have no significant effect on the critical velocity of rebound within the accuracy of the method. The test materials in this study were steel, aluminium, molybdenum, and Tedlar. Even though the particle bounce can generally be avoided with greased or porous surface materials in impactors, there were relatively small differences in the rebound sensitivity of these hard test materials. On the other hand, the particle material may have a substantial effect on the critical velocity. This was confirmed by the comparison between the results of this study for ammonium fluorescein particles and the results of Arffman et al. (2015) for silver particles. Both of these results were determined with the same method and the impacts were checked to be close-to-normal with respect to the obliquity. The comparison showed that the critical velocity was approximately two orders of magnitude higher for ammonium fluorescein than for silver at the particle size of one micron.

The results of this study for ammonium fluorescein particles on a steel surface agreed well with the previous results of Wang and John (1988) for the same materials. The agreement practically connects our method based on the VNAI and numerical simulations to the set of previous critical velocity results for micron-sized particles. Since many of the methods applied in the size range above 1 μm are not applicable in the nanoparticle size range, this connection is an important link between the nanoparticles and micron-sized particles. We also saw a similar difference between our results and the results of Wall et al. (1990) with the corresponding materials that was seen by Wang and John (1988) in their study. The direct measurement of the incident and rebound velocity in accurately normal collisions, such as performed by

Wall et al. (1990), may result in a higher critical velocity than the critical velocity determined using an impactor with close-to-normal impacts. However, this difference is relatively small compared to the effect of the particle material and very oblique impacts outlined above.

Acknowledgments

The authors thank Dr. Mari Honkanen at the Department of Materials Science (TUT) for the scanning electron microscopy images.

Funding

Heino Kuuluvainen acknowledges the TUT's graduate school for financial support.

ORCID

Heino Kuuluvainen  <http://orcid.org/0000-0002-6003-3547>
Juha Harra  <http://orcid.org/0000-0002-4642-8526>

References

- Arffman, A., Kuuluvainen, H., Harra, J., Vuorinen, O., Juuti, P., Yli-Ojanperä, J., Mäkelä, J., and Keskinen, J. (2015). The Critical Velocity of Rebound Determined for Sub-Micron Silver Particles with a Variable Nozzle Area Impactor. *J. Aerosol Sci.*, 86:32–43.
- Arffman, A., Marjamäki, M., and Keskinen, J. (2011). Simulation of Low Pressure Impactor Collection Efficiency Curves. *J. Aerosol Sci.*, 42(5):329–340.
- Bateman, A., Belassein, H., and Martin, S. (2014). Impactor Apparatus for the Study of Particle Rebound: Relative Humidity and Capillary Forces. *Aerosol Sci. Technol.*, 48(1):42–52.
- Berglund, R., and Liu, B. (1973). Generation of Monodisperse Aerosol Standards. *Environ. Sci. Technol.*, 7(2):147–153.
- Brach, R., Dunn, P., and Li, X. (2000). Experiments and Engineering Models of Microparticle Impact and Deposition. *J. Adhesion*, 74(1–4):227–282.
- Chang, M., Seongheon, K., and Sioutas, C. (1999). Experimental Studies on Particle Impaction and Bounce: Effects of Substrate Design and Material. *Atmos. Environ.*, 33(15):2313–2322.
- Chen, S., Li, S., and Yang, M. (2015). Sticking/Rebound Criterion for Collisions of Small Adhesive Particles: Effects of Impact Parameter and Particle Size. *Powder Technol.*, 274:431–440.
- Dahneke, B. (1971). The Capture of Aerosol Particles by Surfaces. *J. Colloid Interf. Sci.*, 37(2):342–353.
- Dzubay, T. G., Hines, L. E., and Stevens, R. K. (1976). Particle Bounce Errors in Cascade Impactors. *Atmos. Environ.*, 10(3):229–234.
- Froeschke, S., Kohler, S., Weber, A. P., and Kasper, G. (2003). Impact Fragmentation of Nanoparticle Agglomerates. *J. Aerosol Sci.*, 34(3):275–287.

- Ihalainen, M., Lind, T., Arffman, A., Torvela, T., and Jokiniemi, J. (2014). Break-Up and Bounce of TiO₂ Agglomerates by Impaction. *Aerosol Sci. Technol.*, 48(1):31–41.
- Kang, M., Cho, H.-J., Kwak, H., and Park, K. (2015). Evaluation of Particle Bounce in Various Collection Substrates to be used as Vaporizer in Aerosol Mass Spectrometer. *Aerosol Sci. Technol.*, 49(5):332–339.
- Kuuluvainen, H., Saari, S., Mensah-Attipoe, J., Arffman, A., Pasanen, P., Reponen, T., and Keskinen, J. (2016). Triboelectric Charging of Fungal Spores During Resuspension and Rebound. *Aerosol Sci. Technol.*, 50(2):187–197.
- Matsusaka, S., Maruyama, H., Matsuyama, T., and Ghadiri, M. (2010). Triboelectric Charging of Powders: A Review. *Chem. Eng. Sci.*, 65(22):5781–5807.
- Pajunoja, A., Lambe, A., Hakala, J., Rastak, N., Cummings, M., Brogan, J., Hao, L., Paramonov, M., Hong, J., Prisle, N., Malila, J., Romakkaniemi, S., Lehtinen, K., Laaksonen, A., Kulmala, M., Massoli, P., Onasch, T., Donahue, N., Riipinen, I., Davidovits, P., Worsnop, D., Petäjä, T., and Virtanen, A. (2015). Adsorptive Uptake of Water by Semisolid Secondary Organic Aerosols. *Geophys. Res. Lett.*, 42(8):3063–3068.
- Rennecke, S., and Weber, A. P. (2013). The Critical Velocity for Nanoparticle Rebound Measured in a Low Pressure Impactor. *J. Aerosol Sci.*, 58:135–147.
- Saukko, E., Kuuluvainen, H., and Virtanen, A. (2012). A Method to Resolve the Phase State of Aerosol Particles. *Atmos. Meas. Technique*, 5(1):259–265.
- Seipenbusch, M., Toneva, P., Peukert, W., and Weber, A. P. (2007). Impact Fragmentation of Metal Nanoparticle Agglomerates. *Part. Part. Sys. Character.*, 24(3):193–200.
- Stace, A. (2015). Molecular Dynamics Study of the Surface Scattering and Capture of Nanoparticles at High Velocities. *J. Aerosol Sci.*, 83:32–38.
- Stöber, W., and Flachsbart, H. (1973). An Evaluation of Nebulized Ammonium Fluorescein as a Laboratory Aerosol. *Atmos. Environ.*, 7(7):741–748.
- Vanderpool, R., and Rubow, K. (1988). Generation of Large, Solid, Monodisperse Calibration Aerosols. *Aerosol Sci. Technol.*, 9(1):65–69.
- Virtanen, A., Joutsensaari, J., Koop, T., Kannosto, J., Yli-Pirilä, P., Leskinen, J., Mäkelä, J. M., Holopainen, J. K., Pöschl, U., Kulmala, M., Worsnop, D. R., and Laaksonen, A. (2010). An Amorphous Solid State of Biogenic Secondary Organic Aerosol Particles. *Nature*, 467(7317):824–827.
- Wall, S., John, W., and Wang, H.-C. (1990). Measurements of Kinetic Energy Loss for Particles Impacting Surfaces. *Aerosol Sci. Technol.*, 12(4):926–946.
- Wang, H.-C., and John, W. (1988). Dynamic Adhesion of Particles Impacting a Cylinder, in *Particles on Surfaces 1: Detection, Adhesion, and Removal*, K. L. Mittal, ed., Plenum Press, New York, pp. 211–224.
- Xie, J., Dong, M., and Li, S. (2016). Dynamic Impact Model of Plastic Deformation between Microparticles and Flat Surfaces Without Adhesion. *Aerosol Sci. Technol.*, 50(4):321–330.

Paper IV

Heino Kuuluvainen, Sampo Saari, Jacob Mensah-Attipoe, Anssi Arffman, Pertti Pasanen,
Tiina Reponen, and Jorma Keskinen,

“Triboelectric charging of fungal spores during resuspension and rebound”

Aerosol Science and Technology, vol. 50, no. 2, p. 187–197, 2016

doi: 10.1063/1.4852795

© Taylor & Francis Group



Triboelectric charging of fungal spores during resuspension and rebound

Heino Kuuluvainen^a, Sampo Saari^a, Jacob Mensah-Attipoe^b, Anssi Arffman^a, Pertti Pasanen^b, Tiina Reponen^{b,c}, and Jorma Keskinen^a

^aDepartment of Physics, Tampere University of Technology, Tampere, Finland; ^bDepartment of Environmental Science, University of Eastern Finland, Kuopio, Finland; ^cDepartment of Environmental Health, College of Medicine, University of Cincinnati, Cincinnati, USA

ABSTRACT

The triboelectric charging of fungal spores was experimentally characterized during rebound and resuspension. A fungal spore source strength tester (FSSST) was used as a primary aerosol generator for spores of three fungal species and two powders (silicon carbide and silver). The critical velocity of rebound was determined using a variable nozzle area impactor (VNAI), and the charging state of particles after resuspension and rebound was measured using the FSSST, different impactor setups, electrometers, and optical particle counters. In the impactor setups and the FSSST, five different surface materials relevant for indoor environments were used (steel, glass, polystyrene, paper, and polytetrafluoroethylene). The critical velocity of rebound was determined to be 0.57 m/s for fungal spores, which is relatively low compared to silicon carbide and previous results for micron-sized aerosol particles. Based on the rebound impactor measurements, we were able to define the crucial parameters of charge transfer for different particle–surface material pairs. A contact charge parameter, which describes the triboelectric charging during rebound, was found to have a negative correlation with the charging state of the particles after the resuspension from an impactor. This connects the triboelectric charging during rebound and resuspension to each other. Based on the contact charge parameter values, quantified triboelectric series could be formed. The results of this work show that fungal spores can be charged both positively and negatively during rebound and resuspension depending on the fungal species and surface material.

ARTICLE HISTORY

Received 7 October 2015
Accepted 20 December 2015

EDITOR

Jian Wang

IV

1. Introduction

Fungal spores are present in outdoor and indoor air, often as a dominant biological component. As primary biological aerosol particles (PBAP), they can act as cloud condensation nuclei and ice nuclei, contributing to cloud formation and global climate (Després et al. 2012). Fungal spores also have adverse health effects. Respiratory diseases and allergies may arise from the inhalation of fungal spores (Douwes et al. 2003). Water damages and subsequent mold growth in buildings can lead to the release of fungal spores and degrade the indoor air quality (Mendell et al. 2011). The identification of indoor mold problems is usually based on the analysis of contaminated building structures or collected fungal spore samples. However, to understand the dynamics of fungal spores in indoor environments, their physical properties should also be studied in the aerosol phase.

Various offline techniques have been used to collect fungal spores, such as an Andersen impactor and filter sampling (Reponen et al. 2011). These methods are well-

established for culture-based and microscopic analyses, and the identification of different species. For measuring the size distribution and concentration of fungal spores, there are more sophisticated online methods based on laser-induced fluorescence (LIF), such as an ultraviolet aerodynamic particles sizer (UV-APS, TSI Inc.) and a BioScout (EnviroNics Ltd.). A comparison of these two instruments was performed by Saari et al. (2014). So far, most studies focused on the size distributions of fungal spores have been conducted in the laboratory settings. The spores have been found to form rather monodisperse particle size distributions in the size range of 2–3 μm (Cho et al. 2005; Saari et al. 2015). In these experiments, a fungal spore source strength tester (FSSST) was used to generate the aerosol samples of known fungal species. The tester was introduced by Sivasubramani et al. (2004) and it has been used in several other studies.

The settling velocity of fungal spores is in the order of 1–10 mm/s (Hussein et al. 2013) and their deposition onto different surfaces in indoor environment is

CONTACT Heino Kuuluvainen ✉ heino.kuuluvainen@tut.fi Department of Physics, Tampere University of Technology, Korkeakoulunkatu 3, 33720 Tampere, Finland.

Color versions of one or more of the figures in the article can be found online at www.tandfonline.com/uast.

© 2016 American Association for Aerosol Research

relatively fast. Furthermore, fungal spores can easily be resuspended from different surfaces. Everyday indoor activities, such as cleaning, can affect the fungal spore concentrations through resuspension (Reponen et al. 1992; Lehtonen et al. 1993). Another phenomenon that might be relevant especially in ventilation and filtration systems is the rebound of fungal spores from surfaces. In general, the rebound of aerosol particles has been studied in order to design filters and impactors with a low probability of particle bounce (Dahneke 1971; Chang et al. 1999; Mullins et al. 2003). Even if the efficiencies of filters are usually very high, the role of particle rebound can be significant in high-volume filtration used in applications such as indoor air purification and ventilation (Hubbard et al. 2014). For the rebound, there is a crucial parameter called the critical velocity of rebound, the lowest impact velocity with which a particle rebounds from a surface. It has been determined previously for micron-sized aerosol particles with different particle and surface materials (Wall et al. 1990), for submicron silver particles (Rennecke and Weber 2013; Arffman et al. 2015), but not for bioaerosols, such as fungal spores.

In triboelectric charging, charges move from one material to another in contact to equalize their electrochemical potential. A similar charge transfer phenomenon often takes place between an aerosol particle and a surface during rebound or consecutive deposition and resuspension processes. This has been widely studied for medical aerosols and inhalators (Watanabe et al. 2007; Matsusaka et al. 2010). A theoretical point of view and experimental studies for the charge transfer of micron-sized aerosol particles and smooth surfaces were presented by John et al. (1980) and later reviewed by John (1995). More recently, Kuuluvainen et al. (2013) measured the charge transfer in a cascade impactor for nanoparticles. Although triboelectric charging of fungal spores during rebound and resuspension is likely to occur in indoor environments, it has not been studied previously. Airborne fungal spores have been found to carry a net negative charge in most environments (Lee et al. 2004), and their charging state can differ significantly from nonbiological particles (Mainelis et al. 2001). The charging state is especially important in electric fields. Electric fields can be found everywhere in indoor environments, for example, close to electric household appliances. In more specific applications, such as electrostatic filters and samplers, the charging state of fungal spores is a key factor (Han et al. 2011; Tan et al. 2011).

In this study, we present experimental results for the triboelectric charging of fungal spores and the critical velocity of rebound. The main idea of this study was to investigate the behavior of fungal spores on different surfaces relevant for indoor environments. In addition to

spores of three fungal species, two reference materials were used, and the results were compared to the theoretical knowledge and previous studies. An extensive dataset of charge transfer parameters and quantified triboelectric series for different materials is provided.

2. Theoretical background

2.1. Resuspension

Resuspension is the detachment of a particle from a surface and its transport away. In more specific terms, re-entrainment and blow-off refer to resuspension by a jet of air. In resuspension, the particle has to overcome the adhesion energy between the particle and the surface. Unlike the static detachment in a centrifuge, the forces required for resuspension can be less than 1% of the static adhesion forces (Hinds 1999). That is usually the case in re-entrainment and blow-off in which rolling and sliding of the particle can be involved before it becomes airborne.

Resuspension is a very challenging phenomenon to investigate both from the point of view of models and experiments. Reeks and Hall (2001) performed experiments in a centrifuge to measure adhesive forces and in a blower to measure the forces required for resuspension. They found a kinetic model called “rock’n roll” to have the best agreement with the experiments. Different types of blow-off experiments are especially relevant for resuspension in outdoor environments mimicking natural wind. In indoor air, everyday activities such as walking or cleaning affect resuspension through mechanical, aerodynamic, and electrostatic disturbance. The effect of walking on resuspension can be studied, for instance, in specific chambers where both aerodynamic and mechanical disturbance are generated in a reproducible way (Gomes et al. 2007). Boor et al. (2013) reviewed previous studies on resuspension in indoor environments and found fundamental differences between monolayer and multilayer deposits.

2.2. Triboelectric effect

Everyday static electricity is usually triboelectric. When two dissimilar materials are brought into a contact and separated, one will become positively and one negatively charged. The transferred charge depends on the electrochemical potential of the materials and the contact area. Different combinations of insulating and conductive materials can be treated differently from a theoretical point of view (Lowell and Rose-Innes 1980). However, the triboelectric effect is in general poorly understood

and experiments are usually not reproducible (Ireland 2009; Castle 1997).

In triboelectric series, materials are listed according to their charge affinity with relation to other materials. The materials on the top of the series are most willing to donate electrons and the materials on the bottom of the series most willing to steal electrons. In general, the triboelectric series found in the literature are approximate, qualitative, based on a single experimental setup, and not reproducible. However, it is also possible to obtain quantitative or semiquantitative triboelectric series by measuring the charge, charge affinity, or charge density with relation to a reference material (Park et al. 2008; Diaz and Felix-Navarro 2004).

2.3. Charge transfer during rebound

The charge transfer of an aerosol particle to a surface during rebound can theoretically be divided into the transfer of preliminary charge and triboelectric contact charging. John et al. (1980) formulated a model where both of these factors were theoretically derived for a spherical particle and a smooth surface starting from the elasticity theory of Hertz. As a result, the total charge transferred during rebound could be written as

$$q_{\text{tot}} = q_c + \beta q_0, \quad [1]$$

where q_c is the contact charge, q_0 is the preliminary charge, and β is a parameter describing the precharge sensitivity of the process. John et al. (1980) also measured q_c and β values experimentally for sodium chloride, methylene blue, potassium biphthalate, and aluminum particles on different metal surfaces. They found contact charge values usually in the order of 100 elementary charges per particle using impact velocities around 70 m/s. Furthermore, the contact charge was proportional to the cube of the particle diameter and directly proportional to the impact velocity. In some studies (Yamamoto and Scarlett 1986; Watanabe et al. 2007), a concept of an equilibrium charge has been used to describe the transferred charge during rebound. The equilibrium charge means the value of the preliminary charge with which the total charge transferred is zero.

In this study, the charge transfer during rebound was characterized according to the theory presented above. This means that the transferred charge was defined to be the average charge transferred from a single particle to a surface. The contact charge is the transferred charge to the same direction for a preliminarily neutral particle. In addition to the study by John et al. (1980), the same notation has been used in other studies (John 1995; Kuuluvainen et al. 2013). On the other hand, the

transferred charge in the resuspension experiments was defined from the viewpoint of a particle, as a charge obtained by a resuspended particle. This is reasonable because we are finally interested in the charge obtained by the particles.

3. Methods

3.1. Sample preparation and aerosolization

Spores of three different fungal species were used in the experiments: *Aspergillus versicolor* (A.v.), *Cladosporium cladosporioides* (C.c.), and *Penicillium brevicompactum* (P.b.). A detailed description of the fungal spore sample preparation can be found in a previous study (Saari et al. 2015). Briefly, 0.5 ml of fungal spore suspension was inoculated on an agar plate for each sample. Then, the inoculated agar plates were incubated in a conditioned chamber at a room temperature and at a relative humidity of 95–97% for a growth period of one month. The chamber was exposed to daylight (6 h) and darkness (18 h) throughout the growth period. Before aerosolization, the samples were dried in a laminar flow hood overnight to reduce humidity on the culture surface and improve the release of spores.

In addition to the fungal spores, two reference materials were used. Because the reference materials had to be comparable to the fungal spores, only solid powders or dusts with a similar size distribution were used. The first reference material was silicon carbide (SiC) standard test dust (Particle Technology Ltd., 0.5–10 μm). Material density of silicon carbide is 3.2 g/cm^3 . The second reference material was commercial silver powder with the particle diameter of 0.7–1.5 μm and near-spherical morphology (Inframat Advanced Materials, purity 99.95%).

The aerosolization was carried out using a fungal spore source strength tester (FSSST). In the FSSST, a generation substrate with fungal spores is placed below a multiple-nozzle plate. When an air stream is driven through the nozzles, the spores are blown off and aerosolized. The aerosol sample comes out from the center of the instrument. In this study, we used a total flow of 25 lpm through the FSSST. Since the FSSST was also used to study the resuspension from different surfaces, the fungal spores were generated either directly from the agar growth plates or from substrates with different materials including steel, glass, polystyrene, paper, and polytetrafluoroethylene (PTFE). Moving the fungal spores from the growth plates onto the different substrates was carried out using glass beads with a diameter of 425–600 μm (Sigma-Aldrich Co.). First, spores were attached on glass beads by gently shaking them on an agar growth plate. After that, the glass beads were moved

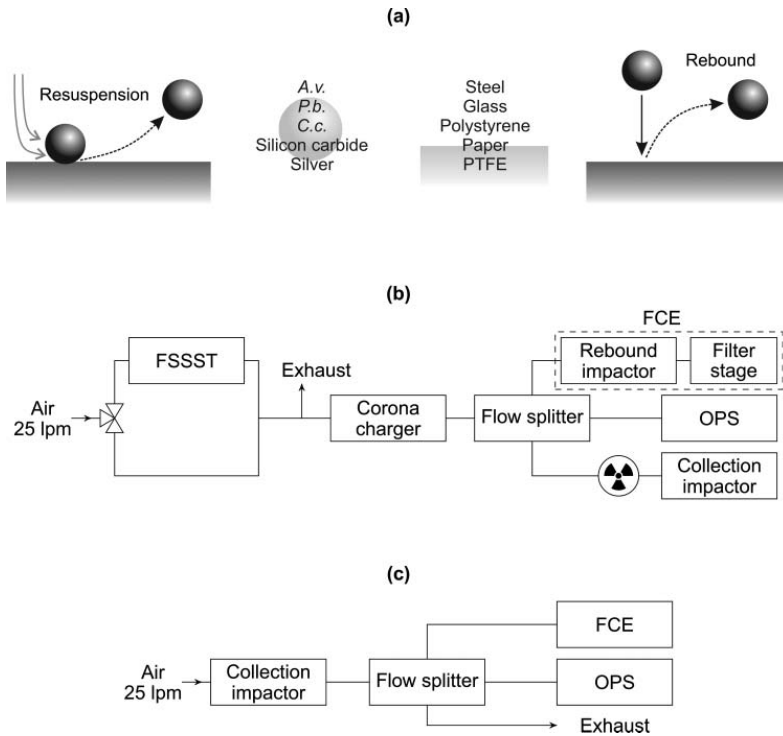


Figure 1. (a) Resuspension and rebound was studied for five particle materials and five surface materials. The fungal species were *Aspergillus versicolor* (A.v.), *Penicillium brevicompactum* (P.b.), and *Cladosporium cladosporioides* (C.c.). PTFE is the abbreviation for polytetrafluoroethylene. (b) A schematic for the measurement setup for the rebound experiment, the resuspension experiment with a fungal spore source strength tester (FSSST), and the impactor collection. (c) A schematic for the measurement setup for the resuspension experiment with an impactor. The Faraday-cup electrometers (FCE), impactors, and filter stage were parts of an electrical low-pressure impactor (ELPI).

onto a studied substrate and shaken again. With this procedure, a relatively thin and smooth layer of fungal spores was obtained on different substrates. The reference particle materials, silicon carbide and silver, were also generated using the FSSST and different substrate materials. Glass beads were used to spread the powder or dust and smoothen the layer. Figure 1a schematically shows the studied phenomena of this study with a list of particle and surface materials.

3.2. Rebound experiment

Figure 1b shows a schematic of the first measurement setup. The main purpose of this setup was to measure the charge transfer of particles during rebound. In addition, the resuspension experiment with the FSSST and impactor collection for further experiments were conducted. At first, filtered air (25 lpm) was led through the system bypassing the FSSST. A sample substrate loaded with fungal spores or reference material was installed

and the air flow was turned into the FSSST. After that, the aerosol was passed through a corona charger and a flow splitter to measuring devices. A single measurement took as long as measurable concentrations were obtained from the FSSST, usually about 2 min. This was referred as a single aerosol sample and the rebound experiment consisted of altogether 133 aerosol samples. The corona charger was a charger of an electrical low-pressure impactor (ELPI, Dekati Ltd.) (Keskinen et al. 1992), and it was turned on and off to obtain varying state of preliminary charge for the particles used in the rebound experiment. For each material pair, at least three samples were measured directly from the FSSST and at least three samples were measured using the corona charger after the FSSST. The whole system was installed vertically starting from the corona charger and the length of the sample lines was optimized, in order to minimize inertial collisions with the sample lines and subsequent losses or change of charge in the system. A special flow splitter (Model 3708, TSI Inc., Shoreview, MN, USA) was used

in order to ensure comparable aerosol samples for different measuring devices.

An optical particle sizer (OPS, Model 3330, TSI Inc.) was used to measure the particle size distribution and number concentration. The operation of the OPS is based on single particle counting and optical size measurement. In these experiments, the sample flow to the instrument was 1 lpm and averaged data was saved every 10 s for the data analysis. The impactor setup used to measure the charge transfer of particles during rebound consisted of a single ELPI impactor stage (stage number 8, cutoff 0.92 μm) and a filter stage placed downstream. The impactor stage was chosen to have impact velocities high enough for particle rebound with fungal spores and reference materials. The impactor and filter stages were installed into an ELPI unit so that we were able to measure electric current from the impactor stage and filter stage with the electrometers. By summing up these two currents, we obtained the total current corresponding to a Faraday-cup electrometer measurement. The compact installation into the ELPI unit practically excluded the effect of particle losses to the relation of these two currents. The flow through the impactor was 10 lpm. The impactor stage was modified so that different substrate materials could be used as an impaction plate. The materials were the same as in the FSSST generation except growth substrate agar which was used only in the FSSST. Steel, polystyrene, and glass substrates were purified with isopropanol, flushed with distilled water, and finally dried with pressurized air. Paper and PTFE substrates were only flushed with clean pressurized air. From the fungal spores, *A.v.* was measured with all the surface materials, including steel, glass, polystyrene, paper, and PTFE, but *P.b.* and *C.c.* were measured only with steel and glass. The reference particle materials silicon carbide and silver were measured with all the surface materials.

To process the data, the average total charge transferred during the rebound was calculated using the total flow through the impactor, the electric current signal measured from the impactor stage, and the total concentration measured with the OPS before the impactor. We assumed that all the particles bounced in the impactor in order to obtain the amount of charges per particle after the rebound. This assumption is supported by the critical velocity results and calculated impact velocities in the rebound impactor as shown later. All the measurement data was averaged over the aerosol sample time. The preliminary net charge of particles was calculated similarly using the total current (the sum of the impactor and filter

stage currents) instead of the impactor stage current. This was carried out for all the aerosol samples.

3.3. Resuspension experiments

The first resuspension experiment was carried out using the FSSST with different surface materials and measuring the charging state of particles downstream. In addition, the resuspension from different surfaces was studied in an impactor with more sophisticated deposition and blow-off processes. A single ELPI impactor stage (stage number 9, cutoff 1.6 μm) was used as a collection impactor with various substrate materials. The impactor was chosen so that it would collect majority of the studied particles. The substrate materials and their cleaning procedures were the same as in the rebound impactor. During the first experiment (Figure 1b), an aerosol flow of 10 lpm was led through the impactor during at least three aerosol samples with the same particle material in order to have enough material for subsequent blowoff. The jet velocity in the impactor was calculated to be 22 m/s assuming incompressible flow. Upstream from the impactor, there was a radioactive source which was used to neutralize the particles and collected sample. With this collection procedure, we were able to obtain a very thin layer of particles on the impactor collection substrate where most of the particles were in a direct contact with the substrate material and net neutral.

Figure 1c shows the setup for the resuspension experiment with an impactor. After finishing the collection, a relatively high flow (25 lpm), corresponding to a jet velocity of 54 m/s, was led through the collection impactor in order to blow off the collected particles. The charge and concentration of resuspended particles were measured with a Faraday-cup electrometer and with an OPS downstream from the impactor. Altogether 20 aerosol samples of resuspended particles were measured. Some of the material pairs were measured only once and some of them were repeated.

3.4. Critical velocity experiment

A variable nozzle area impactor (VNAI) introduced by Arffman et al. (2015) was used to measure the critical velocity of rebound for fungal spores (*A.v.*) and silicon carbide particles (SiC). The VNAI is a new type of a slit impactor where the slit length and the impact velocity can be changed without changing the impact conditions. The flow through the impactor was 1 lpm and it was used in ambient pressure. The impaction substrate in the VNAI was machined aluminum and it was cleaned with isopropanol and flushed with distilled water before the experiment.

The collection efficiency of the VNAI was determined by measuring the particle concentration before and after the impactor with an OPS and a LAS-X II (Particle Measuring Systems Inc.), respectively, and measured as a function of the slit length. After that, the onset of rebound and the corresponding critical slit length were determined from the experimental data and exploited to calculate the critical velocity using CFD simulations. A detailed description of the computational part of the analysis is seen in the study of Arffman et al. (2015). In the critical velocity experiment, the setup was similar to the one used in the rebound experiment (Figure 1b), but the rebound impactor was replaced by the VNAI and the LAS-X II in series. Altogether 28 aerosol samples were generated with the FSSST and measured with slit lengths 3–30 mm for the fungal spores and silicon carbide particles. The corona charger was either turned on or off but it was found to have no effect on the measurement.

4. Results and discussion

4.1. Generated particles

First, we focus on the results obtained for the FSSST as a primary particle generator. Figure 2 shows the number size distributions as a function of the optical particle size measured with the OPS. These distributions are averaged over 22–47 aerosol samples for each particle material. No differences were seen

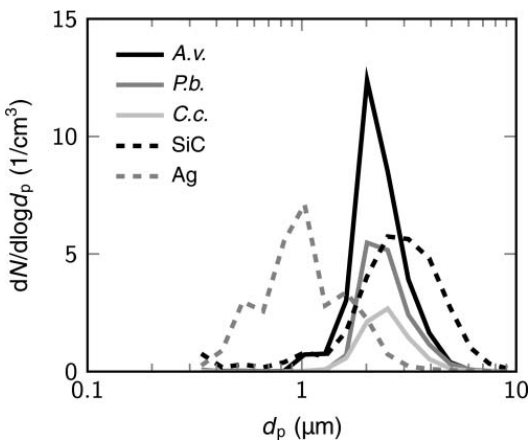


Figure 2. The number size distributions of different particles from a fungal spore source strength tester (FSSST). *A.v.*, *P.b.*, and *C.c.* are abbreviations for fungals species *Aspergillus versicolor*, *Penicillium brevicompactum*, and *Cladosporium cladosporioides*, respectively. Ag refers to silver and SiC to silicon carbide.

between different generation substrates (data not shown). The size distributions of different fungal spores were very similar: relatively narrow and peaking around 2–3 μm . Previously, the aerodynamic size of *A.v.* fungal spores was measured to be 2.8 μm (Saari et al. 2015). The silicon carbide particles had approximately the same size as the fungal spores but slightly a wider size distribution. In the silver size distribution, the peak was around 1 μm and the size distribution was much wider having actually two side peaks on the both sides. However, if we take into account the density of silver (10.49 g/cm^3) and assume that the optical size corresponds the physical size of the sphere, the aerodynamic size would be around 3 μm . It is preferable that all the particles correspond to each other in the aerodynamic size range. The average impact velocity in the rebound experiment for 2.8 and 3 μm particles (aerodynamic size) was calculated to be 25 and 26 m/s , respectively.

4.2. Critical velocity of rebound

Figure 3 shows the collection efficiency of the VNAI as a function of the slit length measured for *A.v.* fungal spores on an aluminum surface. By decreasing the slit length from 30 mm down to 20 mm, the collection efficiency increased. After that, nearly all the particles were collected, until, at the slit length of 16.2 mm, the collection efficiency began to decrease again. This is the critical slit length corresponding to the onset of rebound and the

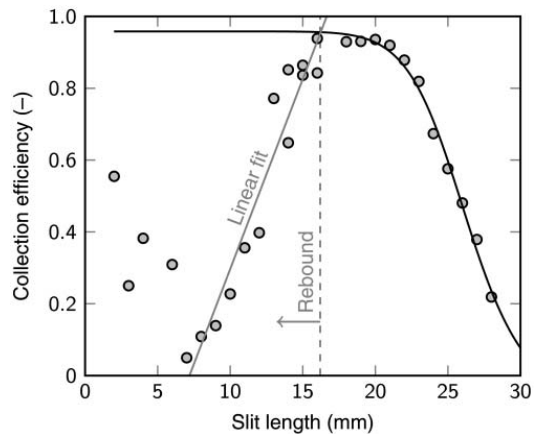


Figure 3. The measurement of the critical velocity of rebound for *Aspergillus versicolor* fungal spores on an aluminum surface. The onset of rebound can be seen as a drop in the collection efficiency curve.

Table 1. The critical velocity of rebound (v_{crit}) for *Aspergillus versicolor* (*A.v.*) fungal spores and silicon carbide (SiC) particles. Also, the aerodynamic size of the particles (d_a) and the critical slit length (L_{crit}) are shown.

Material	d_a (μm)	L_{crit} (mm)	v_{crit} (m/s)	v_{crit} limits (m/s)
<i>A.v.</i>	2.8	16.2	0.57	[0.25, 0.65]
SiC	3	11.4	2.5	[2.3, 3.0]

critical velocity of rebound. It was determined from the measurement data by searching the intersection of a linear fit and the collection efficiency curve. Finally, the critical velocity of rebound was calculated to be 0.57 m/s. Lower and upper limits for the critical velocity can be seen in Table 1. These are based on a sensitivity analysis in which 1 mm is subtracted and added to the critical slit length and the corresponding critical velocities calculated.

For silicon carbide, the critical velocity of rebound was determined to be 2.5 m/s (Table 1). This is almost five times higher than for fungal spores. Both of these values are in good agreement with the previously reported critical velocities for micron-sized aerosol particles and different material pairs (Wall et al. 1990). With respect to these previous results, the fungal spores bounce very easily and the silicon carbide particles require more energy to rebound than other types of particle materials on average. However, more recently published results by Arffman et al. (2015) for silver particles on an aluminum surface predict critical velocities even much lower in the order of 10^{-2} m/s for the particle sizes above 1 micron. These results show that the critical velocity of rebound can be highly dependent on the particle and surface material.

4.3. Charging during rebound

Based on the measurement of the critical velocity and the calculated average impact velocities, it is most likely that nearly all the particles bounced in the rebound experiment, which was an assumption in the data processing. Figure 4 shows the average transferred charge as a function of the preliminary net charge separately for *A.v.* fungal spores and silicon carbide particles on glass and PTFE substrates. Each data point represents a single aerosol sample. When the aerosol was measured directly from the FSSST, it had a negative or close to zero preliminary charge. Using the corona charger after the FSSST resulted in clearly positive preliminary charge. The variation of the preliminary charge enables reliable use of linear fits and Equation (1). As seen in Figure 4, the dependence was linear for each of these material pairs.

From the linear fits, we obtained two parameters, the contact charge q_c and the β -parameter, for each material pair. The β -parameter is the slope of the fit, and the contact charge is the transferred charge for preliminarily neutral particles. These parameters with 95% confidence limits can be seen in Table 2 for all the measured material pairs. An overview on the confidence limits of the parameter values indicates that the theory fits into the measurements well. Only a few cases for steel and glass substrates show deviation in this respect. The β -values are mainly between 0.2 and 0.7 (Table 2). Previously, John et al. (1980) have also measured β -values in the same range for some materials such as sodium chloride particles on different metal surfaces. Based on the results of this work, β seems to depend on the surface material. The highest values were obtained for PTFE (average 0.63) and glass (0.51), and the lowest values for paper (0.28) and steel (0.29). For the contact charge parameter, we obtained values from -830 to $+710$ elementary

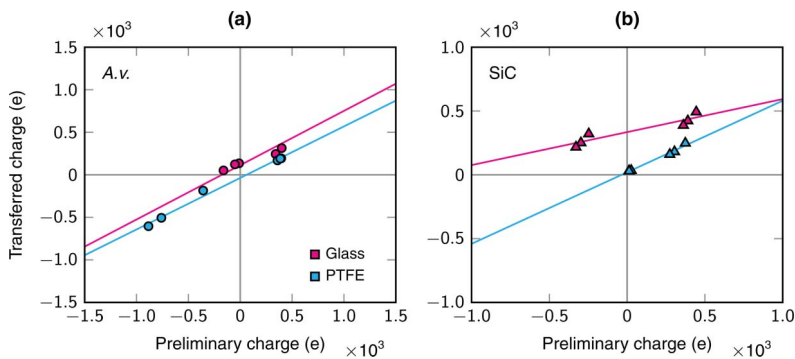


Figure 4. An example of the average transferred charge as a function of the preliminary net charge in the rebound experiment. The data are shown for (a) *Aspergillus versicolor* (*A.v.*) fungal spores and (b) silicon carbide (SiC) particles on glass and polytetrafluoroethylene (PTFE) substrates. The dependence is linear for each material pair, as predicted by the theory of charge transfer.

Table 2. The parameters of charge transfer for different particle and surface materials. The contact charge (q_c) and slope values (β) are obtained from the linear fits based on the theory of charge transfer during rebound. Also, the 95% confidence limits for the parameters are shown. A.v., P.b., and C.c. are abbreviations for fungal species *Aspergillus versicolor*, *Penicillium brevicompactum*, and *Cladosporium cladosporioides*, respectively. PTFE refers to polytetrafluoroethylene, SiC to silicon carbide, and Ag to silver.

Fungal spores			
q_c [limits] (e)	A.v.	P.b.	C.c.
Steel	-193 [-317, -69]	-263 [-317, -209]	-194 [-231, -157]
Glass	113 [32, 194]	-828 [-925, -732]	22 [16, 27]
Polystyrene	42 [24, 61]	—	—
Paper	195 [118, 272]	—	—
PTFE	-37 [-82, 8]	—	—
β [limits] (—)	A.v.	P.b.	C.c.
Steel	0.31 [0.08, 0.53]	0.20 [0.07, 0.33]	0.32 [0.26, 0.37]
Glass	0.64 [0.55, 0.72]	0.78 [0.43, 0.73]	0.42 [0.41, 0.44]
Polystyrene	0.25 [0.20, 0.30]	—	—
Paper	0.17 [0.08, 0.26]	—	—
PTFE	0.61 [0.53, 0.69]	—	—
Reference materials			
q_c [limits] (e)	SiC	Ag	
Steel	709 [603, 815]	-40 [-53, -27]	
Glass	335 [286, 384]	132 [97, 167]	
Polystyrene	104 [93, 115]	18 [16, 20]	
Paper	527 [492, 562]	-16 [-20, -13]	
PTFE	20 [-1, 41]	2 [0, 4]	
β [limits] (—)	SiC	Ag	
Steel	-0.01 [-0.38, 0.38]	0.64 [0.41, 0.87]	
Glass	0.26 [0.12, 0.40]	0.67 [0.17, 1.17]	
Polystyrene	0.32 [0.28, 0.36]	0.27 [0.23, 0.30]	
Paper	0.45 [0.33, 0.58]	0.33 [0.26, 0.40]	
PTFE	0.56 [0.47, 0.66]	0.72 [0.68, 0.75]	

charges which are in the same order of magnitude than the values published by John et al. (1980) for different material pairs. The contact charge values for silver particles were smaller because of the smaller physical size and the theoretical dependence on the cube of the particle diameter. For fungal spores, the contact charges with a steel substrate were negative and close to each other, but with a glass substrate there was a wide variation. P.b. had a highly negative value and other fungal spores had positive values. In applying these parameter values, it is important to remember that the contact charge is directly proportional to the impact velocity.

4.4. Charging during resuspension

Two different experiments were carried out to measure the charging during resuspension. To compare the results of these two experiments, Figure 5 shows the amount of charges per particle measured from the impactor resuspension as a function of the amount of charges per particle from the FSSST resuspension. Despite of the same material pairs, no correlation was seen between these two charges. The net charge from the FSSST varied from -747 to +48 elementary charges and

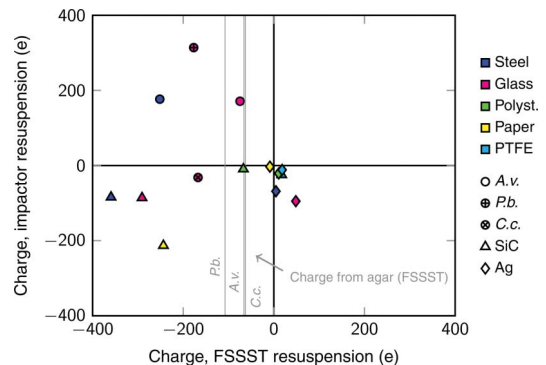


Figure 5. The amount of charges per particle from the impactor resuspension as a function of the charge from the FSSST (fungal spore source strength tester) resuspension. The color and marker shape represent the surface and particle material, respectively. Also, the amount of charges per particle generated from an agar substrate with the FSSST for fungal spores is shown. A.v., P.b., and C.c. are abbreviations for fungal species *Aspergillus versicolor*, *Penicillium brevicompactum*, and *Cladosporium cladosporioides*, respectively. PTFE refers to polytetrafluoroethylene, SiC to silicon carbide, and Ag to silver.

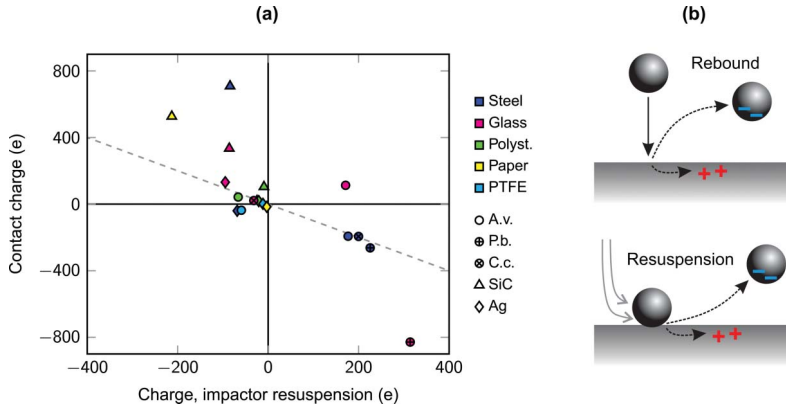


Figure 6. (a) The contact charge parameter as a function of the charge from the impactor resuspension experiment. The color and marker shape represent the surface and particle material, respectively. A dashed line represents the negative one-to-one correlation line. *A.v.*, *P.b.*, and *C.c.* are abbreviations for fungals species *Aspergillus versicolor*, *Penicillium brevicompactum*, and *Cladosporium cladosporioides*, respectively. PTFE refers to polytetrafluoroethylene, SiC to silicon carbide, and Ag to silver. (b) A schematic illustration of the charge transfer during rebound and resuspension. According to the results of this study, the transferred charge is the same.

it was negative or close to zero for all the material pairs. On the other hand, the net charge from the impactor resuspension ranged from -210 to $+310$ elementary charges and both polarities were represented. We conclude that the impactor resuspension with more sophisticated particle deposition process is more reliable to describe the charging during resuspension from different surfaces. It seems that the charging state of particles from the FSSST does not represent the charging state from pure resuspension but it is a product of the sample preparation process, multilayer deposits or collisions after the re-entrainment. It may be that the negative net charge of particles originates from a triboelectric interaction with the glass beads in the beginning of the process. Other option is that the turbulent flow right after the aerosolization creates collisions with the upper parts of the FSSST device and particles are triboelectrically charged during the collisions.

Table 3. Quantified triboelectric series for three surface materials based on the contact charging with *Aspergillus versicolor* (*A.v.*) fungal spores, silver (Ag), and silicon carbide (SiC) particles. As a reference, there is a quantified triboelectric series based on contact charging with a macroscopic object. PTFE refers to polytetrafluoroethylene.

	Gold* q_{ref} (nC)	<i>A.v.</i> q_c (e)	Ag q_c (e)	SiC q_c (e)
Glass	1.3	113	132	335
Polystyrene	0	43	18	104
PTFE	-2.8	-37	2	20

*Diaz and Felix-Navarro (2004).

Figure 6a shows the contact charge parameter obtained from the rebound experiment as a function of the net charge from the impactor resuspension. Even though the data varied widely, a negative correlation between these two quantities could be seen. The negative correlation is reasonable because the contact charge is the transferred charge from a neutral particle to a surface, and the charge from the impactor resuspension is the charge obtained by the particle. This indicates that the triboelectric charging of particles during rebound correlates with the triboelectric charging of particles during resuspension (Figure 6b). For fungal spores, this means that, by investigating their charging properties in a rebound test, it is also possible to predict their behavior during resuspension. This is especially important for indoor environments where the resuspension from surfaces of different materials can affect the charge and dynamics of fungal spores.

4.5. Triboelectric series

The contact charge describes the triboelectric interaction between a particle and a surface. By measuring the contact charge with several material pairs and keeping either the particle or surface material unchanged, it is possible to obtain a quantified triboelectric series. Based on the results of this study, there are several options to form triboelectric series. However, some of the data might not be consistent with each other in this respect. The contact charge values varied widely, especially for steel and paper substrates. Table 3 shows the quantified triboelectric series for glass, polystyrene, and PTFE based on the

contact charging with *A.v.* fungal spores, silver, and silicon carbide particles. The level of contact charge may not be comparable between different particle materials but the series can be compared relatively. All of these three series are consistent with each other and also with the reference adapted from a contact charge measurement between macroscopic objects (Diaz and Felix-Navarro 2004).

5. Conclusions

In this study, we characterized the triboelectric charging of fungal spores. Experiments with a fungal spore source strength tester (FSSST), a variable nozzle area impactor (VNAI), and different impactor setups were carried out. The impactor setups were used for studying particle rebound and resuspension. Altogether, spores of three fungal species, two reference particle materials, and five different surface materials were studied. A critical velocity of rebound was determined using the VNAI, and the net charge of particles was measured after the FSSST resuspension and the impactor resuspension. From the rebound experiment, we were able to define two parameters of charge transfer for each material pair.

The triboelectric charging during rebound was connected to the charging during resuspension through the negative correlation between the contact charge parameter and the net charge measured from the impactor resuspension. This is an important result which combines these two mechanically very different phenomena from the point of view of triboelectric charging. As shown in this study, the charging of fungal spores or other particles during resuspension may not be easy to investigate experimentally. The results from the FSSST resuspension were totally different than the results from the impactor resuspension, even though both of the cases represented similar re-entrainment and the materials were the same. Several issues, such as particle charging before the deposition and multilayered structures on a surface, can disturb the pure triboelectric charging between a particle and a surface during resuspension. Thus, it is important that we can connect resuspension to rebound, the latter of which is easier to control experimentally and understand theoretically. However, this connection and the negative correlation between the contact charge parameter and the charge from the impactor resuspension should be studied more in the future. Especially, different approaches to study the triboelectric charging during resuspension and practical resuspension experiments are required.

The interaction between fungal spores and surfaces is of great interest in indoor air. As relatively large micron-

sized particles, they are constantly depositing on different surfaces and easily resuspended because of various activities or ventilation. In ventilation and filtration systems, they may collide with walls or fibers. In order to characterize the dynamics of fungal spores and predict the concentrations at different locations, it is important to know their charging state after resuspension or rebound. According to this study, the fungal spores bounce with impact velocities higher than 0.57 m/s. The charging state of particles after rebound is dependent on the material pair. This study provides an extensive dataset of charge transfer parameters for different fungal spores and reference particle materials on different surfaces relevant for indoor environments. With these parameters, it is also possible to estimate the charging state of fungal spores after resuspension and form quantified triboelectric series. Fungal spores can be charged both positively and negatively during rebound and resuspension. The absolute values of the net charge measured after rebound or resuspension were mainly in the order of 100 elementary charges per particle. That is almost as high as the charges typically obtained with a corona charger. Thus, the charging state can maintain hours in indoor air and affect the deposition, filtration, and sampling of fungal spores.

Funding

Finnish Distinguished Professor (FiDiPro) program for the Development of Bioaerosols Testing Facilities project through TEKES (1391/31/2011) is gratefully acknowledged. H. Kuuluvainen acknowledges the TUT's graduate school for financial support.

References

- Arffman, A., Kuuluvainen, H., Harra, J., Vuorinen, O., Juuti, P., Yli-Ojanperä, J., Mäkelä, J., and Keskinen, J. (2015). The Critical Velocity of Rebound Determined for Sub-Micron Silver Particles with a Variable Nozzle Area Impactor. *J. Aerosol Sci.*, 86:32–43.
- Boor, B., Siegel, J., and Novoselac, A. (2013). Monolayer and Multilayer Particle Deposits on Hard Surfaces: Literature Review and Implications for Particle Resuspension in the Indoor Environment. *Aerosol Sci. Technol.*, 47(8):831–847.
- Castle, G. (1997). Contact Charging Between Insulators. *J. Electrostat.*, 40–41:13–20.
- Chang, M., Seongheon, K., and Sioutas, C. (1999). Experimental Studies on Particle Impaction and Bounce: Effects of Substrate Design and Material. *Atmos. Environ.*, 33 (15):2313–2322.
- Cho, S.-H., Seo, S.-C., Schmechel, D., Grinshpun, S., and Reponen, T. (2005). Aerodynamic Characteristics and Respiratory Deposition of Fungal Fragments. *Atmos. Environ.*, 39 (30):5454–5465.
- Dahneke, B. (1971). The Capture of Aerosol Particles by Surfaces. *J. Colloid Interf. Sci.*, 37(2):342–353.

- Després, V., Alex Huffman, J., Burrows, S., Hoose, C., Safatov, A., Buryak, G., Fröhlich-Nowoisky, J., Elbert, W., Andreae, M., Pöschl, U., and Jaenicke, R. (2012). Primary Biological Aerosol Particles in the Atmosphere: A Review. *Tellus B* 64:15598.
- Diaz, A., and Felix-Navarro, R. (2004). A Semi-Quantitative Tribo-Electric Series for Polymeric Materials: The Influence of Chemical Structure and Properties. *J. Electrostat.* 62(4):277–290.
- Douwes, J., Thorne, P., Pearce, N., and Heederik, D. (2003). Bioaerosol Health Effects and Exposure Assessment: Progress and Prospects. *Ann. Occup. Hyg.* 47(3):187–200.
- Gomes, C., Freihaut, J., and Bahnfleth, W. (2007). Resuspension of Allergen-Containing Particles Under Mechanical and Aerodynamic Disturbances From Human Walking. *Atmos. Environ.* 41(25):5257–5270.
- Han, T., Nazarenko, Y., Lioy, P., and Mainelis, G. (2011). Collection Efficiencies of an Electrostatic sampler With Superhydrophobic Surface for Fungal Bioaerosols. *Indoor Air*, 21(2):110–120.
- Hinds, W. C. (1999). *Aerosol Technology: Properties, Behavior, and Measurement of Airborne Particles* (2nd ed.), John Wiley & Sons., New York.
- Hubbard, J., Salazar, K., Crown, K., and Servantes, B. (2014). High-Volume Aerosol Filtration and Mitigation of Inertial Particle Rebound. *Aerosol Sci. Technol.* 48(5):530–540.
- Hussein, T., Norros, V., Hakala, J., Petäjä, T., Aalto, P., Rannik, U., Vesala, T., Ovaskainen, O. (2013). Species Traits and Inertial Deposition of Fungal Spores. *J. Aerosol Sci.* 61:81–98.
- Ireland, P. (2009). Contact Charge Accumulation and Separation Discharge. *J. Electrostat.*, 67(2–3):462–467.
- John, W. (1995). Particle–Surface Interactions: Charge Transfer, Energy Loss, Resuspension, and Deagglomeration. *Aerosol Sci. Technol.*, 23(1):2–24.
- John, W., Reischl, G., Devor, W. (1980). Charge Transfer to Metal Surfaces From Bouncing Aerosol Particles. *J. Aerosol Sci.* 11(2):115–138.
- Keskinen, J., Pietarinen, K., and Lehtimäki, M. (1992). Electrical Low Pressure Impactor. *J. Aerosol Sci.*, 23(4):353–360.
- Kuuluvainen, H., Arffman, A., Saukko, E., Virtanen, A., and Keskinen, J. (2013). A New Method for Characterizing the Bounce and Charge Transfer Properties of Nanoparticles. *J. Aerosol Sci.* 55:104–115.
- Lee, S.-A., Willeke, K., Mainelis, G., Adhikari, A., Wang, H., Reponen, T., and Grinshpun, S. (2004). Assessment of Electrical Charge on Airborne Microorganisms by a New Bioaerosol Sampling Method. *J. Occup. Environ. Hyg.* 1(3):127–138.
- Lehtonen, M., Reponen, T., and Nevalainen, A. (1993). Everyday Activities and Variation of Fungal Spore Concentrations in Indoor Air. *Int. Biodeter. Biodegr.*, 31(1):25–39.
- Lowell, J., and Rose-Innes, A. (1980). Contact Electrification. *Adv. Phys.* 29(6):947–1023.
- Mainelis, G., Willeke, K., Baron, P., Reponen, T., Grinshpun, S., Górný, R., and Trakumas, S. (2001). Electrical Charges on Airborne Microorganisms. *J. Aerosol Sci.*, 32(9):1087–1110.
- Matsusaka, S., Maruyama, H., Matsuyama, T., and Ghadiri, M. (2010). Triboelectric Charging of Powders: A Review. *Chem. Eng. Sci.*, 65(22):5781–5807.
- Mendell, M., Mirer, A., Cheung, K., Tong, M., and Douwes, J. (2011). Respiratory and Allergic Health Effects of Dampness, Mold, and Dampness-Related Agents: A Review of the Epidemiologic Evidence. *Environ. Health Perspect.* 119(6):748–756.
- Mullins, B. J., Agranovsky, I. E., and Braddock, R. D. (2003). Particle Bounce During Filtration of Particles on Wet and Dry Filters. *Aerosol Sci. Technol.* 37(7):587–600.
- Park, C., Park, J., Jeon, H., and Chun, B. (2008). Triboelectric Series and Charging Properties of Plastics Using the Designed Vertical-Reciprocation Charger. *J. Electrostat.*, 66(11–12):578–583.
- Reeks, M., and Hall, D. (2001). Kinetic Models for Particle Resuspension in Turbulent Flows: Theory and Measurement. *J. Aerosol Sci.* 32(1):1–31.
- Rennecke, S., and Weber, A. (2013). The Critical Velocity for Nanoparticle Rebound Measured in a Low Pressure Impactor. *J. Aerosol Sci.* 58:135–147.
- Reponen, T., Lehtonen, M., Raunemaa, T., and Nevalainen, A. (1992). Effect of Indoor Sources on Fungal Spore Concentrations and Size Distributions. *J. Aerosol Sci.* 23(1):663–666.
- Reponen, T., Willeke, K., Grinshpun, S., and Nevalainen, A. (2011). “Biological Particle Sampling.” In: *Aerosol Measurement: Principles, Techniques, and Applications*, 3rd ed. P. Kulkarni, P. Baron, K. Willeke, eds. John Wiley & Sons, New York, pp. 549–570.
- Saari, S., Mensah-Attipoe, J., Reponen, T., Vejjalainen, A. M., Salmela, A., Pasanen, P., and Keskinen, J. (2015). Effects of Fungal Species, Cultivation Time, Growth Substrate, and Air Exposure Velocity on the Fluorescence Properties of Airborne Fungal Spores. *Indoor Air*. 25:653–661.
- Saari, S., Reponen, T., and Keskinen, J. (2014). Performance of Two Fluorescence-Based Real-Time Bioaerosol Detectors: Bioscout vs. UVAPS. *Aerosol Sci. Technol.* 48(4):371–378.
- Sivasubramani, S., Niemeier, R., Reponen, T., and Grinshpun, S. (2004). Fungal Spore Source Strength Tester: Laboratory Evaluation of a New Concept. *Sci. Total Environ.*, 329(1–3):75–86.
- Tan, M., Shen, F., Yao, M., and Zhu, T. (2011). Development of an Automated Electrostatic Sampler (AES) for Bioaerosol Detection. *Aerosol Sci. Technol.*, 45(9):1154–1160.
- Wall, S., John, W., and Wang, H.-C. (1990). Measurements of Kinetic Energy Loss for Particles Impacting Surfaces. *Aerosol Sci. Technol.*, 12(4):926–946.
- Watanabe, H., Ghadiri, M., Matsuyama, T., Ding, Y. L., Pitt, K. G., Maruyama, H., Matsusaka, S., and Masuda, H. (2007). Triboelectrification of Pharmaceutical Powders by Particle Impact. *Int. J. Pharmaceutics* 334(1–2):149–155.
- Yamamoto, H., and Scarlett, B. (1986). Triboelectric Charging of Polymer Particles by Impact. *Particle Characterization* 3(3):117–121.

Tampereen teknillinen yliopisto
PL 527
33101 Tampere

Tampere University of Technology
P.O.B. 527
FI-33101 Tampere, Finland

ISBN 978-952-15-3913-8
ISSN 1459-2045